ASSESSING IMMUNE RESPONSES TO ACUTE VIRAL INFECTIONS USING HIGH-PARAMETER FLOW CYTOMETRY

by
Katherine Cascino

A dissertation submitted to the Johns Hopkins University in conformity with the requirements for the degree of Doctor of Philosophy

Baltimore, Maryland
May 2021

Abstract

High-parameter flow cytometry is a crucial tool in immunology to assess kinetics and phenotypes of immune cell subsets in disease. With viral infections that have the potential to establish chronicity such as hepatitis B virus (HBV), productive immune functions must break down in order for a chronic infection to be established. On the other hand, with respiratory viral infections such as SARS-CoV-2, the causative agent of the 2019 global pandemic, infections can range in symptoms from mild or asymptomatic to severe disease requiring hospitalization. In the case of SARS-CoV-2, prolonged severity of disease is believed to be in large part due to aberrant immune responses. In order to better understand what immunologic functions fail and/or become dysregulated, high-parameter flow cytometry can be employed to interrogate exactly which immune cell subsets and/or functional pathways are altered leading to development of a chronic infection or severe disease. Reported here, we have developed two comprehensive flow cytometry panels to assess both global and antigen-specific adaptive immune responses in HBV infection to determine correlates of protection against developing a chronic infection. In addition, we employ two high-dimensional flow cytometry panels that simultaneously assess the immunologic profile and metabolic state of immune cell subsets in severe COVID-19 disease. Using this technique, we identified a metabolically distinct T cell subset unique to COVID-19 subjects compared to acute and chronic hepatitis C virus, severe influenza, and healthy controls. These T cells were found to be undergoing mitochondrial-induced apoptosis and their presence correlated with

lymphopenia in our subjects. In addition, we identified metabolically distinct myeloid-derived suppressor cell populations that were uniquely upregulated in COVID-19 and correlated with disease severity. Overall, the use of high-parameter flow cytometry allows for detailed interrogation of immunologic profiles during disease and has led to the discovery of novel metabolic pathways that can be targeted for treatment of severe COVID-19 as well as helped identify circulating immune cell populations that correlate with disease severity and can be employed as biomarkers of severe disease.

Primary Readers: Andrea Cox and Chloe Thio

Secondary Reader: Joel Blankson

Acknowledgements

There are so many people to thank who have supported me along my journey throughout my PhD. First, I'd like to give a special thank you to my mentors Andrea Cox and Chloe Thio, without whom neither of the projects incorporated in this thesis would have been possible. Your guidance along the way was critical to my development as a scientist. Thank you also to my thesis committee, Bob Siliciano, Jay Bream and Joel Blankson for meaningful contributions during our meetings together. And to Joel for constantly reminding me that I was leaving lab too early (re: 8 or 9pm) and that he would be adding additional years to my PhD….

Thank you to John Hwang and Jeff Quinn, the "world's okayest managers" who keep the lab running no matter what! And to the entire Viral Hepatitis Center, past and present, for guidance, support, friendship, and scientific input.

To my post-doctoral mentors turned friends, a huge thank you to Thomas Liechti in the Vaccine Research Center (VRC) at the NIH and Elizabeth Thompson from the Department of Oncology/BKI. For every day-to-day flow cytometry question I had and for your immense support in running both studies incorporated in this thesis. You made it incredibly fun to do collaborative science.

Thank you to all the faculty, staff and trainees at the VRC for being so welcoming and accommodating to me as an outside collaborator, providing invaluable feedback on experimental design and for being willing to think through scientific questions with me. Thank you also to the faculty and staff at CMM, especially Leslie Lichter and Colleen

Graham, for helping shepherd a naïve first year graduate student all the way through to her PhD.

To the people outside of lab in my life who helped me along the way, thank you Kim Rousseau, Lauren Dennison, Jenny Cascino, Mom, Dad and of course my fiancée, Cameron McGlone. Kim, you have been my rock in and out of lab, always ready to check my math for an experiment or take an impromptu shopping trip and convince me to buy too many things. Lauren, thank you for constantly keeping me laughing with your awkward moments and for being the best roommate turned sister I could have hoped for in Baltimore. To my family, thank you for always supporting me, but for the overtime that was sometimes needed in the rough parts of my PhD. Without everything you've done for me, I could never have made it to this point. Finally, to Cameron, thank you for always being my go-to support system and reminding me that one experiment failing or having to prep for one lab meeting was never the end of the world. I'm beyond lucky to have you in my life.

Table of Contents

List of Tables

List of Figures

Chapter 1: Introduction

1.1 Overview of Innate and Adaptive Immune Responses to Viral Infections

Productive immune responses are crucial to defending the body against infection. A coordinated effort between the first line, non-specific innate immune response and subsequent targeted adaptive immune response together provide the necessary tools to eliminate infection and produce memory against secondary exposure[1]. Below is described the main cell subsets involved in both the innate and adaptive immune response and broadly their roles in protecting against viral infection.

The innate immune system is responsible for the initial detection of a viral infection and for maintaining control of the infection until a specific adaptive immune response can be mounted. The main cell types involved in an innate immune response are monocytes, macrophages, dendritic cells (DCs), natural killer (NK) cells, and granulocytes such as neutrophils, basophils and eosinophils. Recognition of viruses largely occurs through pattern recognition receptors (PRRs) both on the surface of and within innate immune cells including monocytes/macrophages and DCs. PRRs include toll-like receptors (TLRs), NOD-like receptors (NLRs) and RIG-1 like receptors (RLRs) that together function to detect viral RNA, DNA, and structural or non-structural viral components to initiate an immune response[2]. Upon recognition of a virus through PRR detection, macrophages, monocytes and DCs will upregulate co-stimulatory molecules and release pro-inflammatory (IL-1b, IL-18, TNF, IL-6) or anti-viral (type I interferons – IFNα/β) cytokines and chemokines[3].

Proinflammatory cytokines and chemokines attract additional innate immune cells to the site of infection. Neutrophils, often the first cells to arrive at the site of infection, function by phagocytosing foreign material, degranulating antimicrobial enzymes and releasing neutrophil extracellular traps (NETs) to trap microbes at the site of infection[4]. NK cells are an innate lymphoid cell type with cytotoxic potential. In viral infections they have the ability to recognize infected cells that have downregulated MHC Class I molecules and selectively kill those cells[5]. Plasmacytoid dendritic cells (pDCs) are a subset of DCs that are the principle producer of the antiviral cytokine IFNα, making them a crucial innate immune cell subset for viral control[6,7]. Macrophages have many functions and are often classified by their polarization as an M1 or M2 phenotype. M1 macrophages are more antiviral in nature and kill infecting pathogens or compromised cells/tissues, whereas M2 macrophages play a role in wound healing and tissue regeneration[8]. In the context of disease, and most well characterized in cancer, accumulation of an immunosuppressive immature innate myeloid cell type termed myeloid derived suppressor cells (MDSCs) can occur. The exact function and role of these cells is not well characterized but they have been found to accumulate in chronic infection and are thought to be a result of a feedback loop to limit persistent inflammatory signals during chronic infection[9].

After initial recognition of viral infection, the second role of the innate immune system is to direct antigen-specific development of the adaptive immune response. To do this, macrophages and DCs must present viral antigen to adaptive immune cells through their antigen presentation functions, lending to their classification as

professional antigen presenting cells (APCs)[10]. Macrophages and DCs present antigenic peptides in the context of class I or II MHC molecules to $CD8^+$ and $CD4^+$ T cells, respectively[10]. In germinal centers of secondary lymphoid tissues, follicular dendritic cells (FDCs) present intact antigen to B cells[11]. Additional signals from APCs in the form of co-stimulatory molecules and cytokines are required to drive both T cell and B cell differentiation[10].

Once exposed to cognate antigen through APC presentation, adaptive immune cells differentiate into effector cells to drive antigen-specific responses to eliminate a viral infection and memory subsets to persist and rapidly respond in the case of re-exposure to the same infection[12]. The main cells of the adaptive immune response are T cells and B cells. T cells represent the cellular arm of the adaptive immune response and consist of $CD8^+$ T cells and $CD4^+$ helper T cells. $CD8^+$ T cells' primary function is to lyse target cells. They maintain granules of lytic enzymes including perforin and granzyme and upon recognition of cognate antigen presented on MHC Class I from an infected cell, $CD8^+$ T cells degranulate to lyse their target[13]. $CD4^+$ T cells on the other hand mainly exert their function to support other lymphocytes through costimulation and cytokine production. $CD4^+$ T cells promote antibody production from B cells, enhance effector $CD8^+$ T cell responses, and maintain a $CD8^+$ T cell memory pool[14]. $CD4^+$ T cells differentiate into a number of helper subsets including T helper 1 (Th1), Th2, Th17, T follicular helper (TFH) and T regulatory (Treg) cells. Th1 cells mainly produce IFNy and have strong antiviral functions. Th2 cells in turn produce IL-4 and have negative immunopathological effects during viral infection[14]. Th17 cells produce IL-17, a pro-

inflammatory cytokine. While an important cell type in bacterial/fungal infections, the role of Th17 cells in viral infections is still poorly understood[15]. TFH cells provide B cell help in the germinal center through expression of costimulatory molecule CD40L and production of IL-21, both of which are needed by B cells undergoing class-switching and affinity maturation[16]. Finally, Tregs serve a regulatory role to dampen immune responses after control of an infection to avoid unchecked inflammatory processes[17].

The humoral arm of the adaptive immune response consists of B cells and their functions. B cells are also considered professional APCs and can produce cytokines, but their main function is in antibody secretion. Antibodies are central molecules in fighting a viral infection, especially those with neutralizing functions. Neutralizing antibodies bind the surface of a virus in a way that blocks the virus's ability to bind target cell receptors. The virus can no longer enter the cell and replicate, with the result that the infection can be cleared. Antibodies can also serve many additional non-neutralizing functions to aid in the clearance of infections such as complement activation, antibody-dependent cellular cytotoxicity (ADCC) and antibody-dependent cellular phagocytosis (ADCP) by macrophages/DCs[18]. The B cell subsets that secrete high levels of antibodies upon activation are plasmablasts and plasma cells. Plasmablasts are generated shortly after infection or vaccination and are often short-lived[19]. Plasma cells are further differentiated plasmablasts and can be maintained for long-term memory in addition to memory B cells[20]. Together, short-lived and long-lived plasmablasts, plasma cells and memory B cells serve multiple functions in order to defend against viral infection.

The coordinated effort of innate and adaptive immune cell subsets is crucial to defense against invading viral infections. If these functions break down, it can lead to establishment of a chronic infection. Alternatively, if a productive immune response is generated but cannot be dampened after viral control, it can lead to long term negative immune pathologic effects.

1.2 Immunometabolism

Immunometabolism is the recent field of study that examines alterations in metabolic pathways within immune cell subsets that affect immune cell function[21]. While many metabolic pathways have been examined in immune cells, four main pathways described below are glycolysis, tricarboxcilic acid (TCA) cycle, fatty acid oxidation and fatty acid synthesis.

Glycolysis is the multi-enzyme metabolic pathway that converts glucose into pyruvate and ATP in the cytoplasm of cells[22]. The process is an inefficient mechanism for generating ATP compared to the TCA cycle but does not require oxygen. Pyruvate can then be reduced to lactate under hypoxic conditions or shuttled to the mitochondria as a precursor for the TCA cycle when oxygen is present[22]. A famous exception to this rule is the Warburg effect. First described in the 1920s, it was observed that cancer cells preferentially utilize glycolysis even in high oxygen conditions, termed “aerobic glycolysis”[23]. This effect first appeared counterproductive to a highly proliferating cancer cell’s need for energy, but new research suggests the benefit instead lies in facilitation of nutrient uptake that can be converted to biomass (nucleotides, amino acids, lipids)[24].

Indeed, the rapidity by which an immune cell can increase glycolytic function as well as the utility of increasing biomass make glycolysis the metabolic pathway utilized by activated/effector macrophages[25], DCs[26], NK cells[27], T cells[28] and B cells[29] during normal immune functioning.

The TCA cycle on the other hand has been shown to be the main metabolic pathway utilized by quiescent cells in non-proliferative settings[21,30]. As a hub of cell metabolism, the TCA cycle utilizes multiple metabolic substrates including acetyl-CoA, the product of oxidized pyruvate generated during glycolysis, and in turn produces additional metabolites. In addition, the TCA cycle is tightly coupled with mitochondrial electron transport chain activity, which results in efficient production of ATP through oxidative phosphorylation (oxphos)[31]. Interestingly, in M1 macrophages, the TCA cycle is broken in two stages to aid in antimicrobial function. These breaks lead to citrate accumulation for additional fatty acid synthesis to increase membrane mass for antigen presentation, and succinate accumulation to aid induction of IL-1β through HIF-1α[32,33].

Another important metabolic pathway for immune cells is fatty acid oxidation or the reverse, fatty acid synthesis. Fatty acid oxidation is used to break down short to long-chain fatty acids within the mitochondria to produce intermediates acyl-CoA, NADH and $FADH_2$ that are incorporated into the TCA cycle for generation of ATP through oxphos[34]. The pathway is used by non-inflammatory immune cell subsets that tend to have increased longevity such as Tregs, memory T cells and M2 macrophages[21]. Fatty acid oxidation helps regulate the balance between T cell effector and regulatory function by promoting Treg development and inhibiting polarization to T effector cells[28].

At the same time, long-lived memory $CD8^+$ T cells utilize fatty acid oxidation as a means to maintain energy needs but stay poised to respond quickly to antigen stimulation[35]. The reverse of this pathway, fatty acid synthesis, is an important metabolic process to generate lipids needed for cellular growth and proliferation[21]. Utilizing TCA cycle intermediates, mainly citrate, fatty acid synthesis occurs in the cytoplasm and results in production of *de novo* fatty acids. This process has been shown to promote a pro-inflammatory immune cell state. For example, LPS and cytokine signaling can trigger fatty acid synthesis in macrophages[36].

Overall, it is clear that metabolism can directly affect and/or regulate immune cell function. Through broad immunometabolic approaches, increased details about the functional state of immune cell subsets can be determined in both health and disease.

1.3 Hepatitis B Virus Clinical Characteristics and Immunology

Despite the availability of treatment strategies and a preventative vaccine, hepatitis B virus (HBV) remains a significant global health burden. Over 2 billion people have been infected with HBV worldwide, and an estimated 257 million people are chronically infected. Chronic HBV infection (CHB) increases the risk to develop severe liver disease, cirrhosis, and hepatocellular carcinoma, resulting in over 887,000 deaths each year[37,38]. Interestingly, the rate of progression to chronic infection differs dramatically based on age of exposure to the virus. Most adults who acquire an acute HBV infection go on to control their infection with only a small subset (5-10%) progressing to CHB. In contrast, the majority of neonates (90-95%), especially those born to hepatitis B e antigen

(HBeAg) positive mothers, progress to a chronic infection[38,39]. As many have hypothesized, this difference in infection outcome based primarily on age of exposure hints at a central role of functional and specific immune responses against HBV in controlling infection.

Current therapeutic strategies to treat HBV have their limitations. The prophylactic HBV vaccine has been implemented in childhood vaccination strategies worldwide in over 180 countries since 1992. This has significantly decreased the incidence of newly acquired CHB around the world[38,40]. However, mother-to-child transmission still accounts for 40-50% of new HBV infections due to poor implementation of vaccine programs in HBV endemic regions[41]. In addition, prophylactic vaccination has no effect for the over 250 million people already chronically infected with HBV. For those with CHB, antiviral drugs approved for treatment fall into one of two categories: interferon-α (IFN-α) or nucleos(t)ide reverse transcriptase inhibitors (NRTIs)[42]. These treatments are considered a partial cure in that they suppress viral replication and significantly decrease the risk of morbidity and death related to CHB but require lifelong treatment due to stable maintenance of HBV DNA in the infected liver. The main goal of current treatment strategies, therefore, is to achieve a functional cure, which is defined as sustained viral suppression *off treatment*. A functional cure would mimic natural resolution of an acute HBV infection and would likely induce robust HBV-specific immune responses[42,43].

In order to determine whether robust HBV-specific immune responses are important as a potential functional cure strategy, the role of the adaptive immune

response in resolving acute HBV infections must be well understood. The following sections will provide an overview of what is known about global and antigen-specific T cell and B cell responses during HBV infection and the gaps in our understanding that need to be addressed before a functional cure for HBV can be achieved.

1.3.1 HBV Structure and Life Cycle

HBV is the prototype member of the *Hepadnaviridae* family of small hepatotropic DNA viruses. It contains a partially double-stranded, enveloped DNA genome 3.2 kb in size. The genome codes for four overlapping open reading frames (ORFs) that produce all seven of the HBV proteins[44]. The largest ORF encodes the viral polymerase (HBV pol). HBV pol has reverse transcriptase activity and is able to generate the full HBV genome from its genomic RNA intermediate. The second largest ORF encodes the three envelope proteins, small, medium and large that collectively make up the hepatitis B surface antigen (HBsAg). All three proteins share the same C terminal region that makes up the small HBsAg protein. Medium HBsAg contains the preceding preS1 sequence in addition to small HBsAg, while large HBsAg contains a unique preS2 region, preS1, and small HBsAg sequences. The third ORF encodes the structural nucleocapsid core protein (HBcAg) and the upstream precore protein or hepatitis B e antigen (HBeAg) which is not incorporated into virions but instead secreted from infected cells. Finally, the last ORF encodes the HBV x protein (HBx), a small regulatory protein essential for HBV replication[45].

The HBV life cycle initiates when HBV binds to its target cell the hepatocyte through an initial interaction with heparin sulfate proteoglycans (HSPGs) on the cell

surface[46]. The small HBsAg "a determinant region" is responsible for this interaction. Next, the virus binds its main hepatocyte-specific receptor human sodium taurocholate costransporting peptide (hNTCP) through interaction with a preS2 region on the large HBsAg[47]. HBV tropism to the liver is a direct result of the hNTCP receptor, which is exclusively expressed on human hepatocytes[48].

Upon receptor binding and entry, the virus enters the nucleus where the partial double strand is repaired to form episomal covalently closed circular DNA (cccDNA). cccDNA acts as a stable template for transcription of 5 RNA intermediates: pre-genomic RNA (pgRNA, 3.5 kb) which serves as the template for the HBV DNA genomic material, 2.4 and 2.1 kb RNA (transcripts that become L-, M-, and S-HBsAg), 3.5 kb RNA (translated into HBcAg), and a 0.7 kb RNA (translated into HBx)[49]. cccDNA's stability in the nucleus of infected hepatocytes is the cause of HBV viral persistence[44,50].

In order to form new HBV virions, pgRNA is encapsulated within the nucleocapsid (HBcAg) in association with HBV pol. Once packaged, pgRNA is reverse-transcribed by HBV pol to produce the partially double-stranded HBV viral DNA genome[51]. The reverse-transcription step will occasionally produce a minor DNA product, double-stranded linear DNA (dslDNA) which is also secreted as a virion and represents 10% of plasma HBV DNA[52]. dslDNA is able to stably integrate into the host genome and is a secondary source of HBsAg production[53]. Finally, the viral particle is enveloped in association with HBsAg, and although still poorly understood, is thought to exit the hepatocyte through a pathway involving the endosomal sorting complex required for transport (ESCRT) pathway and multivesicular body (MVB) formation[54].

Ultimately however, low amounts of virus are produced from infected cells; an estimated 1-10 virions per day[55].

A unique feature of HBV is its ability to over-produce HBsAg with release of subviral particles (SVPs). SVPs are spherical or filamentous lipid particles lacking HBV genomic material and HBcAg, but containing small HBsAg, and to a lesser degree medium and large HBsAg. SVPs are produced in 10,000 fold excess to fully intact virions[56]. This leads to high levels of circulating HBsAg that is thought to contribute to HBV immune tolerance and exhaustion. Although a relatively small virus, HBV both stably maintains its cccDNA genome in the nucleus and uniquely overproduces SVPs, together making it a difficult virus to control and treat.

1.3.2 HBV Serology and Clinical Phases of Infection

In the course of a natural HBV infection, serological markers are used clinically to classify patients in multiple phases of infection. Upon acute infection with HBV, the first detectable markers are the viral products HBV DNA followed by HBsAg and HBeAg in serum[50]. HBeAg, the soluble pre-core protein, can be cleared early during an acute infection, but HBV DNA and HBsAg persist throughout the course of clinical symptoms. The first antibody to appear clinically is against HBcAg (anti-HBc) followed soon after by anti-HBeAg (anti-HBe). Development of anti-HBe is observable after HBeAg clearance and is a favorable serologic marker during acute infection. Interestingly, anti-HBc antibodies are not protective, likely due to the ability of the core protein to cross-link B cell receptors (BCRs) and lead to T cell-independent B cell activation and production of

antibody[57]**.** The final serological marker to appear is anti-HBsAg (anti-HBs), although development of anti-HBs occurs only in patients who control their acute infection. Therefore, detection of anti-HBs is considered the clinical sign of resolution of infection. In HBV unexposed individuals, presence of anti-HBs indicates a protective vaccination status. In contrast, transition from an acute infection to CHB is defined by the presence of circulating HBsAg for greater than 6 months *without* development of anti-HBs[58]. Due to this pattern of seroconversion, anti-HBc is used to distinguish individuals who have been exposed to an acute HBV infection, whereas anti-HBs determines positive protection status.

CHB can be further characterized into four sequential phases with distinct serological profiles[59,60]. The first phase is immune tolerance (IT), where patients are HBeAg+, anti-HBe- and have high HBV DNA but normal alanine transaminase (ALT), which is an enzyme produced by hepatocytes. Elevations in ALT suggest hepatocyte destruction. During the immune clearance or immune active phase (IA), HBeAg remains positive and anti-HBe does not develop, while HBV DNA levels are lower than in the IT phase and ALT spikes are observed. Transition to the immune control phase (IC) occurs with a loss of HBeAg and development of anti-HBe, further decrease in HBV DNA and normalization of ALT. Finally, the immune escape or HBeAg negative hepatitis phase (ENEG) maintains HBeAg-, anti-HBe+ seroconversion with elevated HBV DNA levels compared to the IC phase and occasional ALT spikes. The complex nature of CHB natural history underlies the fact that chronic infection is not a static state, and in order to

develop a universal functional cure, changing immune dynamics even within CHB must be considered.

1.3.3 T cell Responses in HBV Infection

It is well established that T cells play an important role in the control of acute HBV infection, with $CD4^+$ and $CD8^+$ T cells exhibiting differing but complementary kinetics and functions. Early chimpanzee studies demonstrated that $CD8^+$ T cells are the main effector cells in the control of acute HBV. With depletion of $CD8^+$ but not $CD4^+$ T cells during the peak of acute HBV infection, the duration of peak infection was significantly prolonged[61]. In addition, only upon the reappearance of $CD8^+$ T cells was decrease in HBV DNA observed in the liver. Finally, full clearance of HBV DNA occurred without appearance of anti-HBs and only upon full restoration of $CD8^+$ T cell frequencies, demonstrating a central role of $CD8^+$ T cells in viral control.

Interestingly, the method by which $CD8^+$ T cells exert their effector function against HBV relies heavily on their non-cytolytic ability to produce cytokines[61,62]. In a transgenic mouse model, $CD8^+$ production of IFNy and TNF was shown to inactivate intracellular HBV replication without hepatocyte lysis. As a vital organ for life, cytotoxic destruction of all infected hepatocytes during HBV infection would lead to unsustainable loss of liver function and this is likely the reason for a prominent role of non-cytolytic cytokine production in productive control of the virus. A follow up study performed in chimpanzees supported the transgenic mouse findings and showed that 90% of HBV DNA was eliminated from the liver through non-cytolytic functions early in the acute

HBV infection course (weeks 8-12)[63]. Only later were the presence of T cells detected in the liver (weeks 16-18) and their migration correlated with increased liver damage and serum ALT levels. The T cell dynamics of early non-cytolytic viral control followed by cytolytic activity and liver damage was also confirmed in a cohort of acutely infected humans[64].

Further T cell depletion studies in chimpanzees revealed that $CD4^+$ T cell priming of CD8 effector function is critical to maintaining a self-limited acute infection[65]. When $CD4^+$ T cells were depleted prior to inoculation with an HBV dose that is typically cleared from a healthy animal, a chronic infection was established and no HBV-specific intrahepatic $CD8^+$ T cell responses were detectable. In contrast, if $CD4^+$ T cells were depleted after the onset of peak infection (6 weeks after inoculation), the animals were able to control their infection as expected. Overall, these data show the important kinetics of productive $CD4^+$ priming of $CD8^+$ T cells in the control of an acute HBV infection, as well as the unique non-cytolytic function of $CD8^+$ T cells.

HBV-specific T cell responses are responsible for the HBV control dynamics described above, and it is believed that breakdown of these responses is largely responsible for progression to CHB. Profiling of HBV-specific T cells has revealed that their presence in both acute HBV infection and CHB occurs at low frequencies. For $CD8^+$ T cells, only 0.01% to 2% of total circulating CD8s are HBV-specific, depending on infection status[47]. Specificity against HBsAg, nucleocapsid (HBcAg and HBeAg), HBx and polymerase have all been observed[66–69].

Identification of HBV-specific T cells has mainly been performed by one of two methods. Direct *ex vivo* characterization using multimer staining has allowed for the identification of multiple dominant epitopes, mainly HLA-A2 restricted, in HBsAg (env 183-191 and env 335-343), HBcAg (core 18-27) and HBV polymerase (pol 455-463 and pol 575-583)[70]. Although this method has the advantage of identification through TCR specificity alone, it suffers from the limitations of necessitating HLA typing of subjects and narrowing the scope of analysis to only a few specific epitopes from individual antigens. An alternative method used to identify HBV-specific T cells is *in vitro* peptide pool stimulation. Peptide pool stimulation followed by ELISpot or intracellular cytokine staining (ICS) allows for identification of HBV-specific T cells based on their activation and/or production of cytokines. This method is limited in that identification occurs as a functional readout rather than TCR specificity but has the benefit of allowing for assessment of entire HBV antigens and determining functionality simultaneously.

Both methods described have been utilized to assess HBV-specific T cell responses in acute and chronic HBV infection. During acute infection, a strong and multi-specific T cell response has been observed against HBcAg, HBsAg and HBV polymerase[64,68,71,72]. Frequencies of HBcAg-specific T cells are often detected at highest levels, followed by HBV pol-specific and finally HBsAg-specific cells[71]. In contrast, HBV-specific T cell responses in CHB are infrequent and typically found mainly against HBcAg and HBV polymerase[69,73]. The limited detection of HBsAg-specific T cells in CHB is thought to be a result of T cell deletion, as their frequencies correspond strongly with amount of circulating HBsAg[70,74]. Further role of circulating HBsAg in limiting HBV-

specific T cell responses was shown in a study stratifying CHB patients by HBsAg levels. Investigators observed greater HBV-specific $CD4^+$ T cell responses (as shown by IFNy, TNF and IL-2 production) upon HBcAg and HBsAg peptide pool stimulation in $HBsAg^{lo}$ individuals (<500 IU/mL)[75]. In contrast to this finding, another study showed that instead duration of HBsAg exposure, rather than quantity of circulating HBsAg, had a greater effect on HBV-specific T cells, specifically leading to deletion of HBsAg-specific cells[76].

Typically, functional readouts show that peripheral blood mononuclear cells (PBMCs) from CHB patients lack the ability to produce cytokines and proliferate in response to peptide pool stimulation with HBV antigens, whereas PBMCs from acute individuals can[73]. Interestingly, one study analyzed frequency and function of HBV-specific T cells in CHB after long-term effective therapy with nucleos(t)ide analogues (NUC) and found that NUC treated HBsAg- individuals were able to respond to peptide pool stimulation after *in vitro* culture, with the highest frequency of cells producing IFNy followed by TNF then IL-2[69]. This finding suggests that functional impairment of T cell responses observed in CHB may not be a permanent state.

It is widely believed that the lack of HBV-specific T cell response in CHB is a result of persistent exposure to a high level of antigen leading to T cell dysfunction and/or exhaustion. To address this hypothesis, multiple studies have assessed the phenotypic profiles of HBV-specific T cell responses with a focus on inhibitory and/or exhaustion marker expression. It has been observed that HBV-specific $CD8^+$ T cells have high frequencies of $PD\text{-}1^+$ cells in acute and CHB, but these frequencies decline upon control of an acute infection[70,73]. Interestingly, HBV-specific $CD8^+$ T cells demonstrated

co-expression of PD-1 with CD127, which is believed to represent a phenotype of semi-productive memory, and only upon subsequent downregulation of CD127 do these cells become severely exhausted[73,77]. It was observed that the majority of HBcAg-specific and HBV polymerase-specific $CD8^+$ T cells in CHB patients with low viral loads demonstrate this memory-like $CD127^+PD\text{-}1^+$ phenotype, further characterized by expression of the transcription factor TCF1 that controls cell proliferative capacity[74]. However, HBV polymerase-specific cells examined in this study had a subset of cells with the $PD\text{-}1^+CD127^-$ terminally exhausted phenotype, accompanied by higher KLRG1 expression, further supporting that these cells are more terminally exhausted and highlighting the heterogenous nature of HBV-specific T cell exhaustion phenotypes based on their targeted antigens[78]. In support of these findings, a recent high-parameter analysis of HBV-specific $CD8^+$ T cell phenotypes and functions in CHB patients was performed using multiplexed direct *ex vivo* tetramer staining[79]. Results showed that HBV-specific T cell phenotypes are extremely heterogenous, and that accumulation of inhibitory receptors did not directly correlate with dysfunction. Rather than identifying terminally exhausted phenotypes, the authors described their observations as a "functional adaption." This concept has also been proposed for T cells in cancer, whereby T cells adjust their functional capacity to the lesser needs of an established chronic infection or cancerous state[80].

Additional exhaustion markers besides PD-1 have been shown to be upregulated on $CD8^+$ HBV-specific T cells in CHB including CTLA-4, LAG3, TIM-3, 2B4 and CD160. Targeting these molecules via inhibition *in vitro* can partially restore HBV-specific $CD8^+$ T

cell function[81–84]. To date, a handful of clinical trials have also been undertaken to assess the efficacy of immune checkpoint blockade for the treatment of CHB. One study was aimed to assess efficacy of PD-1 checkpoint blockade on hepatocellular carcinoma[85]. While treatment was well tolerated and a log decline in HBsAg was observed in 6% of CHB patients, T cell responses were not interrogated. Another phase 1b study examined PD-1 blockade in a group of HBeAg-, virally suppressed CHB patients[86]. One of 14 patients experienced a functional cure, with most others demonstrating modest decrease in HBsAg over time (up to 0.5 IU/mL after 24 weeks post treatment). HBcAg- and HBsAg-specific T cell frequencies in this study did not increase after anti-PD-1 treatment, and maximal T cell responses as shown by fluorospot occurred in the patient with functional cure.

In summary, HBV-specific T cells are crucial to the control of HBV infections. However, the dynamics of their functionality is extremely complex. Restoration of HBV-specific T cell capacity in CHB for the goal of establishing a functional cure will likely necessitate previously attempted strategies of checkpoint inhibitor blockade against upregulated exhaustion markers, but clearly, additional modulation is needed. If in fact these HBV-specific cells have entered a “functionally adapted” state, perhaps more than just immunomodulation will be needed. Although not directly assessed in any studies, if HBV-specific T cells have undergone epigenetic modifications to establish a “functionally adapted” state, perhaps drugs targeting epigenetic alterations would be beneficial. In addition, HBsAg-specific T cell frequencies are extremely low in CHB, and strategies to

generate new HBsAg-specific T cells will also need to be considered, in parallel to methods to eliminate circulating HBsAg.

1.3.4 B cell Responses in HBV Infection

To date, study of the humoral response during HBV infection has been largely neglected despite the understanding that B cells must play an important role in the control of acute HBV. In the course of a natural HBV infection, HBV-specific B cells are activated upon antigen exposure to produce antibodies that target multiple HBV proteins. Antibodies produced against HBcAg, HBeAg, HBx, HBV pol and all three HBsAg (L-, M-, S-) proteins have been observed[47,87]. While only a small subset of these antibodies, mainly those targeting the pre-S1 domain of large HBsAg and the a-determinant region of small HBsAg, have been shown to be neutralizing (reviewed in 87), the timing of seroconversion against different antigens helps to determine each clinical phase of HBV infection (see ***1.3.1 HBV serology and clinical phases of infection***). Importantly, induction of anti-HBs is considered the clinical indication of recovery from an acute HBV infection and demonstrates the role antibodies against HBsAg play in controlling infection. In addition, anti-HBs serves a protective function against acquisition of HBV, highlighted by HBIG administration to limit maternofetal transmission or reinfection after liver transplantation, and through successful prophylactic induction of anti-HBs as the protective mechanism of the HBV vaccine[40,50,88,89].

Although B cell mediated antibody production is clearly important for control and prevention of HBV, additional B cell functions also play a crucial role. This fact is

highlighted in studies of hematologic malignancies using $CD20^+$ depleting rituximab that showed a 5-20% risk of HBV reactivation in previously recovered patients[90–92]. Plasmablasts and plasma cells, the most robust producers of antibodies, downregulate CD20 and are not depleted upon rituximab treatment indicating additional B cell functions such as antigen presentation and cytokine production are important for long-term HBV control[93].

Initial examinations of B cells in HBV focused on global phenotypes and functions. In CHB, B cells demonstrate increased activation profiles with reduced proliferative capacity[94,95]. Activation signatures determined by $CD69^+$ and/or $CD71^+$ B cells occurred in both naïve and memory B cell subsets. When categorized by CHB disease phase, the majority of polyclonal B cell activation was observed in the immune active (IA) phase[95]. Multiple groups have also described increased frequencies of circulating IL-10 producing regulatory B (B reg) cells in CHB[96,97]. Presence of these cells was shown to downregulate $CD4^+$ T helper functions *in vitro* and suggests B regs serve a pathogenic role in suppressing HBV-specific immunity in CHB. Overall, these data describe a hyperactive yet dysfunctional global B cell state with concomitant increase of B reg activity, indicating a high degree of dysregulation in the global B cell compartment during CHB.

The phenotype and function of HBV-specific B cells has only recently begun to be examined. Two seminal studies reported the *ex vivo* detection of HBsAg-specific B cells in CHB, ending a decades-long debate about whether these cells were in fact present in CHB[98,99]. The lack of detection of anti-HBs in CHB patients was thought to be a result

either of very little anti-HBs production (through the deletion of HBsAg-specific B cells), or that cells were present and producing anti-HBs, but quantities made were insufficient to overcome excess circulating HBsAg. In the latter case, all anti-HBs would be bound up by HBsAg to form rapidly cleared immune complexes[100–102]. Although immune complexes of HBsAg bound to anti-HBs have been observed in CHB[103] (indicating some degree of anti-HBs production), the newest data suggest HBsAg-specific B cells are present but have decreased functionality.

HBsAg-specific B cells were detectable in both acute HBV infection and CHB, however, they were present at very low frequencies in both the periphery and the liver (0.01%-0.4% of $CD19^+$ B cells)[98,99]. It was also shown that HBsAg-specific cells, when sorted and stimulated *in vitro* could not differentiate into antibody producing plasma cells like healthy vaccinated controls. This functional impairment occurred in HBsAg-specific B cells from both CHB and acute HBV patients who were HBsAg+, but in the same patients at the time of seroconversion (HBsAg-, anti-HBs+), functionality was restored[98]. These observations suggest that HBsAg-specific B cell function is negatively affected by circulating HBsAg regardless of HBV infection outcome.

In further support of dysregulated HBsAg-specific B cells is the finding that these cells were enriched for atypical memory B cells (AtMs). AtM B cells, identified by their downregulation of surface markers CD21 and CD27, have been observed at increased frequencies in a number of chronic infections such as *Plasmodium falciparum* (malaria), Mycobacterium tuberculosis (M. tb), human immunodeficiency virus (HIV), hepatitis C virus (HCV), and HBV[104]. These cells typically represent 3-5% of peripheral B cells in

healthy individuals but can expand up to roughly 50% of circulating B cells during chronic infection. AtM B cells express genes not characteristic for memory B cells such as the integrin CD11c and transcription factor Tbet, as well as many known or suspected inhibitory receptors including CD32b, CD72, CD22, PD-1, BLTA, CD85 and Fc like receptors FcRL4 and FcRL5. Overall, these cells appear refractory to expansion and antibody/cytokine production in response to BCR stimulation and are suspected to represent a dysfunctional memory B cell phenotype during chronic infection[104].

In contrast to the findings above, HBcAg-specific cells are present in CHB subjects at increased frequencies and are more functional[105,106]. These cells were shown to be present at higher frequencies than HBsAg-specific B cells in CHB subjects and they could differentiate into antibody secreting plasma cells upon *in vitro* stimulation[105]. In addition, they were not enriched for an AtM B cell phenotype. Interestingly, while HBsAg-specific B cells expressed mainly IgM^+ BCRs, HBcAg-specific cells were largely IgG^+, suggesting HBsAg-specific B cells may not readily enter the germinal center to undergo class-switching and affinity maturation for production of high affinity HBV-specific B cell clones. At the transcript level, HBcAg-specific B cells revealed a differentially expressed gene program compared with HBsAg-specific B cells. HBc-specific cells had increased expression of genes associated with class-switch recombination (*CD99*, *IL6R* and *CXCR3*), while HBsAg-specific B cells had increased expression of *CD31*, a molecule shown to play a role in maintaining B cell tolerance, as well as *NFATC1*, important for B cell homeostasis/apoptosis and finally, higher levels of

TNFRSF13B (TACI) which indicate their similarity to marginal zone-like B cells[105]. To date, HBV-specific B cell responses have only been assessed against HBsAg and HBcAg.

Taken together, these data are consistent with serological observations in HBV infection. Namely that anti-HBc is observed early and throughout infection and HBcAg-specific B cells are detectable at higher frequencies and appear functional. In contrast, anti-HBs does not appear in CHB subjects and HBsAg-specific B cells, while detectable, were present at low frequencies, could not differentiate, did not appear to have entered the germinal center as consistently (mainly express IgM) and had increased frequencies of AtM B cells.

The data also highlight the importance of antigen-specific consideration when designing a functional cure. In order to generate a successful cure strategy, restoring functionality of HBsAg-specific B cells is crucial, while targeting HBcAg-specific cells may not be necessary. To this end, Salimzadeh et al. found that *in vitro* treatment with anti-PD-1 antibodies was able to partially restore HBsAg-specific B cell functionality in CHB subjects[98]. Although anti-PD-1 therapy could serve a role in reversing the apparent dysfunctional B cell compartment in CHB, it is likely not a silver bullet approach. An effective functional cure will most likely involve a multi-pronged strategy including an antigen-specific approach to eliminate circulating HBsAg, a driving factor in mediating HBsAg-specific immune tolerance[107].

1.3.5 Consequences of HBV and HIV Coinfection

Coinfection with HBV and HIV is common, mainly due to similar routes of transmission and geographic overlap of high burden regions[108]. 40 million people are infected with HIV worldwide, and of that number, an estimated 10% are coinfected with HBV[109]. In regions with low endemicity, HBV and HIV are acquired in adulthood usually through sexual or percutaneous transmission, and the prevalence of HBV and HIV coinfections is 5%-7% of HIV infected individuals. However, that prevalence is much higher among men who have sex with men (MSM), between 9%-17%. In areas with high HBV endemicity, HBV transmission occurs perinatally, leading to established HBV infection in early childhood that precedes HIV infection sometimes by decades. Prevalence of HIV/HBV coinfection in these regions is much higher, on average between 10%-20%[108,109].

Coinfection with HIV negatively affects the natural history of HBV infection. HIV infected individuals are 6 times more likely to develop CHB compared to HIV uninfected persons[110,111]. In addition, HIV infection decreases the rate of HBeAg clearance and increases HBV replication as seen by circulating DNA levels[112,113]. Even after acquiring protective anti-HBs, indicative of a controlled HBV infection, HIV-infected individuals are at risk of losing anti-HBs and reactivating their HBV infection with reappearance of HBsAg and HBV DNA (known as reverse seroconversion)[114,115]. Finally, HIV infection accelerates the progression of HBV-related liver disease. Cirrhosis is more common and liver-related mortality is 17 times more likely in coinfection[116]. Interestingly, coinfection with CHB in HIV infected persons increases the risk of hepatotoxicity from antiretroviral therapy (ART) drugs 3-5 fold[117]. Decisions on treatment strategies for HIV/HBV

coinfected patients is also complicated by the fact that multiple nucleoside analogs are active against both HIV and HBV and careful consideration to avoid emergence of drug-resistant variants must be made.

In summary, coinfection of HIV and HBV can lead to accelerated progression of CHB and liver disease, reactivation in HBV controlled individuals, and overall increased mortality. However, the mechanisms underlying these observations are still poorly understood. Studies that assess the immunologic effects of coinfection may identify novel targets or pathways to reduce mortality and improve outcomes in coinfected patients.

1.4 SARS-CoV-2 Background and Immunology

SARS-CoV-2 is a coronavirus responsible for the coronavirus disease 2019 (COVID-19) pandemic, to date with over 164 million cases worldwide[118]. COVID-19 is characterized by a range of disease severity, from asymptomatic/mild infection to severe disease requiring hospitalization[119]. Those patients who develop severe disease often require supplemental oxygen and/or ventilation and present with pneumonia or acute respiratory distress syndrome (ARDS), resulting in over 3.4 million deaths worldwide[118]. At this time, it is unclear why some patients readily resolve infection while others develop severe symptoms. Specifically, it remains to be determined if severe disease is associated with a failure to generate protective immunity against the virus allowing for prolonged viral replication, overly robust dysfunctional immune responses, or a combination of both.

SARS-CoV-2 is the third highly pathogenic coronavirus (CoV) to demonstrate a zoonotic transmission to humans within the past 20 years[120]. Preceded by the SARS outbreak in 2003 and MERS outbreak in 2012, SARS-CoV-2 shares many features with other CoVs including the unique structural Spike protein, giving the virus the appearance of wearing a crown and to which its name can be attributed. SARS-CoV-2 is an enveloped positive-sense single-stranded RNA virus made up of four structural proteins and multiple accessory proteins[121]. The main structural protein responsible for viral entry is Spike, which becomes activated by its interaction with the transmembrane serine protease TMPRSS2 and binds its primary receptor angiotensin-converting enzyme 2 (ACE2) in order to infect bronchial epithelial cells, pneumocytes and upper respiratory tract cells[122,123].

To date, severe COVID-19 has been associated with multiple changes in peripheral immune profiles, including lymphopenia and increased pro-inflammatory cytokines[124]. Recent studies have broadly assessed immune profiles in COVID-19, revealing alterations in both the lymphocyte and myeloid compartments. Preferential loss of $CD8^+$ T cells, increased plasmablasts, neutrophil expansion, decreased plasmacytoid dendritic cells (pDCs), and differential T cell activation have been observed[125–128]. Although notable, the overall phenotypic characteristics of peripheral cell types shows extreme heterogeneity within severe COVID-19 infections. In addition, these observations are indicative of generalized inflammation and thus fail to distinguish specific host deficiencies in SARS-CoV-2 infection versus other viral infections or inflammatory states. Further studies that assess specific SARS-CoV-2 correlates of disease severity are

necessary in order to identify both biomarkers associated with severe disease and novel treatment strategies to mitigate severe pathologies.

1.5 Flow Cytometry High-Dimensional Panel Design

Recent technological advances in the field of flow cytometry have allowed for the ability to assess increasingly more immunologic information at the single-cell level. In addition to conventional flow cytometry techniques, cytometry by time of flight (CyTOF) and spectral flow cytometry are becoming more commonplace[129,130]. Although this work focuses on conventional flow applications, panel design concepts can be applied to these newer techniques as well. High-dimensional panel design is an ideal strategy for immunophenotyping and immune monitoring studies applied to research areas including infectious disease. Through optimization of comprehensive panels, extensive information can be garnered on a single-cell level from studies with often limited subjects or cell numbers.

The first step in designing a high-dimensional panel is to determine the antigenic markers of interest[131]. Markers can then be categorized by level of importance in the panel. Discrete lineage markers such as CD3, CD4 and CD8 for T cells are given highest priority. These markers are “on/off” and as such will have reliable detection by many antibody clone/fluorophore combinations. Secondary priority is given to markers with well characterized expression patterns that are on a continuum, for example, CD27, CD28, and CD45RA on T cells. Lowest priority is then assigned to markers expressed at low levels or that are uncharacterized, such as activation (CD154, CD69) or exhaustion

markers (PD-1, CTLA-4, TIM-3). Often these markers are phenotypic in nature and may be difficult to optimize in the context of larger panels. While their expression patterns are likely of great interest, they inevitably must be considered last as greater importance lies in establishing cell lineages before their possible phenotypes.

Once the list of markers is identified and prioritized, the second step in designing a high-dimensional panel is to match markers with available fluorophores. Assigning marker/fluorophore combinations is not an exact science but two important factors must be considered: a) Fluorophore brightness. The brightest fluorophores should be paired with low expression markers, either because a low number of molecules are on a single cell, or the marker is only expressed by a small subset of cells. In contrast, dim fluorophores should be assigned to high expression markers. Determining fluorophore brightness can be achieved by using a stain index, which compares the relative brightness of each fluorophore on a given flow cytometer[132]. b) Spillover between detector channels. Detector channels that measure similar wavelengths experience this phenomenon most often (for example B610 and G610 that measure 610nm to 620nm wavelengths)[131]. Signal spillover from one detector channel into another leads to spreading error (called spillover spreading error, or SSE) in the receiving channel and increases exponentially with intensity of the original signal[133]. SSE decreases sensitivity for detection of positive signal in the receiving channel and therefore must be avoided as best as possible. To account for SSE, a spillover spreading matrix (SSM) should be consulted. This matrix is unique to a given cytometer, and reveals detector channel interactions that experience SSE[133]. For channels that cause more spillover, low

expression markers should be assigned to those fluorophores. For a channel that receives spillover from another, highly expressed discrete markers or markers expressed on different cell types should be assigned when possible.

Finally, the third panel design step is to titrate antibodies and test panel iterations to determine the optimized final panel. Antibodies must be titrated and used at an optimal titer to achieve ideal separation between positive and negative populations without using excess reagent[132]. Panel iterations are then performed starting with a subset of lineage markers, mainly those deemed "high priority" to determine whether there are any issues with spillover or compensation[131]. If not, this original iteration becomes the backbone that further iterations are built off of. Proper single stain controls are also crucial at this step to generate accurate compensation. Single stains should be as bright or brighter than the signal detected on cells when applying the full panel[134]. Antibodies can then be added incrementally to assess whether their addition leads to disruptions with panel sensitivity for all markers. The result of the iterative process is a final panel that includes all desired markers and demonstrates sensitivity for each marker.

Chapter 2: Determining Adaptive Immune Correlates of Acute HBV Control

Due to the fact that the rate of progression to CHB differs largely based on age (5-10% of adults and 90-95% of children), effective adaptive immune responses are likely extremely important determinants of outcome. However, the precise productive immunologic functions that fail during an acute HBV infection and lead to the progression of CHB are still unclear. Our goal is to determine adaptive correlates of acute HBV control that can be used to inform a more effective functional cure.

2.1 Current Limitations to HBV Studies and Description of the MACS Cohort

Although many studies of the immune response to HBV have been performed to date, these analyses often suffer from limitations in comprehensive understanding. These limitations mainly stem from the fact that acute HBV infection cohorts are uncommon. This is because the majority of acutely infected individuals are unaware of their infection status since most acute HBV infections are asymptomatic. Only a small subset of acute subjects experience symptoms including jaundice and fatigue[50]. As a result, acutely infected HBV cohorts often compare symptomatic acute infection to a separate group of CHB subjects who have been infected for many years. These comparisons are problematic for making conclusions regarding productive immune responses in acute HBV because what happens in symptomatic acute infection may not reflect the immune response during asymptomatic cases. Also, immune responses in CHB subjects after years of chronic infection may not represent the immunologic failures that occurred

during the acute phase which led to establishment of a chronic infection. Overall, there is a lack of longitudinal sampling in HBV infected individuals, leading to the inability to uncover accurate correlative measures associated with HBV control.

In addition, only recently have immunological studies begun to interrogate at the high-dimensional level antigen-specific responses in HBV subjects. Somewhat surprisingly, no known study to date has incorporated both B cell and T cell analysis into the same HBV samples, leading to a lack of understanding of the interplay between the cellular and humoral adaptive immune responses during HBV infection. To address these issues, we first sought access to samples from the Multicenter AIDS Cohort Study (MACS), which has longitudinal sampling and well-defined incident hepatitis B infection.

MACS was established in 1984 as a prospective multicenter study following MSM at risk of HIV infection[135]. In a more recent retrospective study, Falade-Nwulia et al. identified a subset of individuals participating in the greater MACS cohort who experienced an incident HBV infection[136]. These individuals were followed every 6 months throughout their participation in MACS and therefore have longitudinal sampling prior to, during an acute HBV infection, and after outcome of infection is determined (>6 months after proposed exposure date). Our study will include the subset of these men who have PBMCs available at these three time points. Thus, there are 76 men with incident HBV of whom 22 developed CHB and 54 matched men (2-3 per CHB subject) who controlled their infection (Table 2.1). Subjects are matched on sex (all male), age, HIV status, CD4 counts (if HIV infected), and time samples have been stored

in the repository. Of the 22 subjects who developed a chronic infection, 13 are HIV-infected and 9 are HIV-uninfected.

Use of samples from the MACS cohort will allow us to address many of the issues listed above, specifically, the prospective nature of the cohort and subsequent detection of incident HBV infection allows for analysis of subjects with a more typical asymptomatic acute HBV infection course. In addition, subjects were followed longitudinally and therefore samples from an acute infection and after outcome can be compared within the same subject, allowing for potential immune correlates of protection to be identified. Finally, the longitudinal aspect allows examination in those with CHB close to acute infection and after the chronic state has been established. With access to such a unique cohort of HBV infected subjects, we next aimed to establish comprehensive tools to study the adaptive immune response to HBV infection.

2.2 Development of High-Dimensional Flow Cytometry Panels for Immunologic Assessment in HBV

In order to obtain as much immunologic information as possible from our study, we designed two comprehensive high-dimensional flow cytometry panels targeting B cell[137] and T cell phenotypic analysis (Table 2.2 & 2.3). In addition, both strategies incorporate a method to assess antigen-specificity through *ex vivo* tagging of HBsAg-specific B cells, or *in vitro* HBV peptide pool stimulation of T cells. Described below is the rationale for development of the panels and optimization of each panel with multiple non-MACS acute and CHB subjects.

2.2.1 High-Dimensional Characterization of B cells in Chronic Infection

B cells are an important cell type in the prevention and/or control of infections through production of antibodies, professional antigen presentation, and secretion of cytokines[138]. During acute HBV infection, B cells are responsible for the production of antibodies against HBV envelope protein, HBsAg. Induction of anti-HBsAg (anti-HBs) is considered the clinical indication of recovery from an acute HBV infection, and prophylactic induction of anti-HBs is the protective mechanism of the HBV vaccine[40,50]. B cells also help to maintain control of HBV infection after resolution as shown by HBV reactivation in studies using $CD20^+$ depleting rituximab for treatment of hematologic malignancies[90–92]. Although B cells are known to be an important cell type during HBV infection, it still remains unclear how these functions fail in an acute infection and lead to 5-10% of adults and 90-95% of children developing a chronic infection[38]. For this reason, we developed the panel described here to provide a comprehensive tool to study global and antigen-specific B cells during HBV infection.

B cells can be defined by their expression of CD19 and CD20 (Figure 2.1A). We included a dump channel which enables the exclusion of $CD3^+$ T cells, $CD14^+$ monocytes and dead cells in order to increase our resolution between $CD19^+CD20^{+/-}$ B cells and $CD19^-CD20^-$ cell types (Figure 2.1A). In our panel we observed a population of dye aggregates in some phenotypic markers (CD39 and CD43), and thus excluded these aggregates before further analysis of B cells[131,139] (Figure 2.1A).

B cells originate in the bone marrow where they generate a functional B cell receptor (BCR)[140]. After leaving the bone marrow, immature transitional B cells further

mature into antigen-inexperienced naïve B cells in the periphery[141]. Upon antigen exposure, naïve B cells are activated and further differentiate either through germinal center (GC) dependent or independent pathways[142,143]. The fate of a naïve B cell to enter a GC is dependent on its primary BCR affinity for antigen, with the highest affinity cells immediately differentiating into antibody-secreting plasmablasts in a GC independent manner, while lower affinity cells enter the GC and undergo affinity maturation[144]. The GC independent process results in the differentiation of short-lived plasmablasts or memory B cells that produce a rapid response with overall low or medium affinity antibodies against the respective pathogen[145]. Cells that enter the GC undergo class-switching and multiple rounds of somatic hypermutation (SHM) that leads to the selection of high-affinity B cell clones. High-affinity GC B cells egress from the GC as either short-lived plasmablasts, long-lived plasma cells or long-lived memory B cells[146]. Although the mechanisms underlying post-GC B cell fate decisions need further investigation, it is thought that both temporal factors and BCR affinity may play a role[142].

The panel described here includes markers to distinguish many of the B cell developmental stages, with a focus on identifying antigen-specific memory B cells. Transitional B cells can be reliably determined as $CD10^{+}$ and are gated out to focus analysis on mature B cells[147] (Figure 2.1A). $CD10^{-}$ mature B cells can be further divided into plasmablasts ($CD24^{-}CD38^{hi}$) and non-plasmablasts based on the expression pattern of CD24 and CD38 (Figure 2.1B). Plasmablast populations are transient in the periphery and are often upregulated as a result of infection or vaccination[19]. Non-plasmablasts comprise unswitched and class-switched B cells based on the expression or lack of IgD

and IgM. Class-switched cells that are IgM^-IgD^- are indicative of memory B cells derived from a GC, likely including multiple rounds of somatic hypermutation (SHM), and therefore have increased potential to induce productive antibody-mediated effector functions[146]. In contrast, unswitched B cells contain several subsets which can be differentiated by the expression of IgD, IgM and CD27[148]. Naïve B cells express both IgM and IgD but lack CD27 (Figure 2.1B), which is often used as a memory B cell marker. However, in certain circumstances CD27 alone is not a singularly reliable marker for memory B cells[149]. Furthermore, the IgD^+CD27^+ population contains either marginal zone (MZ) B cells (IgM+) or IgM^-IgD^+ memory B cells (Figure 2.1B). The development and function of IgD-only memory B cells remains elusive and awaits further clarification[150,151]. Peripheral MZ B cells are a unique population resembling splenic MZ B cells although their origin has not been definitively clarified[152]. MZ B cells possess "innate-like" polyreactive low-affinity BCRs and are important for glycan-specific antibody responses[153]. Patients undergoing splenectomy exhibit reduced levels of peripheral MZ B cells and show increased susceptibility to bacterial infections[154]. Finally, unswitched B cells contain a subset of IgD^- cells which show high expression of IgM and are defined as IgM-only memory B cells [148,152] (Figure 2.1B).

Although most markers in this panel are aimed at distinguishing conventional B cell subsets (B2), we also included markers associated with non-classical B1 B cells (CD43 and CD5) (Figure 2.1C)[155–158]. This B cell subset is considered "innate-like" and produces T cell-independent, polyreactive, low-affinity IgM antibodies[155]. It has also been shown that human B1 cells play an unexpected role in immunosuppression as a source of anti-

inflammatory cytokine IL-10[155]. Although the exact definition of B1 B cells in humans remains elusive, multiple studies have aimed to address the best gating scheme to define this population, and our panel will contribute to resolve these issues[156–158]. B1 B cells are gated here as $CD27^{+}CD43^{+}$ on non-plasmablasts due to the overlapping expression of CD27 and CD43 on plasmablasts, which has been shown to contaminate the putative B1 B cell subset (Figure 2.1C)[157,158]. This population is further distinguished by expression of IgM and IgD, with a subset of cells IgM^{+} and/or IgD^{+}. B1 B cells can also produce low-affinity IgA, and $IgM^{-}IgD^{-}$ cells are likely IgA^{+} [155]. CD5 was originally used as the primary marker to classify human B1 cells similar to mice, but it has become increasingly clear that in humans, CD5 is also expressed on a number of additional B cell subsets including pre-naïve, transitional, and even activated conventional B cells[159]. Therefore, identification of B1 cells here is not based on CD5 expression. However, inclusion of this marker allows for the capability to monitor CD5 expression on B1 cells, which has been suggested to contribute to downregulation in BCR signaling in this population, and appears higher on B1 B cells compared to other B cell and non-B cell subsets in chronic HBV subjects (Figure 2.1C)[160]. Examining the dynamics of these cells during chronic infection will provide unprecedented insight into their possible roles in the development of chronic disease.

Functional subsets of conventional class-switched and unswitched memory B cells can be further refined using CD21 and CD27. In the field of chronic infections, CD21 and CD27 alone are often used to distinguish naïve and memory B cell subsets. However, this analysis leads to complications with the $CD21^{+}CD27^{-}$ population, which is

typically described as naïve B cells and excluded from memory analysis, but also contains a subpopulation of memory B cells known as intermediate memory (IM)[161]. In addition, naïve B cells have been shown to downregulate CD21 in autoimmune diseases and chronic infections, which may lead to contamination of the atypical memory phenotype ($CD21^-CD27^-$)[162–164]. Here, we further characterize the maturation state of switched memory B cells to examine intermediate memory (IM, $CD21^+CD27^-$), resting memory (RM, $CD21^+CD27^+$), activated memory (AM, $CD21^-CD27^+$), and atypical memory (AtM, $CD21^-CD27^-$) subsets (Figure 2.2A). This classification of memory B cell subsets is commonly used to characterize memory B cells in chronic infections including malaria, TB, HIV, HCV and HBV[98,99,104,105]. Chronic subjects have been shown to exhibit elevated levels of global as well as antigen-specific AtM B cells compared to healthy controls, and these AtM B cells appear to be less functional than other memory subsets[104]. Figure 2.2A shows our observation of a similar trend with the increased frequency of AtM B cells identified from the class-switched IgM^-IgD^- population in chronic HBV subjects compared to a healthy control.

A leading hypothesis as to the cause of chronic infections is that prolonged exposure to antigen leads to functional impairment of adaptive immune cells and ultimate persistence of infection[165]. T cell exhaustion has been studied in depth in chronic infections, and only recently has the idea of B cell exhaustion also been suggested. To address this possibility, our panel includes multiple markers to assess the functional capacity of global and HBV-specific B cells during HBV infection. For example, AtM B cells are characterized by increased expression of a number of exhaustion

markers, including, but not limited to, PD-1, FcRL5, CD11c, CD22 and CD32, all of which have been included in this panel[104]. As shown in Figure 2.2B, these exhaustion markers are upregulated on AtM B cells compared with other memory subsets in chronic HBV subjects. Through incorporation of many exhaustion markers, this panel allows for comprehensive analysis of the dynamics of global and antigen-specific AtM B cell phenotypes throughout the course of chronic infections.

Chemokine receptors are important surface proteins that guide trafficking of immune cells in response to chemokine expression gradients[166]. In order to assess the capability of B cells to traffic to different sites during infection, we included analysis of CXCR5 and CXCR3 in this panel (Figure 2.3A). $CXCR5^+$ cells traffic to the lymph node in response to expression of CXCL13 produced by follicular dendritic cells in the GC, and once there, encounter cognate antigen and mount a productive immune response against a pathogen. $CXCR3^+$ cells, in contrast, traffic to sites of inflammation in response to CXCL9-11 secreted by monocytes and fibroblasts at inflamed tissue sites[167,168]. It is unclear whether trafficking of HBV-specific B cells to sites of inflammation such as the liver is necessary for a productive response against HBV, but upregulation in CXCL9-11 has been shown in the liver and is associated with $CXCR3^+$ hepatic infiltrates in HCV infection[169,170].

The costimulatory activation marker CD86 was included in the panel in order to determine the activation status of B cells during infection (Figure 2.3A). CD86 is constitutively expressed on B cells but is upregulated upon B cell activation and will help

determine the functional status of global as well as HBV-specific B cells within this panel[171].

Regulatory molecules BTLA and CD39 were included in the panel to examine the inhibitory status of HBV-specific and global B cell subsets during HBV infection (Figure 2.3A). BTLA is expressed on B cells and upon binding its ligand recruits negative regulator SHP-1 that decreases downstream BCR signaling[172]. CD39 is an ectoenzyme that works in concert with CD73 to produce inhibitory ADO and IL-10, and CD39 expression on B cells is associated with a B regulatory (Breg) phenotype[173]. All markers are shown in Figure 2.3A to have differential expression patterns between $CD19^+$ B cells and $CD19^-$ non-B cells. One marker, CD22, did not demonstrate clear differential staining upon full panel analysis necessitating staining with an FMO control which showed a shift in the CD22+ population with full panel staining compared to FMO (Figure 2.3B).

In summary, we describe here a comprehensive 24-color flow cytometry panel to study global and antigen-specific B cells, their subsets, and phenotypes in humans with chronic infections. Our B cell panel enables B cell analysis at unprecedented depth and holds promise to uncover new patterns and dynamics of B cell subsets and phenotypes that are either beneficial or detrimental in the progression of chronic infections. The added ability to incorporate dual-labeling antigen-specific probes (described below) increases the power to make relevant pathogen-specific conclusions regarding B cell functions in chronic infections.

2.2.2 Optimization of ex vivo HBV-Specific B cell Tagging

An important goal for development of our B cell panel was to incorporate antigen-specificity into our analysis of memory B cells in HBV infection. To identify HBV-specific B cells, a dual labeling strategy that has been previously published was employed[98,105]. Briefly, we obtained recombinant small HBsAg genotype C, manually conjugated to one of two fluorochromes, Dylight 550 or Dylight 650, from Gilead[174]. Dual staining was desired as it has been shown to increase the sensitivity of detecting low frequency antigen-specific B cell populations[175,176]. BCRs specific to small HBsAg will bind the probe-fluorophore reagent in order to tag HBsAg-specific B cells.

Optimization of HBsAg-specific probes was performed using cryopreserved PBMCs from HBV unexposed healthy donor leukopacks (LPs) and a healthy subject followed throughout the course of their HBV vaccination series with Energix-B (AC51, Figure 2.4A)[177]. AC51 was selected as a positive control subject based on a strong response to vaccination as signified by production of antibodies against HBsAg (Figure 2.4B). HBsAg Dylight 550 and HBsAg Dylight 650 were first titrated using half-log dilutions (equal concentrations of each Dylight reagent) on HBV unexposed healthy donor leukopack (LP) PBMCs (Figure 2.4C). Circulating HBV-specific B cells should not be detected in these samples, and they were therefore used as a negative control to find a range of concentrations that would limit non-specific background staining. The range between 0.2ug-0.063ug per 50uL staining reaction was found to have low background and these concentrations were tested on AC51. To determine which probe concentration was optimal, percent HBV-specific B cells for healthy LPs, AC51 (D189)

and three CHB subjects were examined (Figure 2.4D). There was little difference between the detection of HBV-specific B cells in the healthy LPs between probe concentrations, but a decrease in percent HBV-specific cells was observed in AC51 with the lower probe concentration. Therefore, 0.2ug per 50uL staining reaction was determined as the ideal concentration for HBsAg Dylight 550/650 reagents in the panel. Several timepoints were then sampled from AC51 in order to ensure that an expected spectrum of frequencies for HBsAg-specific B cells was observed to provide confidence that accurate detection of very low frequencies of HBsAg-specific B cells was possible (Figure 2.4E).

To confirm that HBsAg-specific B cells being detected were truly HBV-specific, HBsAg Dylight550/Dylight650 double positive cells were sorted and differentiated for 14 days in the presence of CD40L expressing cells, IL-2, and IL-21, as previously described[178]. Supernatants were collected and anti-HBs ELISA was performed on Dylight double positive B cells, Dylight double negative B cells, and CD40L expressing cells only. Only cells sorted from the double positive population produced anti-HBs antibodies, confirming their specificity to HBV and ability to be detected with the HBsAg probes (Figure 2.4F).

In the context of the full panel, dual positive staining can be detected in both chronic HBV subjects as well as vaccinated individuals, but frequencies of circulating HBsAg-specific B cells are low (0.01%-0.04% circulating $CD19^+$ B cells), as previously described (Figure 2.5A)[98,105]. Interestingly, a significant fraction of HBV-specific B cells from chronic subjects were unswitched (IgD^+ and/or IgM^+), and further identified as

naïve B cells (IgD^+CD27^-). Those that were IgD^+CD27^+ were mainly marginal zone B cells (Figure 2.5B). A detailed assessment of HBV-specific B cell phenotypes for CHB vs healthy vaccinated is shown in Figure 2.5C-D. It is important to note from this analysis that our panel enables rigorous gating strategies in order to ensure precise examination of populations of interest, which in our case are memory B cells.

2.2.3 Comprehensive Assessment of T cells in Chronic Infection

T cells play an important role in the control and elimination of pathogens[179,180]. However, when their protective functions are dysregulated it can lead to the development of disease such as chronic infection, cancer, and autoimmunity[181,182]. The ability to profile T cell phenotypes and functions in a high-dimensional fashion allows for comprehensive understanding of T cell dynamics in health and disease.

Although it is well established that T cells play a vital role in control of HBV infection, it remains unclear what T cell functions fail in the progression to CHB[183]. We developed the following panel in order to identify global and antigen-specific T cell functions important for control of HBV infection. Here, we report a comprehensive 30-parameter flow cytometry panel with the capability to assess detailed differentiation, effector functions including activation and cytokine production, and inhibitory status of $CD4^+$, $CD8^+$ and T regulatory cells (Tregs).

All T cells subsets can be reliably identified by their expression of CD3 and further described by expression of either CD8 or CD4 (Figure 2.6A). $CD8^+$ T cells are the main effector T cells, characterized by their ability to lyse infected cells through release

of perforin and granzyme upon recognition of cognate antigen. $CD4^+$ T cells in contrast perform helper functions, mainly cytokine production and co-stimulation to aid differentiation and drive both $CD8^+$ T cell and B cell function[184]. One subset of $CD4^+$ T cells are Tregs, which can be identified as $CD4^+CD25^+CD127^-$ (Figure 2.6B)[17]. Tregs act as negative immune regulators and function to suppress effector immune cell function by a variety of mechanisms. Through upregulation of the high-affinity IL-2 receptor complex (CD25, CD122 and the common gamma chain), Tregs outcompete effector T cells for IL-2, an important growth factor for T cell maintenance. Tregs also produce immunosuppressive cytokines IL-10 and TGFβ, as well as upregulate a number of co-inhibitory receptors including CTLA-4[185]. Finally, Tregs express ectoenzymes CD39 and CD73, which together produce inhibitory ADO[186,187]. We included CD39 in our panel to help distinguish Tregs (Figure 2.6B) as well as to determine whether other T cell subsets aberrantly upregulate the inhibitory molecule in the context of chronic infection.

T cells undergo maturation in the thymus and enter the periphery as mature naïve T cells[188]. Upon antigen exposure they differentiate into effector or memory cells[189]. Memory subsets each have distinct functions and are identified in the periphery with a combination of surface markers CCR7 and CD45RA as follows: Naïve ($CCR7^+CD45RA^+$), T effector memory (Tem, $CCR7^-CD45RA^-$), T central memory (Tcm, $CCR7^+CD45RA^-$) and T effector memory CD45RA expressing (Temra, $CCR7^-CD45RA^+$)[190]. Expression of costimulatory CD27 and CD28 can further distinguish memory subset differentiation status (Figure 2.6C)[190].

The panel described here includes multiple markers to detect T cell activation upon recognition of cognate antigen. CD69 is an early activation marker important for identifying low frequency cytokine producing cells after antigen-specific stimulation *in vitro*[191,192]. In addition, we included the co-stimulatory molecule OX40 in the panel due to its role in promoting T cell survival and proliferation after antigen-specific stimulation (Figure 2.7A)[193]. Interestingly, OX40 was observed to be upregulated on HBV-specific T cells and stimulation with an OX40 agonist was shown to augment HBV-specific T cell responses[194]. We also included the co-stimulatory molecule CD154 (CD40L) (Figure 2.7B). CD154 is expressed on all activated $CD4^+$ antigen-specific T cells and is a crucial co-stimulatory molecule that binds CD40 on B cells to aid the development of high-affinity antibody responses in the germinal center (GC) (Figure 2.7B)[195,196].

In addition to activation markers, we included multiple cytokines (TNF, IFNy, IL-2 and IL-21) and the degranulation marker CD107a in our panel to assess effector functions generated as a result of antigen-specific activation (Figure 2.7B). Cytotoxic $CD8^+$ T cells are important effector cells. Upon recognition of their cognate antigen, lytic vesicles containing perforin and granzyme are triggered to release their contents. CD107a (LAMP-1) is also located within lytic vesicles and upon degranulation is transiently expressed on the cell surface and allows for the identification of degranulated cells[197]. TNF is a pro-inflammatory cytokine produced early after activation and helps recruit neutrophils and monocytes to the site of infection as well as plays a role in tissue remodeling[190,198]. IFNy is an antiviral cytokine associated with a Th1 helper $CD4^+$ T cell response and effector $CD8^+$ T cell responses[199]. In the context of HBV

infection, TNF and IFNy production from effector $CD8^+$ T cells has been shown to mediate non-cytopathic clearance of HBV DNA from infected hepatocytes[62]. IL-2 is an important cytokine for T cell differentiation and survival. Mainly produced by $CD4^+$ and $CD8^+$ T cells, it provides survival and proliferation signals to lymphocytes[200]. Finally, IL-21 is a critical cytokine for T follicular helper cell (Tfh) mediated maturation of B cells to produce high-affinity antibodies[201]. Strong T cell stimulatory signals provided by phorbol myristate acetate (PMA) and Ionomycin can stimulate T cells in vitro to express and produce co-stimulatory molecules, degranulation markers and cytokines. Therefore, we utilized PMA/Ionomycin stimulation to optimize our panel and detect our cytokines of interest (Figure 2.7A-B)[202].

Chemokine receptors are important surface proteins that guide trafficking of immune cells in response to chemokine expression gradients[166]. We included CXCR5 and CXCR3 in our panel to assess trafficking of global and antigen-specific T cells. $CXCR5^+$ cells traffic to the lymph node in response to expression of CXCL13 produced by follicular dendritic cells in the GC while $CXCR3^+$ cells instead traffic to sites of inflammation in response to CXCL9-11 secreted by monocytes and fibroblasts at inflamed tissue sites (Figure 2.8A)[167,168].

Checkpoint inhibitory molecules normally function to downregulate immune responses after effector functions have occurred to avoid overexuberant immune activation[203]. However, in the context of cancer and chronic infection, persistent antigen exposure aberrantly drives the upregulation of inhibitory molecules leading to cellular exhaustion phenotypes[204]. To assess the degree of T cell dysfunction in global and

antigen-specific T cells during chronic viral infection, we included multiple inhibitory markers PD-1, TIM-3, CTLA-4, and TIGIT in our panel. These inhibitory molecules were all chosen for their current clinical significance, with strategies to block checkpoint inhibition through each of these markers currently being tested in clinical trials (Figure 2.8B)[205].

Recent work has shown in chronic infections that T cells exhibiting an exhausted phenotype are not all created equal. The combination of PD-1, CD127 and transcription factor TCF1 expression help determine multiple stages of memory cell exhaustion[77,206]. TCF1 is a transcription factor and chromatin remodeling protein in the canonical WNT signaling pathway and shows varying expression throughout the course of T cell differentiation[207]. Expression of TCF1 indicates the proliferative capacity of T cells, with higher expression occurring in naïve and memory cells capable of proliferating. For exhausted T cells in chronic infection, PD-1^{+}CD127^{+} cells often share similarities with conventional effector T cells but show signs of exhaustion through PD-1 expression and functionally less ability to proliferate or produce cytokines. However, these cells do express TCF1 and therefore maintain minimal effector function[208]. PD-1^{+}CD127^{-} cells on the other hand typically lack TCF1 expression and show upregulation of additional exhaustion markers. These cells are considered terminally exhausted with no proliferative or cytokine production capacity[74,206,209]. Figure 2.8C shows the differential expression of PD-1 and CD127 on CD8^{+} memory T cells and subsequent TCF1 expression on each subset. In the CHB subjects assessed, TCF1 expression is high in both CD127^{+}PD-

1^+ and $CD127^-PD\text{-}1^+$ populations, but decreased expression is observed in a subset of $PD\text{-}1^-$ cells, demonstrating the ability of our panel to assess these differences.

Finally, in order to detect more detailed T cell differentiation states related to chronic infection, we included CD161 and KLRG1 in our panel. CD161 is a C-type lectin receptor mainly expressed on NK cells, but also expressed on a subset of T cells. On T cells, intermediate expression is associated with productive effector function, while high expression instead represents a subset of dysfunctional cells (Figure 2.8D)[210]. In chronic HCV and HBV infection, intrahepatic virus-specific $CD8^+$ T cells were found to express CD161 on Tem cells, but these cells proliferated poorly *in vitro*[211]. KLRG1 is also primarily an NK cell receptor, but on T cells it is classically associated with antigen-experienced T cells that have undergone senescence[212]. The senescent phenotype is supported by the observation that frequency of KLRG1 expression increases with age. However, KLRG1 also possesses an ITIM motif and is considered a putative co-inhibitory receptor (Figure 2.8E)[212].

Taken together, our comprehensive T cell panel offers the unique opportunity to assess multiple T cell effector functions including activation, cytokine production, trafficking and exhaustion as well as provides the chance for unprecedented assessment of T cell differentiation states associated with productive and/or dysfunctional responses in chronic infection. The panel has been optimized not only with robust, non-specific activation of PMA/Ionomycin, but validated using both acute and chronic HBV subjects exposed to overnight peptide pool stimulation with pools composed of overlapping peptides from three HBV-specific antigens: HBsAg, HBcAg and HBV pol

(see ***2.2.4 Optimization of in vitro Peptide Pool Stimulation for HBV-specific T cell Identification*** below). The panel described here has the ability to identify functional antigen-specific T cells through activation and cytokine production, as well as assess global and antigen-specific phenotypes associated with productive and/or dysfunctional immune responses.

2.2.4 Optimization of in vitro Peptide Pool Stimulation for HBV-specific T cell Identification

In order to identify HBV-specific T cells, we sought to optimize an *in vitro* peptide pool stimulation strategy that would enable us to assess T cell responses to multiple HBV antigens. To this end, we designed three overlapping peptide pools consisting of peptides 15 amino acids in length with an 8 amino acid overlap that span the entire protein sequence for large HBsAg (Surface pool, also containing the sequence for medium and small HBsAg), HBeAg/HBcAg (Core pool, containing peptides that cover both the pre-core and core sequences) and HBV pol (Pol pool) (Table 2.4)

PBMCs from two acute HBV subjects and two CHB subjects were stained for flow cytometric analysis of activation and cytokine production after overnight peptide pool stimulation (Figure 2.9A). Consistent with the literature, cytokine production from acute HBV subjects was robust while minimal cytokine production was observed in CHB subjects (data not shown)[213]. Interestingly, cytokines in acute subjects came exclusively from $CD4^+$ T cells, with no production observed from $CD8^+$ T cells. As $CD8^+$ T cell responses are reported in the literature, we hypothesized that either our intracellular

cytokine staining (ICS) assay was not sensitive enough to detect possible low-frequency $CD8^+$ T cell responses, our peptide pools were not optimized for $CD8^+$ T cell stimulation, or that our timing for HBV peptide pool stimulation was not ideal to detect $CD8^+$ T cell cytokine production.

To address this discrepancy, we performed an ELIspot assay on isolated $CD8^+$ T cells from one acute HBV subject and observed spot formation below background levels for cells stimulated with all three peptide pools (Figure 2.9B). As ELIspot is known to be more sensitive than ICS in detecting cytokine production after T cell stimulation[214], we concluded that lack of sensitivity in our ICS assay was not the cause of no observable $CD8^+$ T cell cytokine production since we also did not observe responses in our ELIspot assay with similar timing of stimulation between the two assays.

While our peptide pool stimulation protocol is an overnight stimulation of 14-16 hours, most ICS experiments performed on HBV samples in the literature occur after an 8-10 day expansion of PBMCs with peptide pools before a secondary overnight pulse stimulation. To determine whether our lack of $CD8^+$ T cell responses was due to timing, or if the peptide pools were not optimized to detect $CD8^+$ cytokine production, we performed a 10 day expansion on one acute HBV subject prior to overnight pulse stimulation with each HBV peptide pool. We found that 10 day expansion did in fact allow for detection of HBV-specific $CD8^+$ T cell responses (Figure 2.9C). Therefore, we concluded our peptide pools can in fact stimulate $CD8^+$ T cell responses but the timing of stimulation is not ideal to detect HBV-specific $CD8^+$ T cell cytokine production. Although useful in determining that our experimental methods work, we must acknowledge that

the optimization here was performed on only one to two acute HBV subjects. It remains possible that in our larger cohort, detection of $CD8^+$ T cell cytokine production will be possible in a subset of subjects after overnight stimulation. In addition, our inclusion of multiple activation markers in the panel will allow for identification of antigen-specific $CD8^+$ T cells that are activated after peptide pool stimulation regardless of whether they are functionally able to produce cytokines.

2.3 Perspectives and Future Directions

The study described within this chapter has been designed as a first of its kind to uncover adaptive immune correlates of acute HBV infection control. To date, it remains unclear why many adults who acquire an acute HBV infection are able to control the infection readily while a small subset progress to CHB. Likely, there is a crucial role played by productive adaptive immune responses that has yet to be fully understood.

Through access to a longitudinally followed cohort with well-defined incident HBV infection, as well as the development of two comprehensive flow cytometry panels to profile at the high-dimensional level both B cell and T cell responses, we aim to uncover antigen-specific and/or global adaptive immune cell parameters that differ in the acute stage of infection and correlate with productive outcomes.

Efforts are currently ongoing to finish acquisition of our samples and analyze results, but we hope to report our findings in the literature soon.

Table 2.1. Characteristics of Multicenter AIDS Cohort Study Participants.

		HIV uninfected		HIV Infected	
Outcome		Control	Chronic	Control	Chronic
Number of subjects (% total cohort)		22 (29%)	9 (12%)	32 (42%)	13 (17%)
Sex	Male	22	9	32	13
Treatment*		0	0	7	1

Subjects matched on age, HIV status, CD4 T cell count (for HIV infected) and time in repository.
*Treatments include Iam, tdf, Iam/tdf, ftc/tdf, lam/ftc/tdf.

Table 2.2. High-dimensional B cell flow cytometry panel.

Specificity	Fluorochrome	Purpose
HBsAg	Dylight 550/Dylight 650	HBV-specific B cell tag
CD19	APC-H7	Lineage B cells
CD20	BV786	
CD10	PE-Cy5	Differentiation B cells
CD27	PE-CF594	
CD21	BUV496	
IgM	AF700	
IgD	BB790	
CD24	BUV395	
CD38	BUV661	
CD5	PE-Cy5.5	
CD43	BV605	
CD86	BUV737	
CXCR3	BV421	Trafficking
CXCR5	PE-Cy7	
CD11c	BB630	Inhibitory/Exhaustion Marker
CD39	BV711	
PD-1	FITC	
FcRL5	BB660	
BTLA	BB700	
CD22	BUV805	
CD32	BV750	
CD3/CD14	BV510	Dump
Viability	Live Dead Aqua	Viability/Dump

Table 2.3. High-dimensional T cell flow cytometry panel.

Specificity	Fluorochrome	Purpose
CD3	BUV496	Lineage T cells
CD4	BUV805	
CD8	BV510	
CD45RA	APC H7	Subsets T cells
CCR7	BUV395	
CD25	BUV563	
CD127	PE Cy5	
KLRG1	PE CF594	Proliferative Capacity
TCF1	AF488	
CD161	BV605	
CD27	BV786	Activation
CD28	BV570	
CD69	PE Cy5.5	
CD40L	BV650	
OX40	BV711	
CXCR5	BB790	Trafficking
CXCR3	PE	
PD-1	BUV661	Inhibitory/Exhaustion Marker
TIM-3	BUV737	
CTLA-4	PE Cy7	
Tigit	BB660	
CD39	BB630	
IFNy	BB700	Cytokines
TNF	BV750	
IL-2	BV421	
IL-21	AF647	
CD107a	AF700	
Viability	Live Dead Blue	Viability

Table 2.4. HBV Peptide Pools

Peptide Pool	HBV Antigen	Peptides per pool	Concentration for Stimulation
Core Pool	HBeAg, HBcAg	26	2ug/mL/peptide
Polymerase Pool	HBV Polymerase	120	2ug/mL/peptide
Surface Pool	HBsAg (L-, M-, S-)	56	2ug/mL/peptide

Overlapping peptides designed from HBV genotype A sequence. Each peptide is 15 amino acids in length with an 8 amino acid overlap.

Figure 2.1. Gating strategy for the 24-color panel to assess B cells in HBV infection.

A. Gating of B cells from viable $CD3^{-}CD14^{-}$ cells in PBMC is depicted. Dye aggregates were removed from analysis. Mature B cells were defined as $CD10^{-}$ B cells. B. $CD10^{-}$ mature B cells can be divided into $CD24^{-}CD38^{hi}$ plasmablasts and non-plasmablasts (upper left plot). Non-plasmablasts can be further characterized based on their surface expression of Ig classes IgM and IgD. IgM/IgD double negative cells are defined as class-switched memory B cells. Surface expression of IgM, IgD, or in combination characterizes unswitched B cells (upper right plot). Unswitched B cells can be further delineated into naïve B cells ($IgD^{+}CD27^{+}$), IgM-only memory B cells ($IgD^{-}CD27^{+/-}$) and $IgD^{+}CD27^{+}$ cells (lower left plot). The latter population contains $IgM^{+}IgD^{+}CD27^{+}$ marginal zone B cells and $IgM^{-}IgD^{+}CD27^{+}$ IgD-only memory B cells (lower right plot). C. Gating of $CD27^{+}CD43^{+}$ non-classical B1 B cells within non-plasmablast cells is shown for chronic HBV patients (upper left plot). Gating on non-plasmablasts is important due to overlapping CD43 expression on plasmablast cells (upper right plot). B1 cells can be divided into unswitched (IgM^{+} and/or IgD^{+}) or $IgM^{-}IgD^{-}$ switched cells (lower left plot). CD5 expression is higher on B1 B cells compared with non-B cells, plasmablasts, and total B cells (lower right plot). Plots show three concatenated CHB subjects.

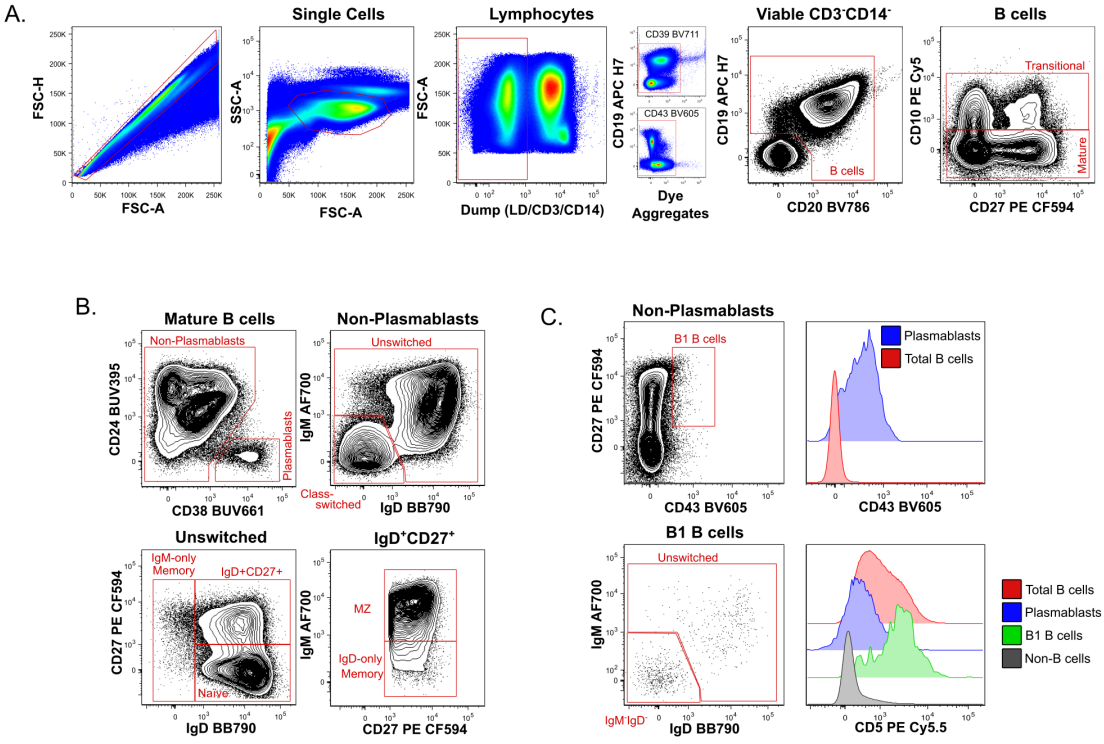

Figure 2.2. Increased frequency of AtM B cells in CHB and higher inhibitory/exhaustion marker expression.

A. Class-switched B cells can be further classified based on their expression of CD21 and CD27. Here, class-switched memory B cells are defined as follows: $CD21^{+}CD27^{-}$ intermediate memory (IM), $CD21^{+}CD27^{+}$ classic resting memory (RM), $CD21^{-}CD27^{+}$ activated memory (AM), and $CD21^{-}CD27^{-}$ atypical memory (AtM). An increased frequency of AtM B cells is observed in CHB subjects compared to healthy controls. B. Expression levels of phenotypic markers associated with chronic infections were examined on the four memory B cell subsets, IM, RM, AM and AtM to show increased expression of all markers on AtM B cells in chronic HBV infection. Chronic HBV plots show three concatenated CHB subjects.

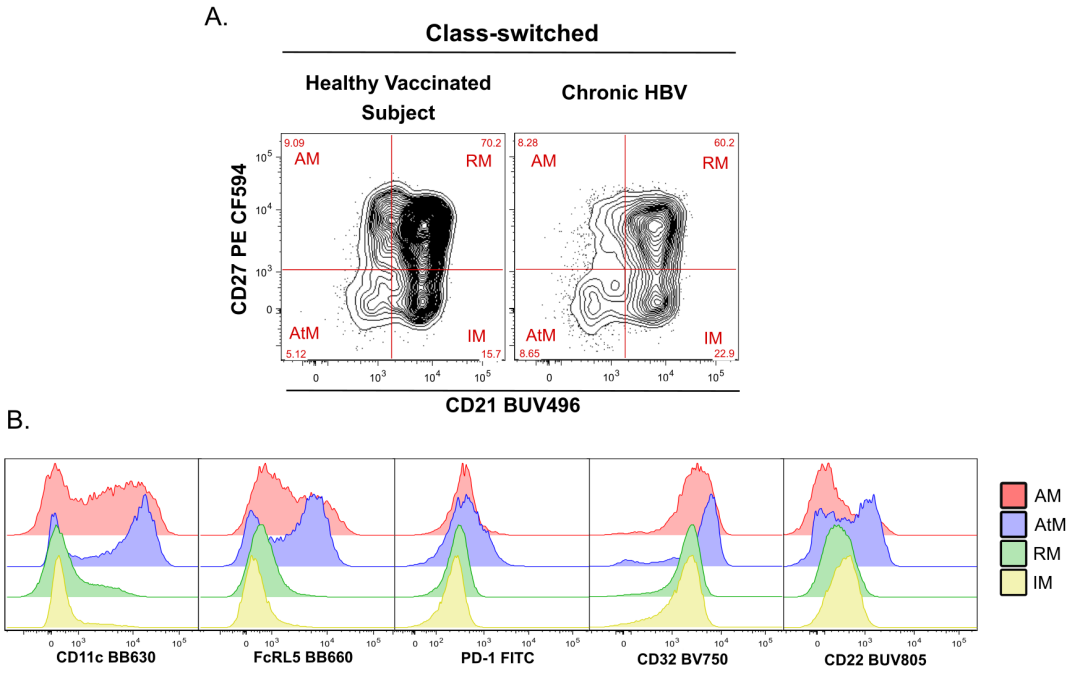

Figure 2.3. Unique expression of all phenotypic markers observed with full panel staining.

A. Expression pattern of phenotypic markers on viable $CD3^{-}CD14^{-}$ cells is shown. The marker CD19 is used on the y-axis to visualize unique expression patterns of phenotypic markers on B cells. All plots show three concatenated CHB subjects. B. FMO control for CD22 shows sufficient separation of $CD22^{+}$ B cells from non-B cells despite dim staining of CD22 BUV805. One chronic HBV subject was stained with the full panel as well as CD22 FMO.

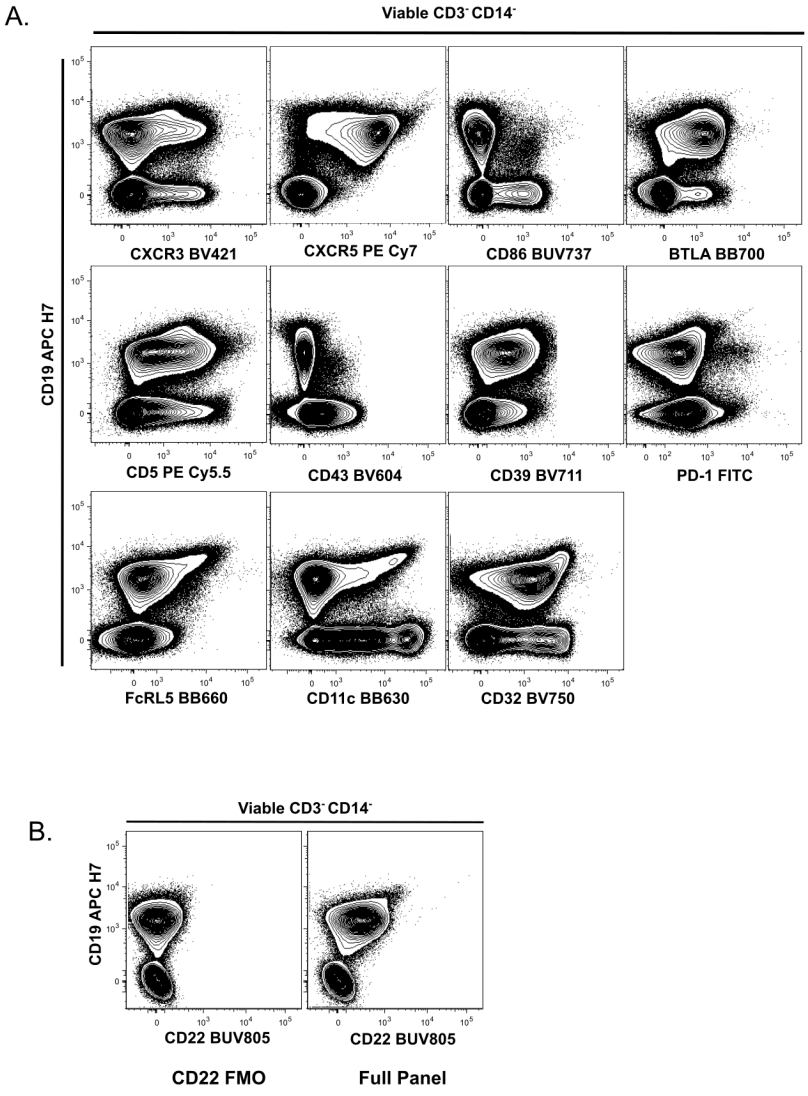

Figure 2.4. Optimization of HBsAg Dylight probes to detect HBsAg-specific B cells.

A. Timeline of sample acquisition throughout course of HBV booster vaccination with ENERGIX-B for healthy vaccinated subject AC51. Sampling occurred immediately before the first booster (D0), 7 days after the first booster (D7), 32 days after the first booster (D32), 12 days after second booster (D47) and 7 days after third booster (D189). B. Plasma antibody titers against HBsAg (anti-HBs) over time. Increase in anti-HBs from baseline shows response to vaccination. Dots indicate sample mean OD450 and are plotted against time points when samples were collected, arrows indicate when boosters occurred. Samples were run in duplicate, error bars=SD. C. Half-log titrations of HBsAg Dylight 550/650 probes on healthy HBV unexposed leukopak (LP) subjects (LPs, top row, 5 concatenated subjects) to determine probe concentrations with minimal non-specific background staining. Two concentrations of HBsAg Dylight probes with lowest background were tested on PBMC from AC51 D189 (bottom row) to confirm the detection of double positive HBV-specific B cells. D. HBV-specific B cell frequencies from PBMC samples stained with either 0.2ug/50uL or 0.063ug/50uL of the Dylight 550 and Dylight 650 labeled HBsAg probes. HBV-specific B cells were defined as double positive for HBsAg probes. Data includes 5 healthy HBV unexposed donor LPs and 4 total HBV exposed individuals (1 healthy subject with HBV booster vaccination (AC51) and 3 chronic HBV (CHB) subjects). Black dots are CHB subjects that were only tested at one concentration. Colored dots show individual subjects at each concentration tested. Bar indicates median value of each group. E. Time course analysis of AC51 to validate use of 0.2ug HBsAg Dylight 550/650 per 50uL staining reaction. HBV-specific B cells are detected at a greater frequency over time, with little non-specific background staining. F. HBsAg Dylight 550/650 double positive cells were sorted and stimulated with CD40L expressing feeder cells, IL-2, and IL-21 for 14 days. Supernatants were run on anti-HBs ELISA and the specificity of the HBsAg Dylight 550/650 detection method was confirmed as only double positive cells produced anti-HBs. For staining reactions (C & E), HBsAg Dylight 550 and Dylight 650 were added at equal concentrations in 50uL staining reactions. Optimization was performed on a smaller panel of B cell markers for all figures, and plots were pre-gated on viable, $CD3^-$, $CD14^-$, $CD19^+$, $CD10^-$, $CD27^+CD21^+$/$CD27^+CD21^-$/$CD27^-CD21^-$ B cells. Anti-HBs ELISA (Abnova, cat# KA0287).

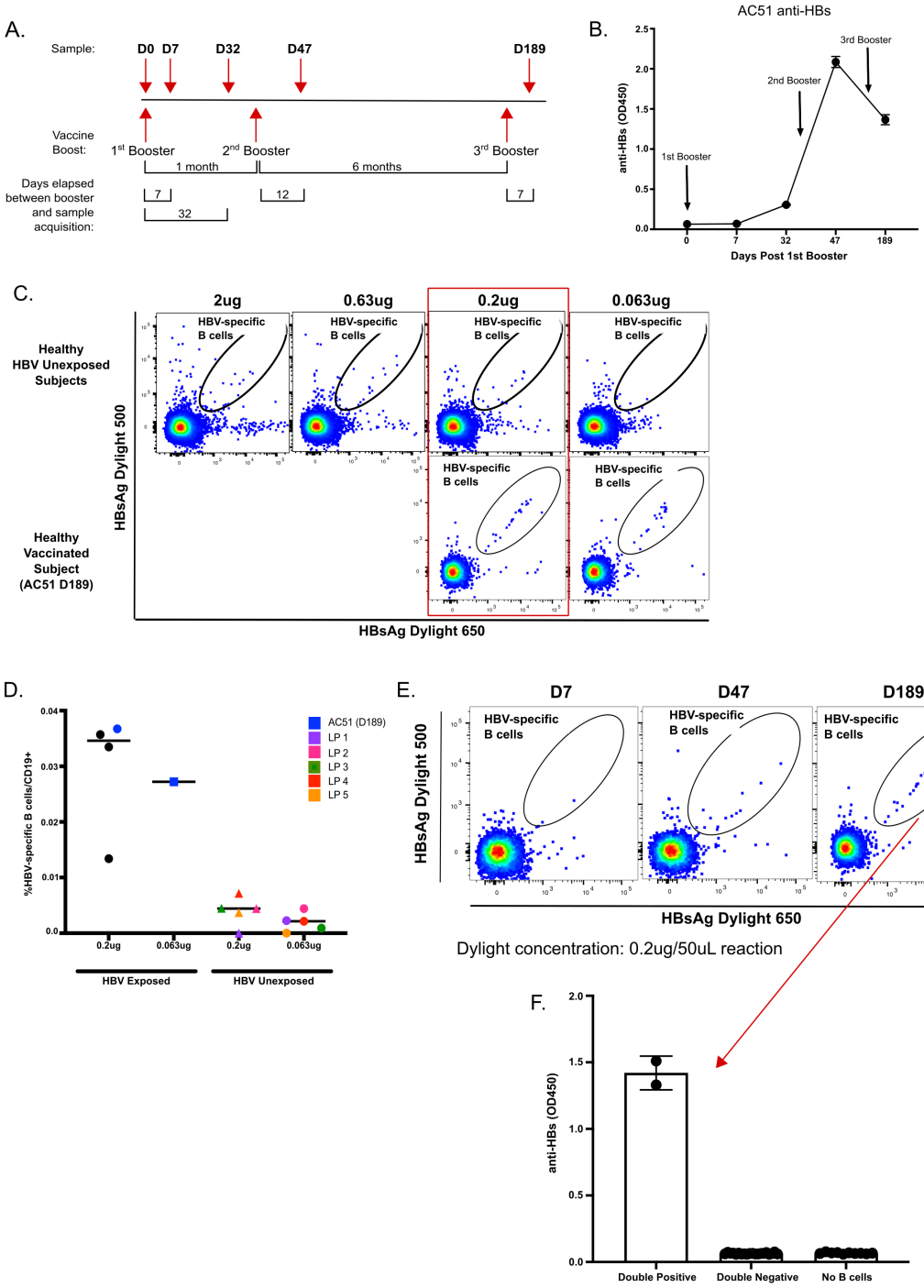
A.
Sample:
D0 D7 D32 D47 D189
Vaccine Boost:
1st Booster
2nd Booster
3rd Booster
1 month
6 months
Days elapsed between booster and sample acquisition:
7
12
7
32
B.
AC51 anti-HBs
anti-HBs (OD450)
1st Booster
2nd Booster
3rd Booster
Days Post 1st Booster
C.
2ug
0.63ug
0.2ug
0.063ug
Healthy HBV Unexposed Subjects
Healthy Vaccinated Subject (AC51 D189)
HBV-specific B cells
HBsAg Dylight 500
HBsAg Dylight 650
D.
%HBV-specific B cells/CD19+
AC51 (D189)
LP 1
LP 2
LP 3
LP 4
LP 5
0.2ug
0.063ug
HBV Exposed
HBV Unexposed
E.
D7
D47
D189
HBV-specific B cells
HBsAg Dylight 500
HBsAg Dylight 650
Dylight concentration: 0.2ug/50uL reaction
F.
anti-HBs (OD450)
Double Positive
Double Negative
No B cells

Figure 2.5. HBV-specific B cell lineages and phenotypes

A. HBsAg double positive cells within unswitched (first column) and class-switched (second column) subsets are shown for a healthy HBV vaccinated subject (top row) and chronic HBV patients (bottom row). B. HBsAg-specific B cells derived from unswitched B cells were overlaid on total unswitched B cells from the chronic HBV patients. The majority of unswitched $CD27^{+}$ HBsAg-specific B cells represent marginal zone B cells. C. Unswitched and class-switched HBV-specific B cells from 3 chronic HBV (CHB) subjects were concatenated and overlaid on total B cells in CHB to show expression patterns for each phenotypic marker included in the panel for all HBV-specific cells. D. Similar analysis was performed on all HBV-specific B cells from healthy vaccinated subject AC51. All chronic HBV plots show three concatenated CHB subjects.

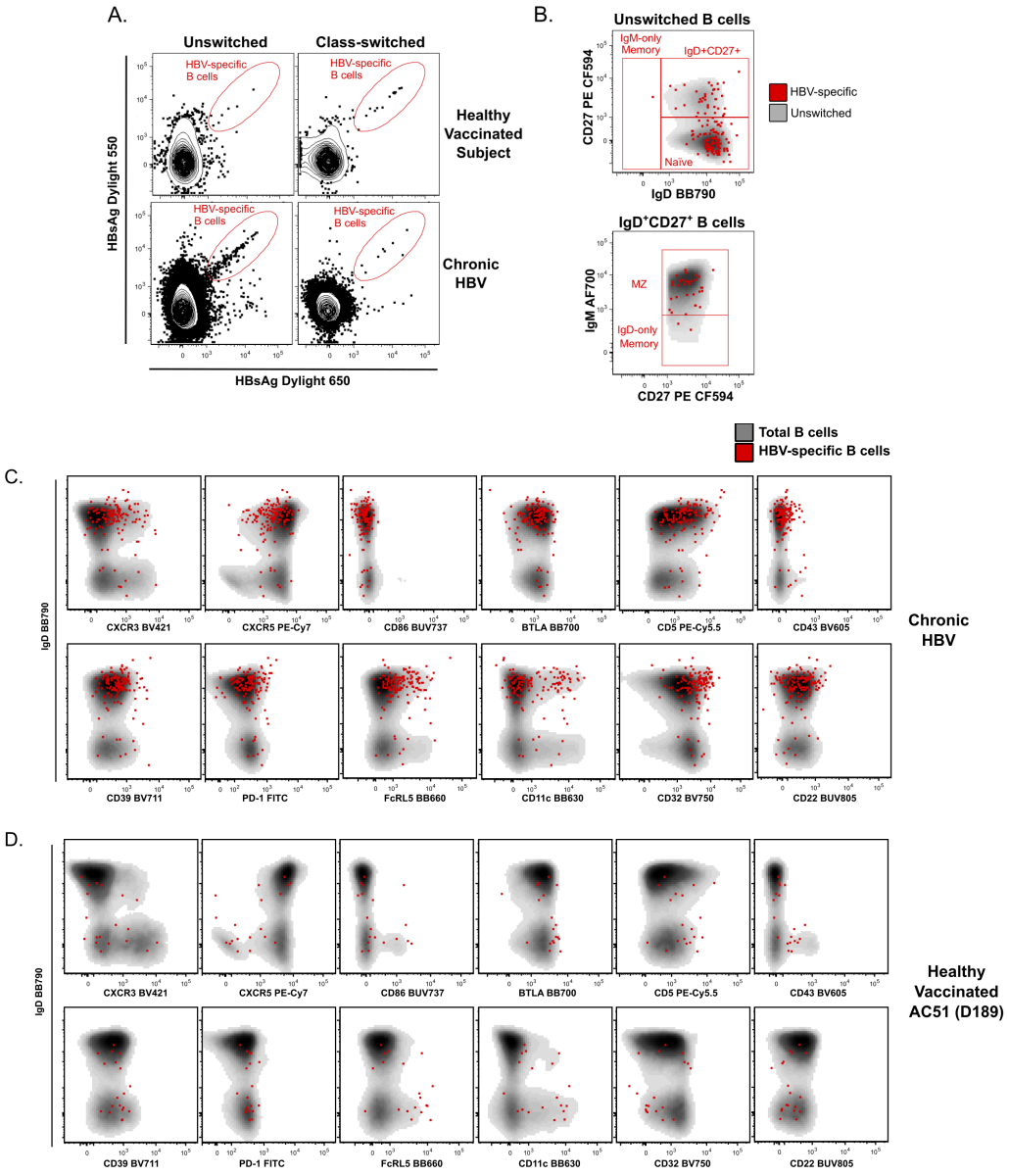

Figure 2.6. Gating Strategy for 28-color panel to assess T cell responses in HBV infection

A. T cells are gated from live, single cell lymphocytes and can be distinguished by $CD3^+$ staining. T cells are further delineated by their unique expression of CD4 or CD8. B. $CD4^+$ T cells contain a population of $CD25^+CD127^-$ T regulatory cells that have increased expression of CD39. C. Both $CD4^+$ and $CD8^+$ T cells contain naïve T cell populations ($CD45RA^+CCR7^+$) and memory subsets. Memory T cells are identified as: T central memory (Tcm, $CCR7^+CD45RA^-$), T effector memory (Tem, $CCR7^-CD45RA^-$) and T effector memory $CD45RA^+$ (Temra, $CCR7^-CD45RA^+$). Expression of CD27 and/or CD28 further distinguishes memory T cell subsets. Gating was performed on two concatenated acute HBV subjects without stimulation.

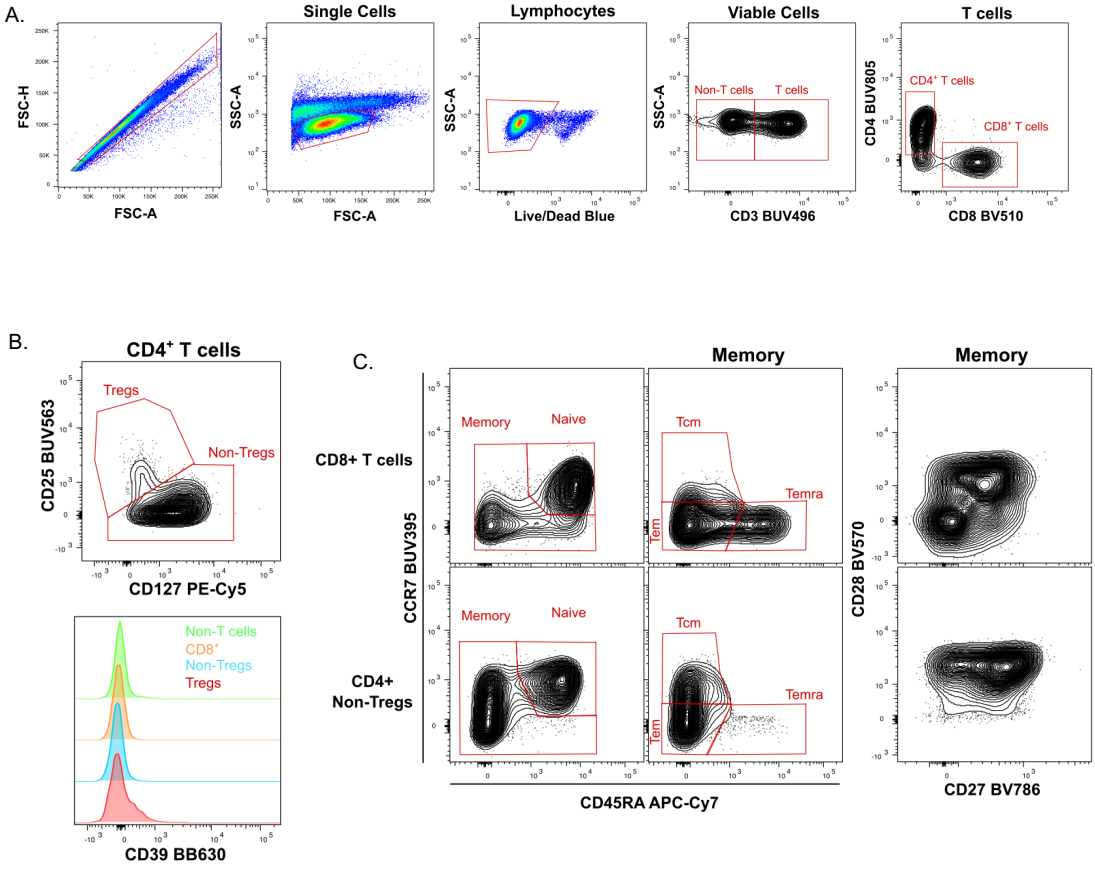

Figure 2.7. PMA/Ionomycin stimulation upregulates activation, degranulation and cytokine production from T cells.

A. Activation markers CD69 and OX40 are expressed upon strong stimulation with PMA/Ionomycin in both $CD4^+$ and $CD8^+$ T cells in a healthy subject. B. Memory $CD4^+$ and $CD8^+$ T cells produce all cytokines assessed by our panel upon stimulation with PMA/Ionomycin. Cytokines are plotted against co-stimulatory molecule CD154 (CD40L) for $CD4^+$ T cells and degranulation marker CD107a for $CD8^+$ T cells to simultaneously show activation and cytokine production. Cytokine production was assessed in a healthy subject.

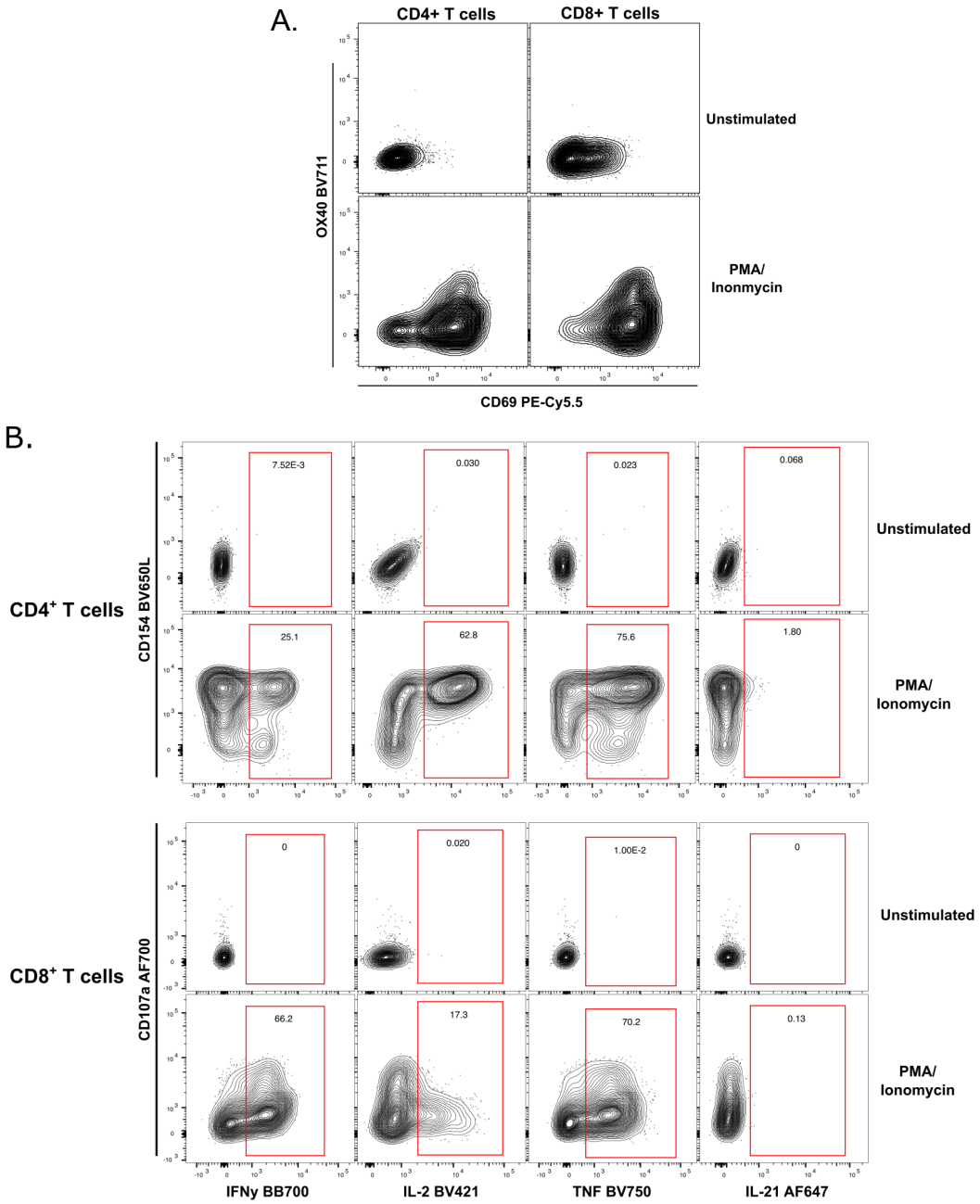

Figure 2.8. All phenotypic markers are detectable in the panel in the context of functionally relevant cell subsets.

A. Chemokine receptors CXCR5 and CXCR3 are detected at higher frequencies in the memory $CD8^+$ T cell compartment (red) compared to naïve cells (blue). Plots show PBMCs from two unstimulated acute HBV subjects. B. Exhaustion markers included in the panel demonstrate differential expression on $CD8^+$ T cells compared to $CD8^-$ T cells (top row) in two CHB subjects. Expression levels are also shown to differ between two acute HBV subjects (naïve = green, memory = orange) and two CHB subjects (naïve = blue, memory = red)(bottom row). PBMCs were stimulated with HBV peptide pools prior to acquisition. C. Expression of PD-1 and CD127 assessed on $CD8^+$ memory T cells from two CHB subjects stimulated with HBV peptide pools (left plot). PD-1^+ cells indicate a partially exhausted state. TCF1 expression was then assessed on $CD127^-PD\text{-}1^-$, $CD127^-PD\text{-}1^+$, $CD127^+PD\text{-}1^-$ and $CD127^+PD\text{-}1^+$ populations to determine further terminal exhaustion status (right quadrant). D. Differential expression of CD161 is shown on $CD8^+$ Tem cells from two CHB subjects stimulated with HBV peptide pools compared to Tcm and Temra subsets. E. KLRG1 expression was observed in acute HBV subjects in the non-T cell compartment. While expressed on T cells, KLRG1 is primarily an NK cell marker and expression here confirms ability to detect the marker in the context of the full panel.

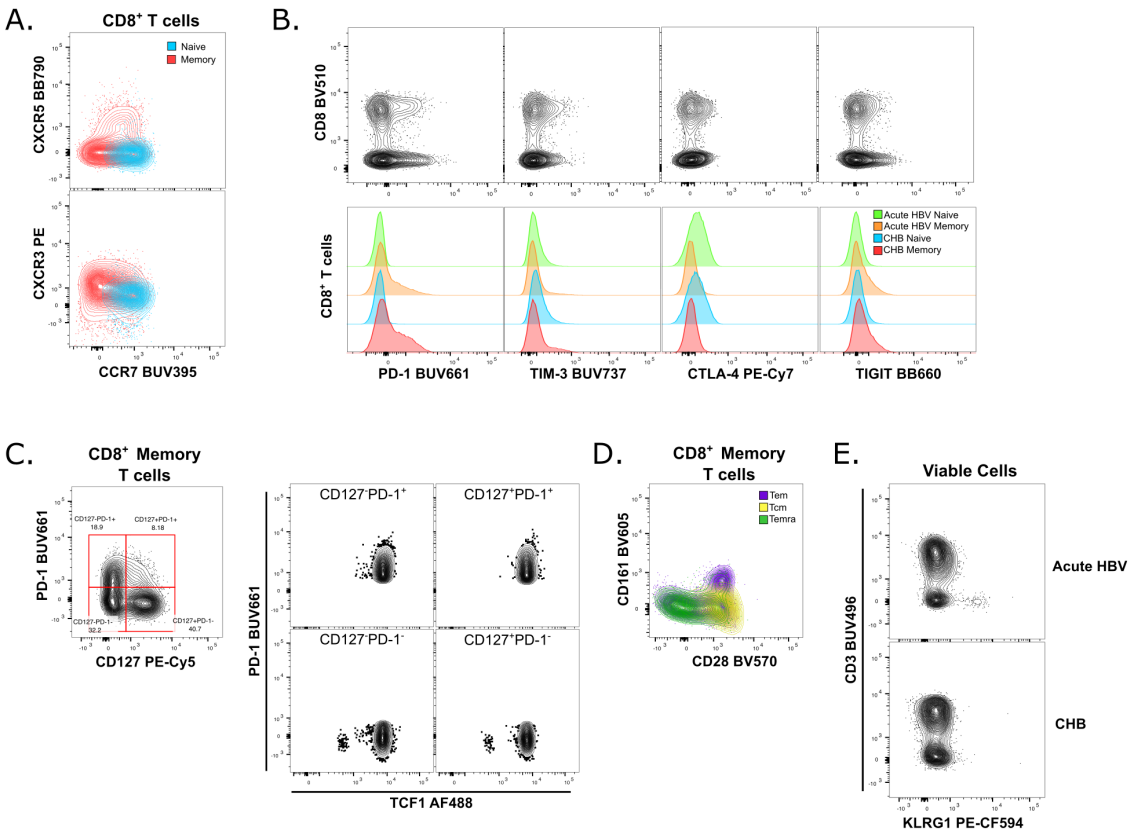

Figure 2.9. Overnight HBV peptide pool stimulation leads to CD4$^+$ T cell cytokine production while 10 day expansion is necessary to elicit robust CD8$^+$ T cell cytokine responses.

A. PBMCs from two acute HBV subjects were rested 6 hours before stimulation with one of three HBV peptide pools for 16 hours overnight in the presence of brefeldin A and monensin. Plots show memory CD4$^+$ or CD8$^+$ T cells with both subjects and all HBV peptide pools concatenated. Overnight stimulation produces robust CD4$^+$ T cell responses to HBV peptide pools but little CD8$^+$ cytokine production. B. IFNy ELIspot was performed on isolated CD8$^+$ T cells after 6 hour rest to determine whether more robust IFNy production could be observed with the more sensitive cytokine assay. Data are reported as IFNy spot forming colonies per 1 million cells and each dot represents one replicate well. Red line indicates limit of detection of the assay. Representative images from wells stimulated with each peptide pool are shown to the right. C. PBMCs from one acute HBV subject were rested 6 hours before stimulation for 10 days in culture with one of three HBV peptide pools and rIL-2. Half of the culture media with rIL-2 was replaced at days 3 and 7, then again at day 9 without rIL-2 replacement. On day 10 cells were restimulated for 16 hours with the same peptide pool they were expanded with. Plots show memory CD4$^+$ or CD8$^+$ T cells with all HBV peptide pools concatenated.

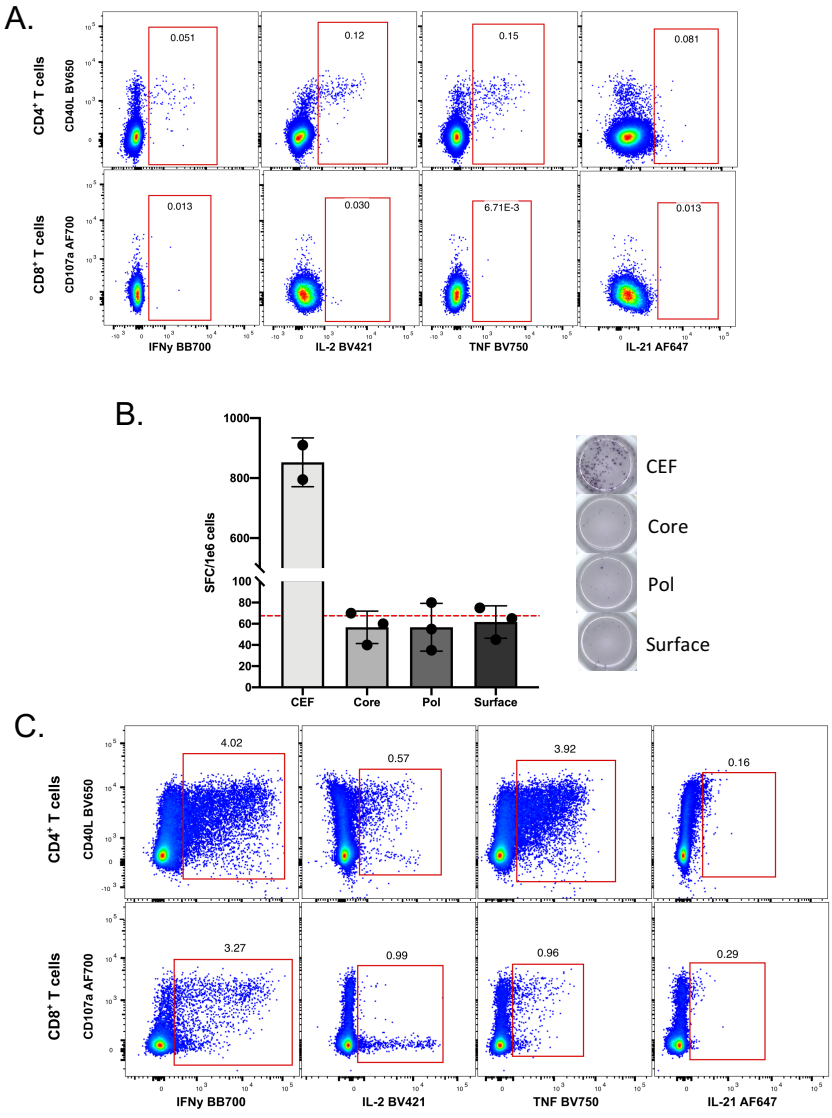

Chapter 3: Metabolic Programs Define Dysfunctional Immune Responses in Severe COVID-19

It is unclear why some SARS-CoV-2 patients readily resolve infection while others develop severe disease. By interrogating metabolic programs of immune cells in severe and recovered COVID-19 patients compared to other viral infections, we identified a unique population of T cells. These T cells express increased VDAC1, accompanied by gene programs and functional characteristics linked to mitochondrial dysfunction and apoptosis. The percentage of these cells increases in elderly patients and correlates with lymphopenia. Importantly, T cell apoptosis is inhibited *in vitro* by targeting the oligomerization of VDAC1 or blocking caspase activity. We also observe an expansion of myeloid derived suppressor cells with unique metabolic phenotypes specific to COVID-19 and their presence distinguishes severe from mild disease. Overall, the identification of these metabolic phenotypes provides insight into the dysfunctional immune response in acutely ill COVID-19 patients and provides a means to predict and track disease severity and/or design metabolic therapeutic regimens[215].

3.1 Immunometabolic Approach to SARS-CoV-2 Assessment

We hypothesized that interrogation of immunometabolic phenotypes in COVID-19 has the potential to transcend traditional immune cell phenotyping and provide novel insights into distinct functional subsets. To this end, we developed a flow cytometry-based proteomic and epigenetic approach that enables the interrogation of metabolic

programs at the single cell level (Figure 3.1). We focused on three main pathways to characterize the metabolic landscape of immune cells in COVID-19. First, the mitochondrial membrane proteins Voltage Dependent Anion Channel 1 (VDAC1) and Tomm20 were used as surrogates for mitochondrial mass and utilization of oxidative phosphorylation. Second, to evaluate the presence of glycolytic machinery used for glycolysis, the glucose transporter Glut1 and the rate limiting enzyme of glycolysis, Hexokinase II (HK2) were evaluated. Finally, the ability to utilize fatty acid oxidation was measured by the expression of carnitine palmitoyltransferase 1a (CPT1a). Expression of H3K27Me3 was included as a readout for histone methylation which is regulated at multiple levels by metabolites of the TCA cycle[216]. Using this approach, we identified distinct T cell and myeloid subsets in the PBMC of acutely ill COVID-19 patients (COVID-A) that were not found in the PBMC of recovered COVID-19 patients (COVID-R) and patients with hepatitis C virus (HCV) and influenza viral infections. Furthermore, these cells provide important mechanistic insight into the immune dysfunction observed in COVID-A patients and the mechanism of pathogenesis

3.2 Metabolically Distinct T cells in SARS-CoV-2

The high dimensional flow cyotometry-based assay was performed on thawed PBMC from an IRB approved biorepository from patients admitted to the Johns Hopkins Hospital (Table 3.1). We initially focused on T cells within the PBMC given their importance in viral control. Using traditional immunological markers, we observed limited differences in T cell frequencies and phenotype, as previously described (Figure

3.2)[127,217]. Most notably, we detected an increase in the CD4:CD8 ratio and an increase in central memory (Tcm) CD4 T cells in COVID-A patients when compared to healthy controls (Figure 3.2B-C). In addition, when compared to healthy controls, we observed no differences in expression of the classical markers of T cell subsets CD45RA and CCR7 (Figure 3.2E) or the activation markers CD69, Ki67, PD-1, or HLA-DR (Figure 3.2F). Likewise, levels of metabolic enzymes involved in glycolysis and fatty acid oxidation did not differ between the two groups (Figure 3.2G).

In stark contrast, unbiased analysis of T cells employing the combined immune and metabolic markers dramatically segregated T cells from healthy controls and COVID-A (Figure 3.3A). This unique population of T cells found in the COVID-A patients was characterized by robust upregulation of VDAC1 and the epigenetic mark H3K27me3 (Figure 3.3A-B). H3K27me3 is regulated in part by a-ketoglutarate-mediated jumonji demethylases[216], while VDAC1 is a mitochondrial membrane protein involved in metabolite transport, and has been associated with mitochondrial cell death signaling and lupus-like autoimmunity[218,219]. This phenotype was unique in its exclusive upregulation of mitochondrial proteins, without a concomitant upregulation of glycolytic machinery. Classically, upon T cell activation VDAC1 and H3K27me3 expression increase along with the glucose transporter Glut1 and Hexokinase II (HKII), both of which support activation-induced glycolysis. This traditional activation signature was seen upon TCR stimulation of healthy PBMCs in vitro (Figure 3.3C). However, the unique population of H3K27me3^{hi}VDAC1^{hi} T cells in the PBMC of COVID-A patients differ from conventional recently activated T cells because they express relatively low levels of

Glut1 and HKII (Figure 3.3D). The H3K27me3^{hi}VDAC1^{hi} T cells were found both within the naive and memory T cell compartment (Figure 3.3D) and did not demonstrate enrichment for specific TCR clones (Figure 3.3E). Expanded analysis of 55 PBMC samples from 38 COVID-A patients (including sequential samples) revealed that these T cells were markedly upregulated (many exceeding 50% of total T cells) in COVID-A patients and were almost completely absent in healthy controls (Figure 3.3F). Interestingly, while not present in all of the patients queried, every COVID-A patient 70 years of age and older demonstrated frequencies of the H3K27me3^{hi}VDAC1^{hi} T cells which were 40% or greater in their PBMC (Figure 3.3G). Overall, these data reveal a distinct population of H3K27me3^{hi}VDAC1^{hi} T cells in the PBMC of COVID-A patients. The discordance in activation and metabolic phenotypes suggests that these T cells are dysfunctional.

3.2.1 Unique H3K27me3^{hi}VDAC^{hi} T cells Distinguish Acutely Ill COVID-19 Patients from Recovered Patients and Hospitalized Patients Infected with Influenza

By interrogating metabolic programs using our immune-metabolic assay, we were able to identify a unique population of H3K27me3^{hi}VDAC1^{hi} T cells in COVID-A patients. We next wanted to determine if this population of T cells was unique to the COVID-A patients. To this end, we interrogated the PBMC of recovered COVID-19 patients (>28 days from diagnosis, COVID-R) and patients with other viral infections to determine if this phenotype was simply a result of ongoing inflammation or general consequence of viral infection. PBMC were obtained and analyzed from patients with acute and chronic viral hepatitis C infection[220], hospitalized with influenza infection[221], and those who had recovered from COVID-19 (COVID-R)[222] (Table 3.2). There appeared to be only subtle

differences between these groups in $CD4^+$ and $CD8^+$ T cell subsets as defined by traditional markers (Figure 3.2). Yet, when including metabolic markers in the analysis, the COVID-A patients' T cells again segregated compared to other groups as shown by UMAP projections, indicating a distinct subset of T cells unique to COVID-A patients not accounted for by traditional markers (Figure 3.4A-C). $H3K27me3^{hi}VDAC1^{hi}$ T cells were absent in both acute and chronic hepatitis C infection; however, they were present in a subset of both influenza and COVID-R patients (Figure 3.4D-E).

Importantly, although T cells present in severe influenza infection and during recovery maintained elevated VDAC1 and H3K27me3 expression, clustering the $H3K27me3^{hi}VDAC1^{hi}$ CD4 T cells by protein expression of all other markers included in the flow cytometry panel showed that these cells robustly clustered based on disease type, indicating qualitative differences in $H3K27me3^{hi}VDAC1^{hi}$ T cells across disease status (Figure 3.4F). That is, even though T cells expressing H3K27me3 and VDAC1 were present in the PBMC of the influenza and COVID-R patients, they were distinct from the $H3K27me3^{hi}VDAC1^{hi}$ T cells in the PBMC of the COVID-A patients.

For example, as described earlier, the $H3K27me3^{hi}VDAC1^{hi}$ T cells from the COVID-A patients demonstrated significantly decreased expression of Glut1, a metabolic marker associated with T cell effector function, compared with COVID-R and influenza (Figure 3.4G). Notably, the level of Glut1 on the $H3K27me3^{hi}VDAC1^{hi}$ T cells corresponded to disease severity in COVID-A patients. While the most severe patients (requiring mechanical ventilation) expressed significantly lower levels of Glut1, the patients with more mild disease (hospitalized and requiring low or high flow oxygen)

demonstrated H3K27me3^{hi}VDAC1^{hi} T cells with Glut1 levels similar to COVID-R patients and influenza patients (Figure 3.4G). In contrast, H3K27me3^{hi}VDAC1^{hi} T cells from COVID-A patients had significantly increased expression of the mitochondrial protein Tomm20 and KLRG1, a marker associated with T cell senescence and age-related functional defects (Figure 3.4G)[212]. Thus, despite similar levels of H3K27Me3 and VDAC1 expression, the expression of proteins involved in metabolic programming of these cells is distinct between severe acute COVID-19 patients and mild/recovered COVID-19 or hospitalized influenza patients, all of whom recovered. Therefore, these cells represent a population truly unique to acutely ill COVID-19 and may provide insight into the immune dysregulation observed in SARS-CoV-2 infection.

3.2.2 Dysfunctional Mitochondria in T cells of Acutely Ill COVID-19 Patients Leads to Apoptosis in a VDAC1-Dependent Fashion

In order to elucidate the functional significance of these T cells that were highly prevalent in acute COVID-19, single-cell RNA sequencing was performed on six COVID-A patients, all of which had more than 50% of the T cells of interest as determined by flow cytometry, and three healthy controls. Evaluating gene programs enriched in T cells derived from COVID-A patients revealed an upregulation of cell death programs, as has been reported previously (Figure 3.5A, red bars)[223]. Furthermore, these data demonstrated evidence of mitochondrial dysfunction, including downregulation of several programs associated with mitochondria function, organization, respiratory chain complex assembly, oxidative phosphorylation, and electron transport coupled proton transport (Figure 3.5A, blue bars).

To investigate whether elevated levels of VDAC1 and Tomm20 was indicative of altered mitochondrial function in these T cells, we performed electron microscopy on PBMC from additional COVID-A patients and healthy controls to examine the lymphocyte mitochondria. This analysis revealed markedly dysmorphic, irregularly shaped mitochondria with incomplete cristae in lymphocytes from COVID-A patients compared to lymphocytes from healthy controls, consistent with dysregulated mitochondrial function (Figure 3.5B). In addition to displaying morphological characteristics of apoptosis, lymphocytes from COVID-A patients showed prominent degenerative changes including large cytoplasmic vacuoles.

We next performed confocal microscopy of PBMC stained with anti-CD3 and MitoTracker Deep Red, which stains mitochondria. $CD3^+$ T cells from COVID-A patients demonstrated less distinct mitochondrial staining versus healthy controls (Figure 3.5C), consistent with the dysmorphic mitochondria observed by EM. Based on these findings and along with the observed decreased mitochondrial programs by RNA-seq and presence of apoptotic cell morphologies by EM, we hypothesized that VDAC1 might act to facilitate release of mitochondrial cytochrome c to the cytosol, leading to apoptosis[224,225]. We therefore performed immunofluorescence analysis of endogenous cytochrome c and found it to be present in the cytoplasm of a subset of $CD3^+$ T cells from COVID-A patients, whereas in healthy controls, cytochrome c was localized to the mitochondria (Figure 3.5D). Of note, while release of cytochrome c into the cytoplasm can lead to rapid cell death, in our procedure, the cells were fixed immediately after thawing, prior to measurement of endogenous cytochrome c. Employing this technique

enabled us to capture a subset of T cells undergoing active mitochondria-induced apoptosis. Interestingly, the presence of H3K27me3^{hi}VDAC1^{hi} T cells was highly predictive of the development of lymphopenia during the course of hospitalization. We observed a highly significant ($p<0.0001$) negative correlation between the frequency of these cells and the peripheral lymphocyte count as measured after 7 days of hospitalization (Figure 3.5E). This highly significant negative correlation supports the hypothesis that mitochondrial-induced apoptosis is in part contributing to the lymphopenia that develops in the COVID-A patients during the course of their disease[127,226]. Thus, the unique population of T cells found in the COVID-A patients display mitochondrial dysfunction consistent with cytochrome c release into the cytoplasm and subsequent induction of apoptosis. Given these findings and the fact that VDAC1 can facilitate caspase-mediated cell death[224,227], we hypothesized that the high expression of VDAC1 in the setting of dysmorphic mitochondria was directly linked to increased susceptibility to cell death in these T cells.

To test this hypothesis, we cultured PBMC from COVID-A patients and healthy controls for 48 hours in vitro in the presence of media alone, the mTOR inhibitor rapamycin, the VDAC1 oligomerization inhibitor VBIT-4[218,219], or the global caspase inhibitor ZVAD (Figure 3.6A). We observed decreased T cell survival in media alone from the PBMC of COVID-A patients when compared to healthy controls, confirming increased cell death in COVID-A T cells. Interestingly, survival of the COVID-A T cells was rescued with either the VDAC1 oligomerization inhibitor or the pan-caspase inhibitor, but not the mTOR inhibitor. These findings are consistent with the fact that VDAC1

oligomerization and interaction with BCL2 family proteins is thought to enable pore formation within the mitochondrial outer membrane, allowing for cytoplasmic release of cytochrome *c*, which initiates the caspase cascade to induce cellular apoptosis[224,227,228]. Notably, neither VBIT-4 nor ZVAD enhanced survival of the healthy T cells, demonstrating that this mechanism of cell death contributes to loss of viability in the COVID-A T cells but not in the T cells from the healthy controls. Interestingly, the COVID-A T cells treated with ZVAD and VBIT-4 treatment demonstrated robust response to anti-CD3 + anti-CD28 stimulation, similar to the healthy T cells, indicating the ability to functionally rescue the T cells (Figure 3.6B). These data, combined with the observations of increased cytoplasmic cytochrome *c* suggest that VDAC1 is promoting cell death through direct pore formation (Figure 3.6C). However, these observations do not rule out a role for an interaction between VDAC1 and BAX/BAK to promote cell death in these T cells.

In light of the propensity of the T cells from the COVID-A patients to undergo apoptosis, we wanted to verify that our results did not reflect differences in cell survival after freezing. When we compared fresh and frozen PBMC from four COVID-A patients, we observed an increased frequency of the H3K27me3^{hi}VDAC1^{hi} T cells in the freshly stained PBMC (Figure 3.6D) compared to those frozen and thawed. Thus, our studies are potentially underestimating the frequency of these unique T cells in the COVID-A patients.

3.3 B cell Frequencies and Phenotypes Differ in the Memory Compartment in COVID-19

Using our assay, we also interrogated the metabolic programs of B cells and NK cells. In contrast to T lymphocytes, we did not observe marked differences in the frequencies of naïve B cells between any viral infections and the healthy controls (Figure 3.7). Consistent with recent reports, we did observe an increase in the peripheral antibody-secreting cells (ASC) in the COVID-A patients[226]. All of the viral infections were associated with a significant increase in the memory B cells versus healthy controls, while only the COVID-A and hepatitis C patient groups demonstrated an increase in the activated memory B cells. The COVID-A and influenza patient groups both had a higher percent of atypical memory B cells compared to PBMC from the hepatitis C and the COVID-R patient groups. Overall, global UMAP projection demonstrated only subtle phenotypic differences among the different groups in the B cell compartment.

3.4 Unique NK Cell Population in COVID-A Subjects Identified by High Dimensional Phenotyping Analysis

When we examined the NK cells, we found no significant differences in frequency when comparing the COVID-A patients, the COVID-R patients and the influenza patients (Figure 3.8). Conversely, HD flow analysis revealed a population of $CD56^{+}$ NK cells in the COVID-A patients not present in the influenza patients or in the healthy controls. This population was defined by the upregulation of classical activation markers CD69, Ki67, and CD49a and by increased expression of the metabolic markers Tomm20, CPT1a, and HKII. When we compared NK cells from COVID-A patients with COVID-R patients, we

observed differences in $CD56^{+}$ and $CD56^{bright}$ cells driven mainly by differential expression of markers of activation. While the precise significance of these cells is unclear, their generation can potentially provide important clues into the dysregulated systemic inflammation characteristic of acutely ill COVID-A patients.

3.5 Expansion of Neutrophils and PMN-MDSCs in Acute COVID-19

Next, we examined myeloid cells in the PBMC of the COVID-A patients employing our HD immunometabolic assay (Figure 3.9). Consistent with prior reports, acute COVID-19 was associated with a decreased percentage of myeloid dendritic cells (mDC) and plasmacytoid dendritic cells (pDC) in PBMC and limited differences in monocyte populations[226,229] (Figure 3.9A-C). Although cryopreservation is known to affect the recovery of myeloid populations, a rapid protocol to stain cells immediately post thaw was utilized to minimize this effect and allowed for recovery of monocytic and granulocytic cells post-cryopreservation, when compared to freshly isolated cells (Figure 3.9F-G).

Visualization of myeloid cells by UMAP projection revealed two distinct populations, which once again only became apparent upon interrogating metabolism (Figure 3.10A-B). We first identified $CD15^{+}$ granulocytic cells in COVID-A patients, which were entirely absent from the healthy controls (Figure 3.10A-B). Evaluating the granulocytic cells further revealed a combination of low-density neutrophils, basophils, and polymorphonuclear (PMN)-myeloid derived suppressor cells (MDSC) (Figure 3.10C, Figure 3.9). Increased neutrophil counts have been previously observed in COVID-19

patients[226,229] and low-density neutrophils can be found in the PBMC fraction during inflammation, representing both immature neutrophils and activated/degranulated neutrophils[230]. Immunosuppressive PMN-MDSC are often associated with chronic inflammation, as is seen in cancer, obesity and chronic viral infection[231]. Although low levels of PMN-MDSC were detectable in chronic hepatitis C, there were significantly more in COVID-A patients (Figure 3.10C). Of note, the PMN-MDSC expressed the highest levels of VDAC1 within the PBMCs, higher than the H3K27Me3^{hi}VDAC1^{hi} pre-apoptotic T cells (Figure 3.10D). However, in contrast to the VDAC1^{+} T cells, the PMN-MDSC had concurrent upregulation of HKII, which is known to associate with VDAC1 and prevent apoptosis[232]. Thus, the granulocytic suppressor cells (PMN-MDSC) in the PBMC of the COVID-A patients possessed a unique metabolic signature (Figure 3.10E). The expression of VDAC1 and HKII provide further information into the metabolic programing of these cells and may provide potential therapeutic targets for an immunosuppressive MDSC compartment.

3.6 Metabolically Distinct Myeloid Cells in COVID-A with Differential HLA-DR Expression

We next identified a population of monocytic cells present in COVID-A patients that expressed high levels of carnitine palmitoyltransferase 1a (CPT1a), an enzyme found within the mitochondrial membrane that is essential for fatty acid oxidation. Additionally, these myeloid cells also expressed high levels of VDAC1 (Figure 3.11A-B). Interestingly, CPT1a has been associated with both inflammasome activation and ROS production[233,234], and a potential role for inflammasome activation in contributing to the

pathogenesis of SARS-CoV-2 infection has been noted by others[235]. When comparing the myeloid cells found in COVID-A versus COVID-R patients, there was a similar metabolic program driven by high expression of CPT1a and VDAC1, however, there was differential expression of HLA-DR (Figure 3.11C). During acute infection, a large portion of the $CPT1a^{+}VDAC1^{+}$ myeloid cells were $HLA\text{-}DR^{-}$, and thus classified as monocytic MDSC[236] (M-MDSC) (Figure 3.11C). A decrease in HLA-DR expression on myeloid cells during COVID-19 infection has been previously noted by other groups as well[128,235,237]. M-MDSC are known potent suppressors of T cell responses, and in line with this role of immunosuppression, they expressed diminished levels of costimulatory molecules such as CD86 compared to their $HLA\text{-}DR^{+}$ counterparts (Figure 3.11D). Further, they expressed elevated levels of CCR2, indicating recent migration out of the bone marrow (Figure 3.11D).

Conversely, the $HLA\text{-}DR^{+}$ component, composed of both $CD14^{+}$ and $CD16^{+}$ monocytes, was elevated during active infection, and remained high during recovery (Figure 3.11C). $HLA\text{-}DR^{+}$ monocytes are capable of producing robust amounts of cytokines and also providing antigen presentation and T cell costimulation, as indicated by the elevated CD86 expression (Figure 3.11D). The differential expression patterns of these monocytic populations between the infected and recovered patients may represent a shift from immunosuppressive (DR^{-}, MDSC) to a productive immune response (DR^{+}, stimulatory monocytes).

To better understand the function of the two subsets of $CPT1a^{+}VDAC1^{+}$ $HLA\text{-}DR^{-/+}$ cells, we assessed single-cell RNA sequencing data from the PBMC of three COVID-A

patients that had high levels of the CPT1a^{+}VDAC1^{+} myeloid cells, as determined by flow cytometry (Figure 3.11E). The analysis revealed four distinct clusters (Figure 3.11E). Clusters 1 and 3 both had elevated levels of VDAC1 and CPT1a, but cluster 1 expressed relatively lower levels of HLA-DR compared to cluster 3 (Figure 3.11E), corresponding to the two populations of cells identified by flow cytometry. Cluster 3 (HLA-DR^{+}) exhibited gene programs associated with a productive immune response, such as antigen processing/presentation and a type I IFN response (Figure 3.11F). In contrast, cluster 1, which demonstrated decreased HLA-DR expression and contained the cells that were more abundant in acute infection, expressed gene programs associated with reactive oxygen species (ROS) production, exocytosis and targeting proteins to the membrane surface (Figure 3.11F). Therefore, the gene programs supported the hypothesis of an increased immunosuppressive myeloid compartment during acute infection, which transitions into an immunostimulatory profile during resolution. Specifically, the HLA-DR^{-} cluster expressed high levels of genes for secreted alarmins such as S100A9 and S100A8 and chemokines such as CXCL2 and CXCL3[238] (Figure 3.11G). Overall, our data demonstrate that the immune activating DR^{+} cells are present in both the COVID-A and COVID-R patients (Figure 3.11H). However, the DR^{-} M-MDSC suppressor cells are found in the COVID-A patients but not the recovered COVID patients (Figure 3.11I).

The dichotomy based on HLA-DR expression of these metabolically unique cells and association with productive or inhibitory immune responses prompted us to examine the relationship between the HLA-DR^{+} and HLA-DR^{-} CPT1a^{+}VDAC1^{+} myeloid cells and disease severity. The CPT1a^{+}VDAC1^{+} HLA-DR^{-} cells represent less than 0.5% of

total PBMCS of COVID-R patients, however, the percentage of these cells is significantly higher in COVID-A patients requiring mechanical ventilation (on average 3.5% of PBMCs) than in COVID-A patients with less severe disease (0.7% of PBMCS) (Figure 3.11J). While we do not observe these cells in the (non-respiratory) hepatitis C infected patients, the DR^- cells are present in the influenza patients (Figure 3.11I,J). However, the overall percentage of these cells in the influenza patients is significantly lower than that of the severe COVID-A patients. All influenza patients recovered and this finding is consistent with the fact that although these patients have been hospitalized, they are more in line with the mild COVID-A patients and overall, far less ill than the severe COVID-A patients.

3.7 The Unique T cell and Myeloid Subsets in PBMC of Acutely Ill COVID-19 Patients Distinguishes Disease Severity

Finally, while our immune-metabolic approach has defined previously undescribed T cell and myeloid subsets in the COVID-A patients that provide insight into the mechanism of immune dysfunction and pathogenesis, we wondered whether the presence of these cells could be exploited to predict and track severity of disease. To this end, we used a random forest model to identify features most important in distinguishing COVID-19 patients from healthy controls, influenza, or between disease severity and recovery (Figure 3.12). We found that the proportion of $H3K27Me3^{hi}VDAC1^{hi}$ CD4 T cells was highly predictive when comparing healthy controls to COVID-19 (Figure 3.12A). Alternatively, when distinguishing between disease severity or between an otherwise similar respiratory viral disease, the innate compartment was highly informative (Figure 3.12B-C). As previously described, the absence of pDCs was able to distinguish mild from

severe COVID-19 (Figure 3.12C). However, we also found that the HKII^{+} PMN-MDSC cells we identified were associated with severe disease and could readily discriminate severe COVID from influenza, recovered and healthy controls (Figure 3.12A-B,D). In addition, CPT1a^{+}VDAC1^{+} myeloid cells (particularly the presence of HLA-DR^{-} M-MDSCs) were associated with more severe disease (Figure 3.12C). Finally, as prior publications have shown the association between COVID-19 severity and age, sex, and BMI, we further added these variables to our COVID-19 severity analysis[127] (Figure 3.12E). The feature importance analysis confirmed that in our data set sex and BMI are among the most important features in predicting COVID-19 severity. Interestingly, they were less predictive than the percentage of VDAC1^{+}CPT1a^{+} myeloid cells, pDC, and H3K27Me3^{hi}VDAC1^{hi} CD4^{+} cells (Figure 3.12E). Adding the percentage of VDAC1^{+}CPT1a^{+} myeloid cells, pDC, and H3K27Me3^{hi}VDAC1^{hi} CD4^{+} improved prediction of COVID-19 severity compared to basic clinical information (Figure 3.12F), highlighting the important contribution of the immune cell populations identified to disease severity. This model was validated using an additional 18 COVID-A patients and 5 COVID-R patients not studied in the original cohort (Figure 3.12G).

3.8 Perspectives and Future Directions

Considering that metabolic reprogramming plays an integral role in immune cell differentiation and function, we devised an assay to interrogate metabolic programs at a single cell level. Previous studies examining PBMC from COVID-19 patients have revealed generalized changes in cellular subsets and cytokines consistent with increased inflammation[127,128,226,229]. In contrast, by employing our approach we were will able to

identify robust, distinct T cell and myeloid subsets that were unique to the PBMC of the COVID-A patients. These previously undescribed populations of cells provide important insight into the immune dysfunction and pathogenesis of SARS-CoV-2 infection. Furthermore, as well as defining novel immune cell subsets, our approach reveals a new line of inquiry to understanding immune responses in general during infection, inflammatory diseases, and cancer.

Institutional safety protocols led to certain experimental limitations of our study. For example, mitochondrial studies had to be performed on fixed cells limiting the use of certain dyes and limiting our ability to extend the depth of our studies concerning mitochondrial dysfunction. Nonetheless, we employed 3 different microscopic techniques (Figure 3.5) to prove this point. Along these lines, the fact that the VBIT-4, the inhibitor of VDAC1 aggregation, promotes survival in the T cells from the COVID-19 patients but not healthy controls supports a role for VDAC1 in promoting cell death. While we also observe cytochrome *c* in the cytoplasm of such T cells, we have not definitively proven that VDAC1 pore formation leading to cytochrome *c* in the cytoplasm is the definitive/sole mechanism of cell death. Additionally, while our study is highlighted by insightful comparisons between SARS-CoV-2 infected patients and hospitalized influenza infected patients, limited availability of cells from the influenza cohort precluded more in depth functional comparisons between the two sets of patients.

In trying to understand the mechanism of pathogenesis of SARS-CoV-2 infection, there has been much focus on over exuberant immune responses and cytokine

storm[226,235,239]. In contrast, our data has revealed the presence of cells consistent with dysfunctional and suppressive immune responses. T cells play a critical role in both killing virally infected cells and providing help for effective and prolonged anti-viral antibody production[240]. Our data reveals the presence of populations of H3K27me3^{hi}VDAC1^{hi} T cells in the COVID-A patients. These cells expressed low levels of Glut1, the glucose transporter necessary to support glycolysis during effector responses. While increased VDAC1 levels in and of themselves might simply represent increased mitochondrial mass, we observed parameters indicative of mitochondrial dysfunction and apoptosis signaling in these cells, including altered mitochondrial ultrastructure and release of mitochondrial cytochrome *c* into the cytosol. Furthermore, observed loss of cell viability was reversed by treatment with the pan-caspase inhibitor Z-VAD, suggesting caspase dependent apoptosis. Rescue from cell death was likewise achieved by inhibiting VDAC1 oligomerization, further supporting a mitochondrial mediated cell death program. VDAC1 is the most prevalent protein in the mitochondrial outer membrane, and acts as the main transporter of nucleotides and metabolites across the mitochondrial membrane[241]. By interacting with pro-apoptotic BCL2 family members, VDAC1 oligomerization may allow for pores large enough for release of cytochrome *c* into the cytoplasm[224]. In addition, VDAC1 has also been shown to facilitate BAX/BAK mediated cell death[242–244].

The prevalence of the H3K27me3^{hi}VDAC1^{hi} T cells increased with age and such cells were observed in all of the patients over 70 years of age in our study. Interestingly, increased age is a known risk factor for severe COVID-19 and aging is associated with a

decline in lymphocyte mitochondrial fitness and activity[245,246]. Additionally, increased prevalence of the H3K27me3^{hi}VDAC1^{hi} T cells correlated with lymphopenia in the COVID-A patients. Lymphopenia has previously been described as a prominent feature of COVID-19 and our data suggest that mechanistically this may be due in part to mitochondrial-induced cell death[124]. To this end, our data support direct T cell death, as opposed to trafficking to inflamed organs such as the lung[247]. Further, this dysregulated T cell immunity could contribute to a lack of or waning protective immunity or impair the functionality of pre-existing cross-reactive T cell immunity[248,249]. Alternatively, it is possible that increased cell death of T cells is driving some of the dysregulated inflammation and autoimmune-like features characteristic of COVID-19. Finally, our data suggest that therapeutically targeting mitochondrial (metabolic) dysfunction might represent a successful strategy for abrogating disease.

The precise inflammatory mediators leading to the generation of the H3K27me3^{hi}VDAC1^{hi} T cells has yet to be determined. Several lines of evidence indicate that this T cell phenotype is driven by more than the cytokine environment or TCR stimulation alone. Memory T cell subsets are more responsive to secondary cytokine signaling compared to naïve T cells[250], however, elevated VDAC1 and H3K27me3 expression was found equally in the naïve and memory compartment. Further, there was no expansion of specific TCR clones within the H3K27me3^{hi}VDAC1^{hi} phenotype, indicating this is likely not driven by recent antigen-exposure. Because most of the hospitalized COVID-A patients were hypoxic, requiring supplemental oxygen, an interesting possibility is that SARS-CoV-2-induced inflammation in the setting of hypoxia

contributes to the generation of these dysfunctional T cells. Indeed, oxidative phosphorylation is required for maintenance of T cell function and is the predominant metabolic pathway utilized by resting T cells[251]. Thus, COVID-19 hypoxia combined with a specific inflammatory environment may lead to this metabolically dysregulated T cell phenotype.

Previous studies have demonstrated increased inflammation and activation of myeloid cells in COVID-19 patients[226,235,237]. However, it still remains unclear which of these responses are protective and which are pathogenic. Our identification of unique myeloid populations in the COVID-A patients shed light on the role of these cells. $HKII^+$ $VDAC1^+$ PMN-MDSC were exclusively upregulated in the COVID-A patients, suggesting that this population of cells is either contributing to pathogenesis or the consequence of dysregulated inflammatory responses. On the other hand, $CPT1a^+VDAC1^+DR^+$ monocytic cells were found in both the acute and recovered patients. DR^+ monocytes have previously been shown to be associated with productive immune responses in other respiratory viral infections[252] and single-cell RNA sequencing analysis revealed increased antigen processing/presentation and type I IFN responses in such cells. In contrast, the $CPT1a^+VDAC1^+DR^-$ M-MDSC were found exclusively in the COVID-A patients and further, the frequency of these cells was positively correlated with severity of disease. As such, the presence of these suppressor cells seems to be indicative of dysregulated inflammation. Finally, CPT1a has been associated with inflammasome activation, which has been observed in COVID-19 patients, and its role in fatty acid oxidation supports

modulators of either fatty acid oxidation or inflammasome signaling as potentially novel therapeutic targets to mitigate disease.

Finally, the unique cellular subsets described herein represent potentially potent biomarkers to predict and track severity of disease. The importance of the described cell populations is highlighted by their ability to robustly contribute to distinguishing severe and mild COVID-19 and acute COVID-19 from other viral infections. Consequently, tracking these unique cells might identify those at highest risk of disease progression and provide important criteria for enrollment into clinical trials as well as provide a surrogate marker for tracking efficacy of new potential treatments. Together, our data demonstrate the utility of broad immuno-metabolic phenotyping to identify subsets of immune cells that have the potential to not only provide insight into disease pathogenesis and predict severity of disease but also, importantly, to define novel metabolic targets for treatment.

Table 3.1. Characteristics of the 38 subjects with acute COVID-19

Demographics	
Male N (%)	19 (50)
Female N (%)	19 (50)
Mean age (range)	59.7 (20-82)
Mean BMI (range)	32.2 (17.5-51.2)
Current smoker N (%)	0 (0)
Race and Ethnicity	
Race	N (%)
Black	17 (47.5)
White	11 (28.9)
Other*	7 (18.4)
Asian	2 (5.2)
Ethnicity	
Hispanic/Latinx	N (%)
Yes	5 (13.2)
No	32 (86.8)
Maximum Disease Severity**	N (%)
$MinO_2$	14 (36.7)
HFO_2	4 (10.5)
Ventilated Lived	15 (39.5)
Died	5 (13.2)
Comorbidities	N (%)
Hypertension	21 (55.3)
Diabetes mellitus	15 (39.5)
COPD/asthma	12 (25.0)
Coronary artery disease	2 (5.2)
HIV infection	3 (7.9)

*Most self-identified as Hispanic/Latinx.

**Maximum disease severity indicates the most severe COVID-19 disease class for the patient while under observation: $MinO_2$= no or low flow oxygen required, HFO_2= high flow oxygen required, Ventilated= patient required intubation and survived, Died = patient died (ventilated or not)

Table 3.2. Characteristics of Study Subjects

	COVID-A	Influenza	COVID-R	Acute HCV	Chronic HCV
Demographics					
Male N (%)	19 (50)	9 (43)	6 (60)	2 (33)	7 (70)
Female N (%)	19 (50)	12 (57)	4 (40)	4 (67)	3 (30)
Mean age (range)	59.7 (20-82)	46.4 (22-89)	47.8 (18-81)	25.8 (24-28)	30.5 (26-35)

Figure 3.1. Gating strategies for COVID-19 flow cytometry panels.

Representative flow plots from an acute COVID-19 subject show gating of all peripheral immune cell subsets assessed by one of two immuno-metabolic panels (A) T cell panel or (B) Myeloid and B cell panel. C. Metabolic markers included in both panels to assess metabolic state of immune cell subsets.

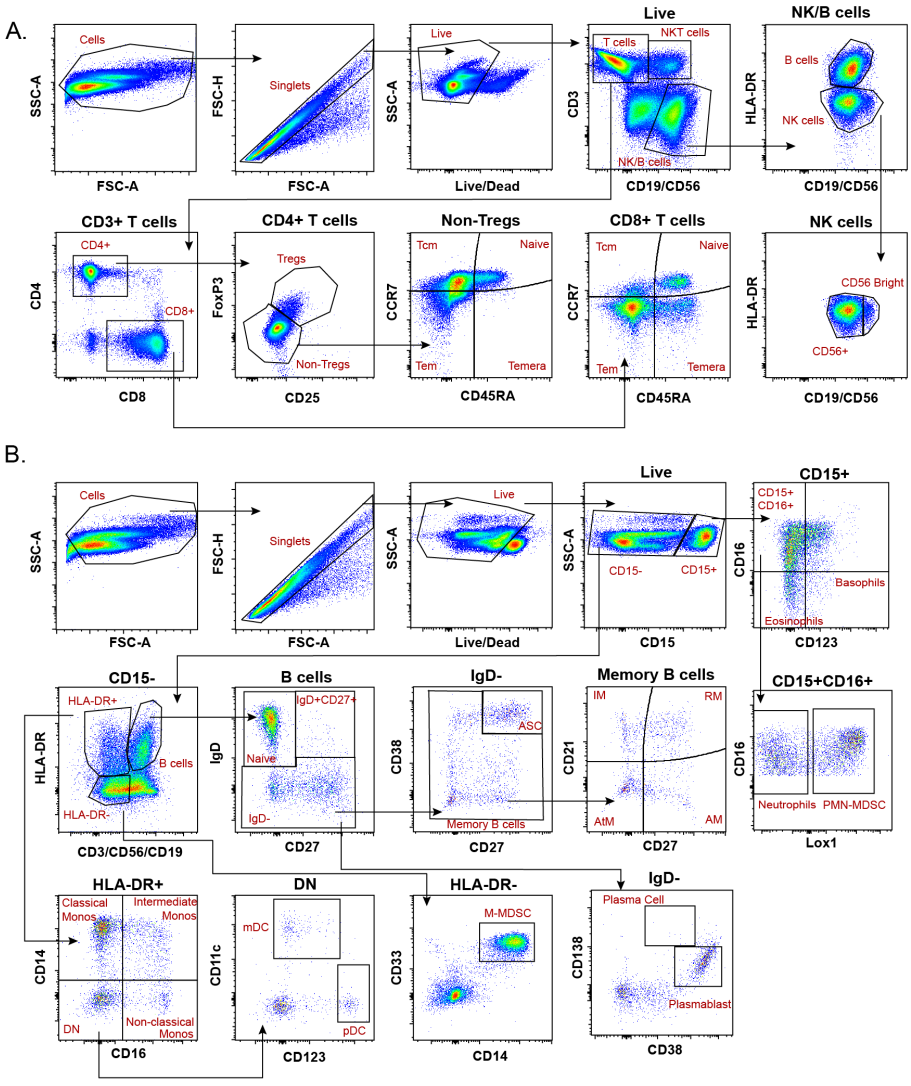

C.

Marker	Purpose
H3K27me3	Histone Methylation
CPT1a	Fatty Acid Oxidation
GLUT1	Glycolysis
Hexokinase II	Glycolysis
Tomm20	OXPHOS
VDAC1	OXPHOS

Figure 3.2. Frequencies of T cell subsets and activation markers reveal few COVID-19 specific differences.

A. Frequency of indicated cell subset as percent of total live cells. Each dot represents one individual, significance tested using unpaired Kruskal-Wallis test compared to healthy control. B. CD4:CD8 ratio. Each dot represents one individual, significance tested using unpaired Kruskal-Wallis test compared to healthy control. C. Frequency of $CD4^+$ and D. $CD8^+$ T cell subsets shown as percent of CD4 or CD8, respectively. Each dot represents one individual, significance tested using unpaired Kruskal-Wallis test compared to healthy control. E-G. UMAP projection of MFI heatmap overlays of indicated proteins. Significance is indicated as compared to healthy control, *p<0.05, **p<0.01,***p<0.001, ****p<0.0001, if no significance is indicated the test is non-significant.

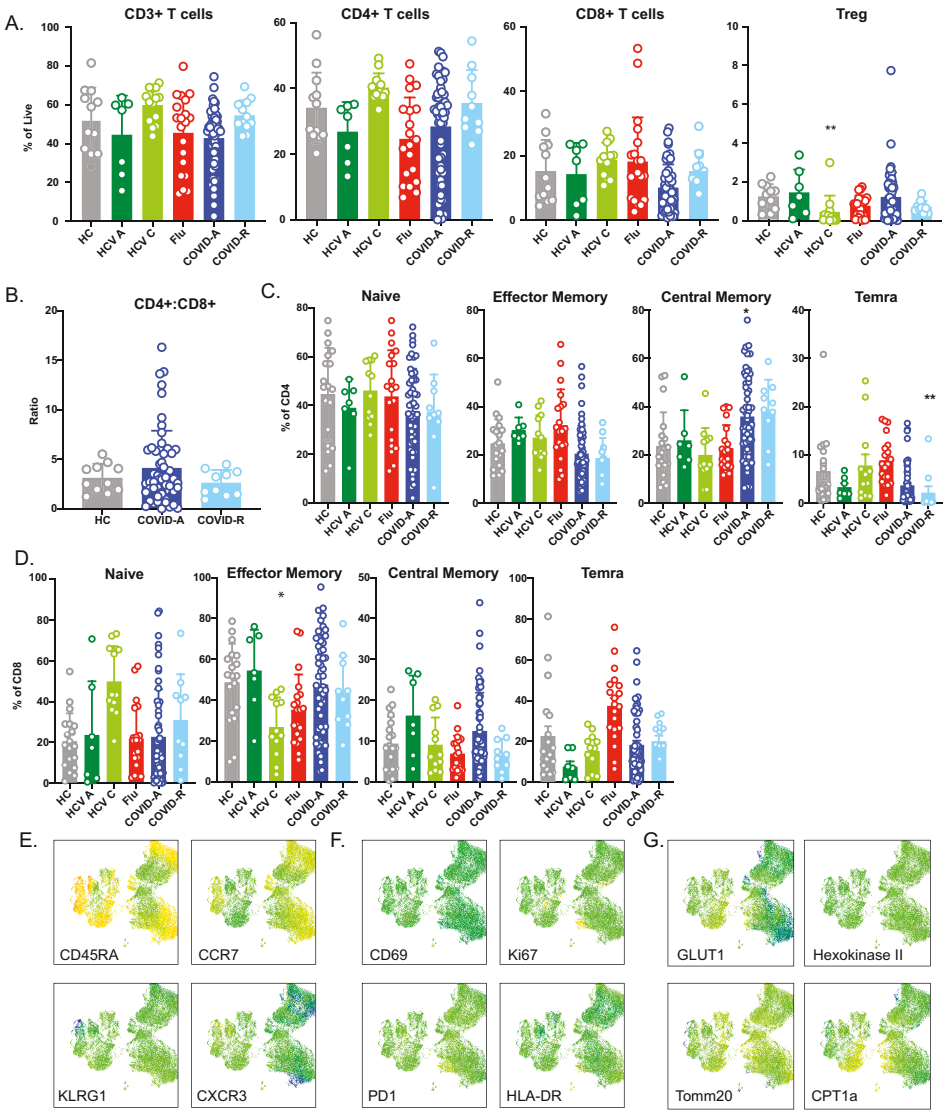

Figure 3.3. Identification of novel metabolically distinct T cells in COVID-19 patients.

A. Concatenated flow cytometry data depicted as UMAP projection of $CD3^+$ T cells from healthy control (HC, grey) and hospitalized acute COVID-19 patients (COVID-A, blue). The two markers discovered to drive segregation of the COVID-A and HC cluster, H3K27Me3 and VDAC1, are depicted as histogram overlays and MFI heatmap overlays on UMAP projection. B. Representative flow plots of $H3K27Me3^+VDAC1^+$ T cells. C. Healthy PBMCs were stimulated for 24 hours with anti-CD3 and anti-CD28 and evaluated for metabolic enzymes using flow cytometry. Representative histograms of unstimulated (grey) and stimulated (purple) cultures. D. Histograms comparing $H3K27Me3^+VDAC1^+$ T cells (pink) and remaining T cells (blue) from concatenated pooled COVID-A donors for indicated proteins. E. TCR Simpson Clonality from sorted $H3K27Me3^+VDAC1^+$ T cells (pink) and remaining T cells (blue). F. Frequency of $H3K27Me3^+VDAC1^+$ as percent of CD4 or CD8 T cells. Each dot represents one patient sample, significance tested using unpaired Mann-Whitney test. G. Frequency of $H3K27Me3^+VDAC1^+$ as percent of CD4 (black) or CD8 (grey) stratified by age of COVID-A patients.

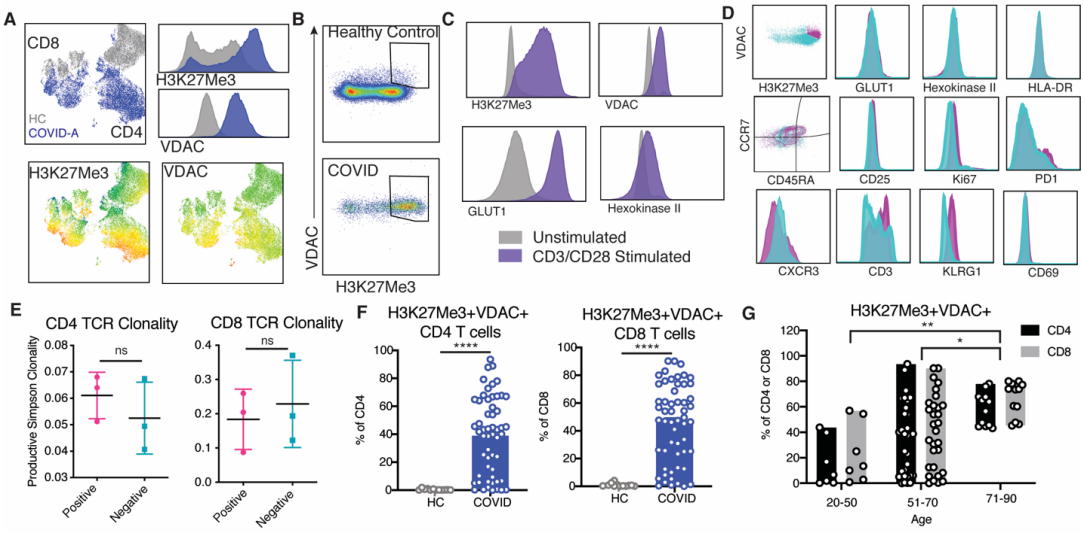

Figure 3.4. Novel H3K27me3^{hi}VDAC1^{hi} T cells are unique in COVID-19 compared with other viral infections.

A. UMAP projection of pooled donors with active infection, color coded by disease. B. UMAP projection of acute and recovered COVID-19 compared to healthy controls. C. UMAP projection of influenza and acute COVID-19 compared to healthy controls. D. Frequency of H3K27Me3^{+}VDAC1^{+} CD4 and CD8 T cells as percent of total live cells. E. Representative gating of H3K27Me3^{+}VDAC1^{+} CD4 T cells from multiple disease states. F. Hierarchical clustering of H3K27Me3^{+}VDAC1^{+} CD4 T cells based on expression (MFI values) of indicated proteins. Comparison of hospitalized acute COVID-19 infection (dark blue), recovered COVID-19 (light blue) and hospitalized influenza (red). G. Normalized MFI of GLUT1, TOMM20 and KLRG1 on H3K27Me3^{+}VDAC1^{+} CD4 T cells in all patients where H3K27Me3^{+}VDAC^{+} T cells compromise greater than 10% of total CD4 population and representative histogram overlays of MFI. Each dot represents one patient sample, significance tested using unpaired Kruskal-Wallis test compared to healthy control (D) or every combination (G). *p < 0.05, **p < 0.01, ***p < 0.001, and ****p < 0.0001.

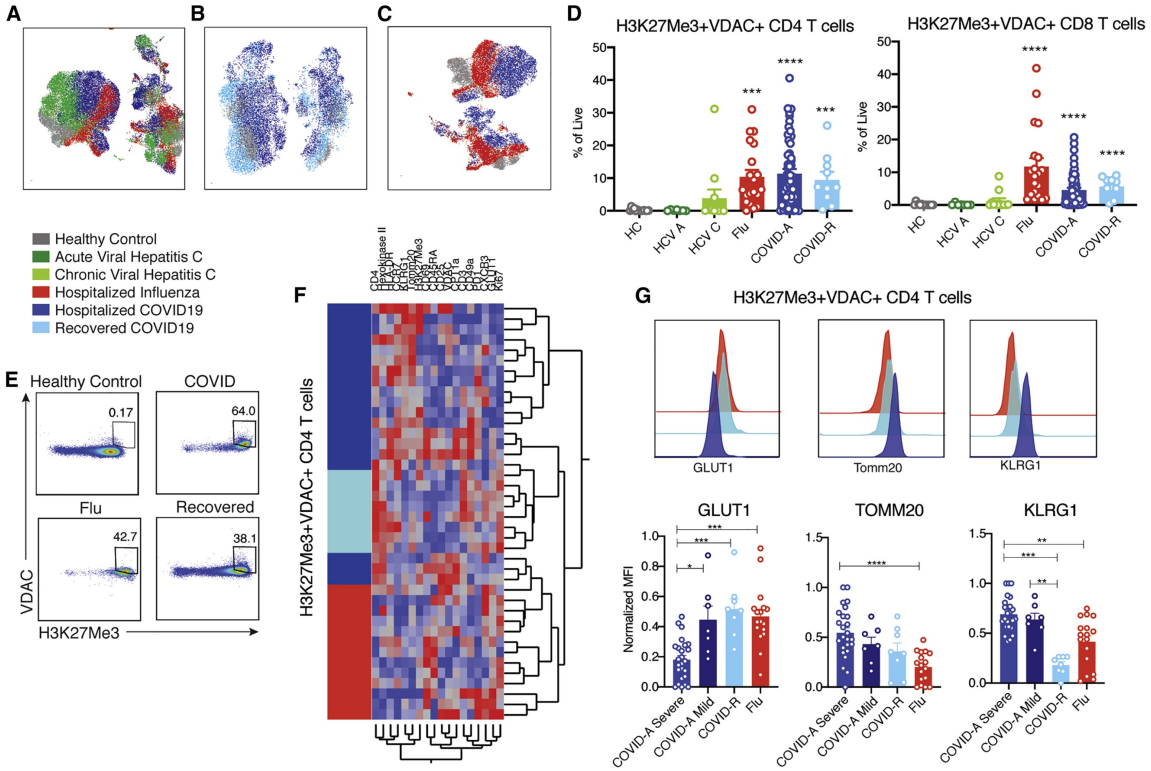

Figure 3.5. T cells from COVID-19 subjects demonstrate parameters of mitochondrial dysfunction and apoptosis signaling, correlating with development of lymphopenia.

A. Single-cell RNA sequencing analysis of 6 COVID-19 subjects and 3 HC were evaluated for $CD3^+$ T cells. Genes distinguishing T cells from COVID-19 patients compared to HC were evaluated for statistical over representation using GO biological processes as gene sets and categorized into higher level annotation using ReviGO. Displayed is the enrichment score for each gene set and color corresponds to programs in upregulated genes (red) and downregulated genes (blue). B. Representative electron microscopy images of PBMCs from a COVID-A patient and a healthy control. C. Representative confocal images of PBMCs from a COVID-A patient and healthy control with mitochondria labeled using MitoTracker Deep Red (pink), $CD3^+$ T cells labeled (green) and nuclei labeled with DAPI (blue). D. Representative fluorescence images of PBMCs from 3 COVID-A subjects and one healthy control (left) immunostained for cytochrome *c* (green) and CD3 (red), and nuclei labeled with DAPI (blue). Plot profiles of intracellular cytochrome *c* fluorescence intensity distribution (right). E. Correlation of lymphocyte count with frequency of $H3K27Me3^+VDAC1^+$ out of total $CD4^+$ T cells from day 0-6 (left) or day 7-14 (right) of study enrollment, including all symptomatic patients. Each dot represents one subject and color corresponds to days since onset of lymphopenia (black = no COVID-19 related lymphopenia developed). Correlation tested using non-parametric Spearman correlation.

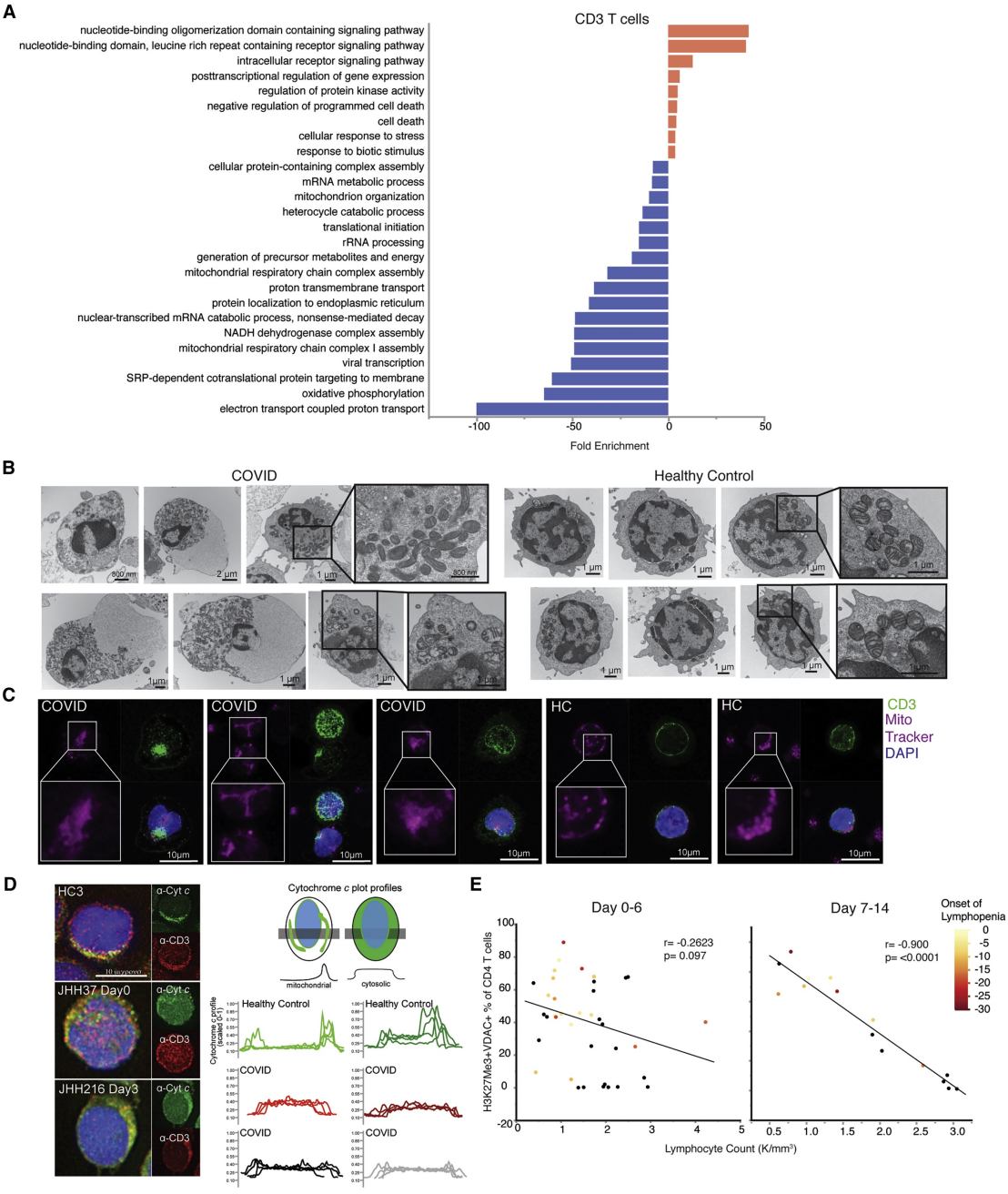
A
CD3 T cells
nucleotide-binding oligomerization domain containing signaling pathway
nucleotide-binding domain, leucine rich repeat containing receptor signaling pathway
intracellular receptor signaling pathway
posttranscriptional regulation of gene expression
regulation of protein kinase activity
negative regulation of programmed cell death
cell death
cellular response to stress
response to biotic stimulus
cellular protein-containing complex assembly
mRNA metabolic process
mitochondrion organization
heterocycle catabolic process
translational initiation
rRNA processing
generation of precursor metabolites and energy
mitochondrial respiratory chain complex assembly
proton transmembrane transport
protein localization to endoplasmic reticulum
nuclear-transcribed mRNA catabolic process, nonsense-mediated decay
NADH dehydrogenase complex assembly
mitochondrial respiratory chain complex I assembly
viral transcription
SRP-dependent cotranslational protein targeting to membrane
oxidative phosphorylation
electron transport coupled proton transport
-100
-50
0
50
Fold Enrichment
B
COVID
Healthy Control
C
COVID
COVID
COVID
HC
HC
CD3
Mito Tracker
DAPI
10μm
D
HC3
α-Cyt c
α-CD3
JHH37 Day0
JHH216 Day3
Cytochrome c plot profiles
mitochondrial
cytosolic
Healthy Control
COVID
Cytochrome c profile (scaled 0-1)
E
Day 0-6
Day 7-14
r= -0.2623
p= 0.097
r= -0.900
p= <0.0001
Onset of Lymphopenia
H3K27Me3+VDAC+ % of CD4 T cells
Lymphocyte Count (K/mm³)

Figure 3.6. Loss of T cell survival can be rescued by targeting VDAC1 or caspases.

A. PBMCs from acute COVID-19 patients or healthy controls were cultured for 48 hours in media, rapamycin (100nM), VBIT-4 (300nM), or ZVAD (60nM). T cell survival was calculated as the percent CD4 or CD8 T cells remaining from initial plating. Significance tested using two-way ANOVA with each drug compared to the media control, n=9. B. T cells were stimulated with anti-CD3/CD28 (purple) for 48 hours and surviving T cells from COVID-19 patients are able to respond by upregulating HLA-DR, CD69, CD25 and GLUT1 to the same extent as healthy controls compared to unstimulated controls (grey). C. Graphical depiction of proposed mechanism of mitochondrial cell death signaling in COVID-19 T cells. D. Representative plots show increased $H3K27me3^{+}VDAC^{+}$ $CD4^{+}$ T cells in a COVID-A subject with cells stained fresh compared to after cryopreservation. *p < 0.05, **p < 0.01, ***p < 0.001, and ****p < 0.0001.

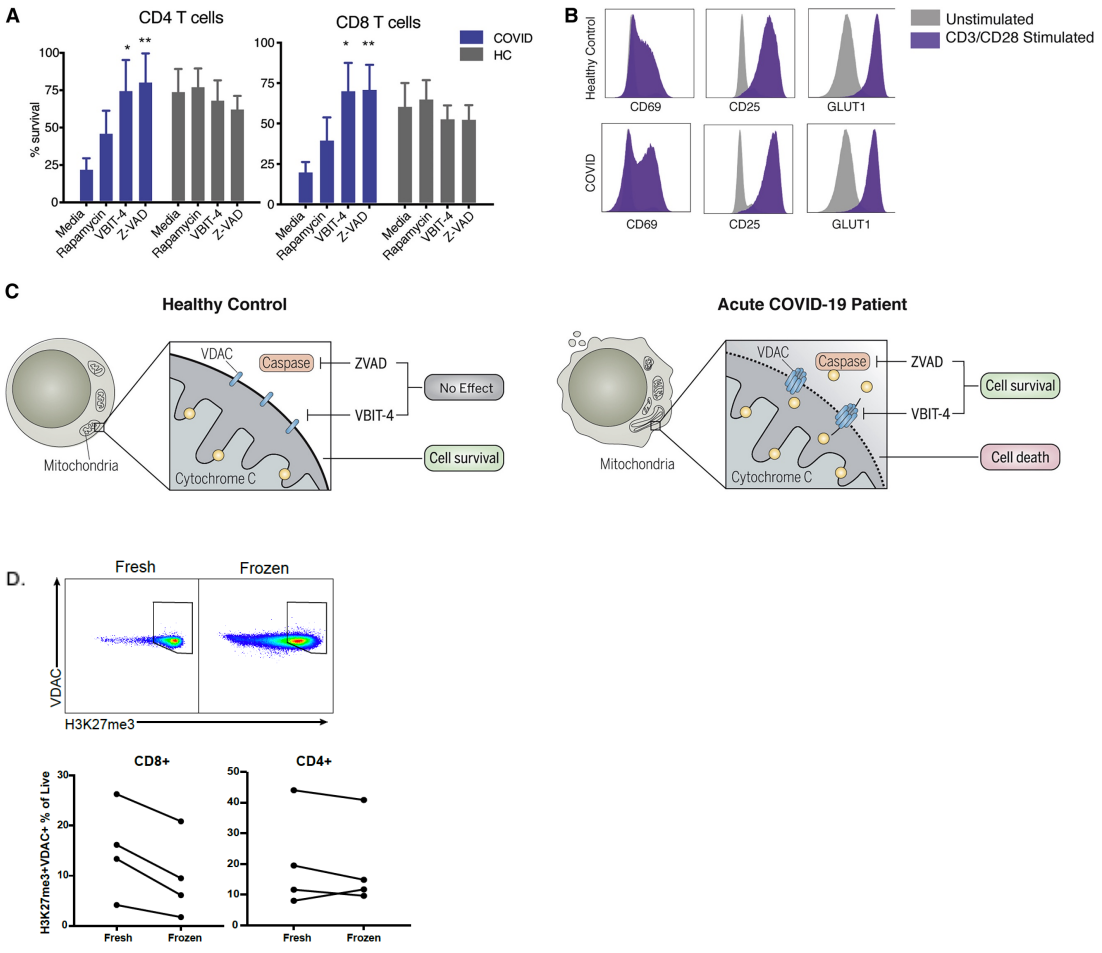

Figure 3.7. B cell frequencies and phenotypes differ in the memory compartment in COVID-19.

A-D. Frequency of indicated cell subset as percent of total live cells. Each dot represents one individual, significance tested using unpaired Kruskal-Wallis test compared to healthy control. (E-F) UMAP projection performed on a subset of COVID-A (blue), hospitalized Flu (red) and HC subjects (grey) (E) or COVID-A (blue) and COVID-R (light blue) (F). Manual gating overlays on UMAP projection color code total B cell (top) and memory B cell (bottom) subsets. UMAP projection MFI heat maps of indicated proteins. Significance is indicated as compared to healthy control, *p<0.05, **p<0.01, ***p<0.001, ****p<0.0001, if no significance is indicated the test is non-significant.

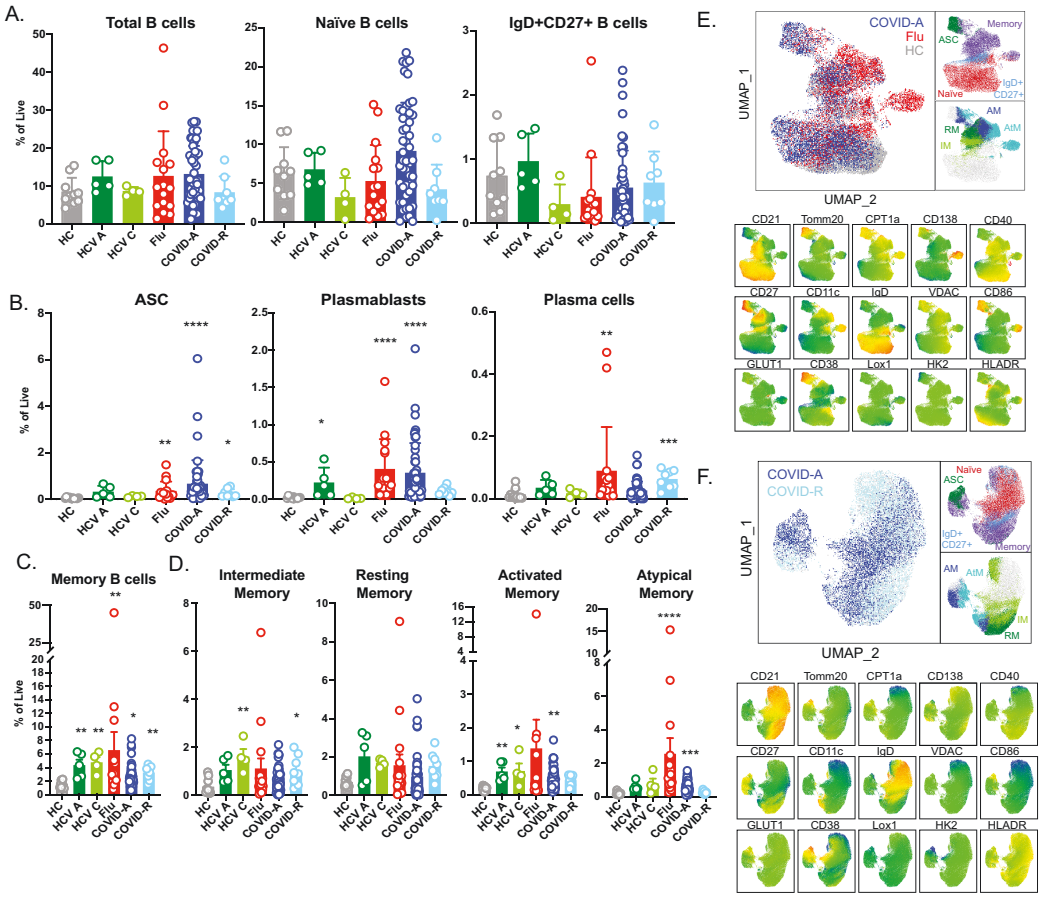

Figure 3.8. Unique NK cell population in COVID-A subjects identified by high-dimensional phenotyping analysis.

A. Frequency of indicated cell subset as percent of total live cells. Each dot represents one individual, significance tested using unpaired Kruskal-Wallis test compared to healthy control. B. UMAP projection of total NK cells performed on a subset of COVID-A (blue), hospitalized Flu (red) and HC subjects (grey) (left). Arrow indicates unique COVID-A specific cluster identified. Manual gating overlays on UMAP projection (top) color code CD56+ (purple) and CD56 bright (pink) cells. UMAP projection MFI heat maps of indicated proteins are shown right. C. Similar analysis as in (B) was performed on a subset of COVID-A (blue) compared to COVID-R (light blue) subjects. Significance is indicated as compared to healthy control, *p<0.05, **p<0.01, ***p<0.001, ****p<0.0001, if no significance is indicated the test is non-significant.

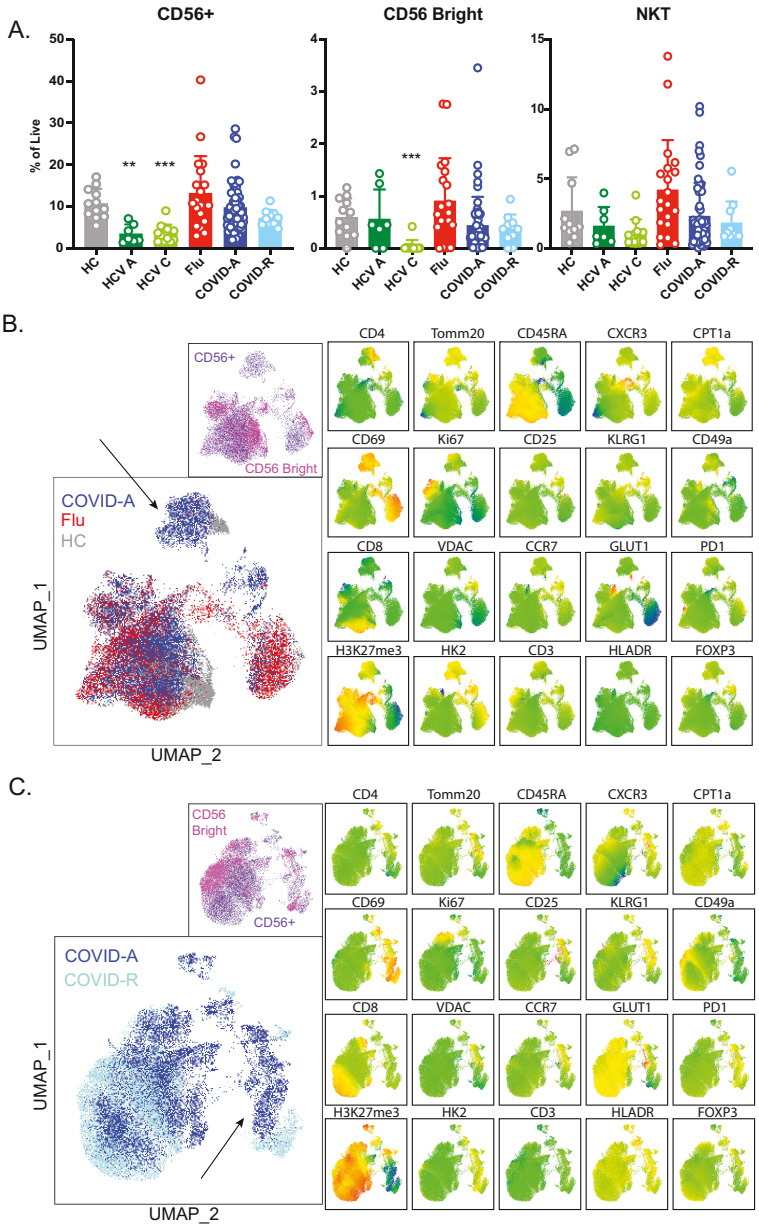

Figure 3.9. Myeloid subsets in viral infections.

A-C. Frequency of indicated cell subset as percent of total live cells. Each dot represents one individual, significance tested using unpaired Kruskal-Wallis test compared to healthy control. D. Frequency of indicated cell subset as percent of total live cells. To assess how dendritic cell frequencies changed in recovery, significance was tested using unpaired Kruskal-Wallis test comparing all possible combinations. E. UMAP projection of total myeloid cells performed on a subset of hospitalized Flu (red) and HC subjects (grey). Manual gating overlays on UMAP projection color code myeloid and B cell subsets in the UMAP space. MFI histogram overlays of $CD14^{+}$ myeloid populations of indicated proteins for hospitalized Flu (red) and HC (grey). Significance is indicated as compared to healthy control (A-C), or between groups (D). F. Frequency of indicated cell subset as percent of total live cells when sample was processed fresh or after cryopreservation (frozen). Each dot represents one individual. Significance tested using Wilcoxon matched-pairs signed rank test. G. Principal component analysis of frequencies of innate cell subsets show differences driven by patient variability and not cryopreservation. *$p<0.05$, **$p<0.01$, ***$p<0.001$, ****$p<0.0001$, if no significance is indicated the test is non-significant.

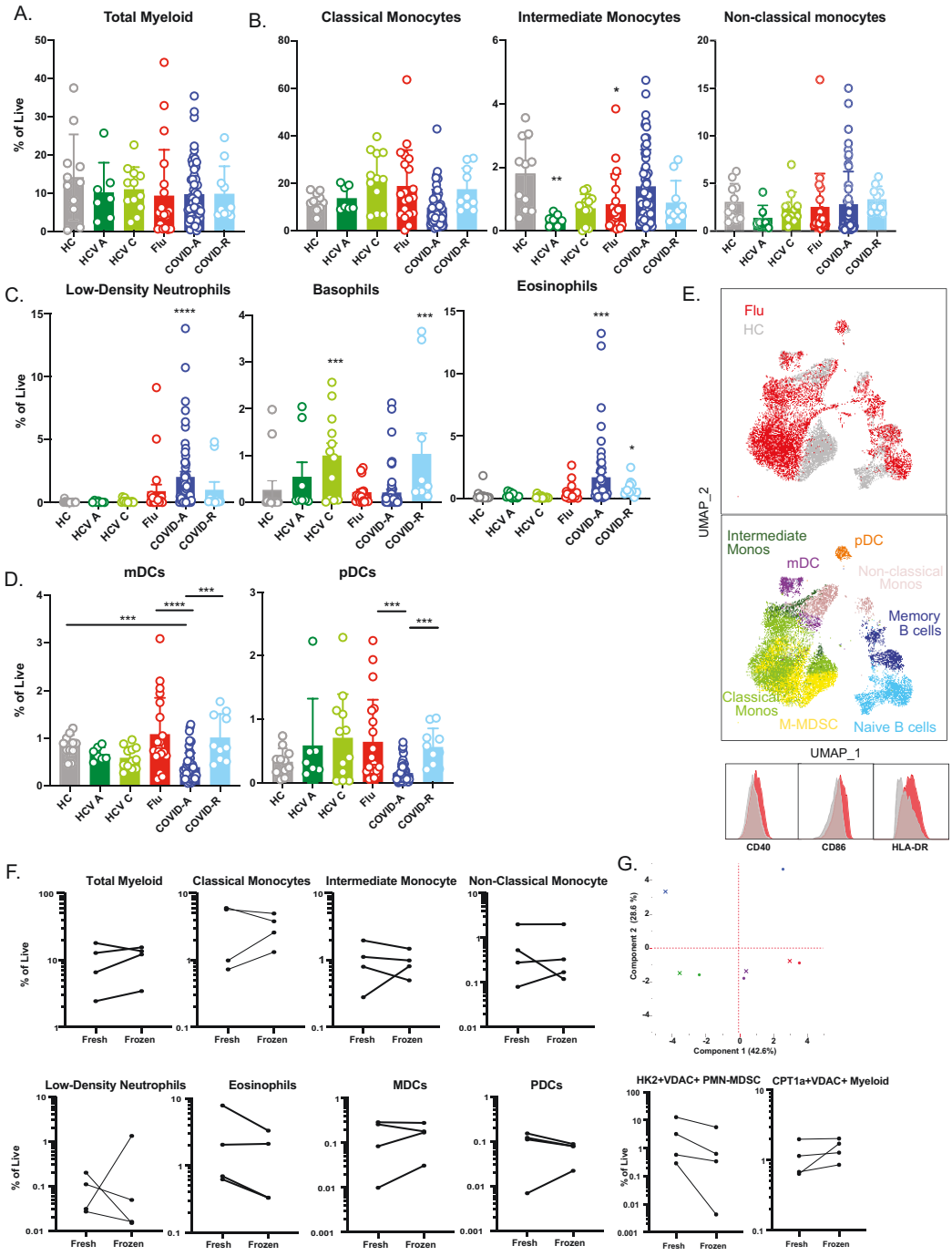
A.
Total Myeloid
% of Live
B.
Classical Monocytes
Intermediate Monocytes
Non-classical monocytes
HC
HCV A
HCV C
Flu
COVID-A
COVID-R
C.
Low-Density Neutrophils
Basophils
Eosinophils
D.
mDCs
pDCs
E.
Flu
HC
UMAP_2
Intermediate Monos
pDC
mDC
Non-classical Monos
Memory B cells
Classical Monos
M-MDSC
Naive B cells
UMAP_1
CD40
CD86
HLA-DR
F.
Total Myeloid
Classical Monocytes
Intermediate Monocyte
Non-Classical Monocyte
% of Live
Fresh
Frozen
Low-Density Neutrophils
Eosinophils
MDCs
PDCs
HK2+VDAC+ PMN-MDSC
CPT1a+VDAC+ Myeloid
G.
Component 2 (28.6 %)
Component 1 (42.6%)

Figure 3.10. Metabolically distinct granulocytic immunosuppressive myeloid derived suppressor cells in PBMC of COVID-19 patients.

A. Concatenated flow cytometry data depicted as UMAP projection of $CD3^{-}CD19^{-}CD56^{-}$ myeloid cells from healthy control (HC, grey) and acute COVID-19 patients (COVID-A, blue). B. UMAP projection of MFI heatmap overlays of indicated proteins. C. Representative gating of $CD15^{+}$ granulocytic subsets basophils, eosinophils, neutrophils and PMN-MDSC across all disease states studied. D. Flow plot comparing HKII and VDAC1 expression in HC T cells (grey), COVID-A T cells (dark blue) and COVID-A PMN-MDSC (light blue). E. Frequency of indicated cell subset as percent of total live cells. Each dot represents one patient sample, significance tested using unpaired Kruskal-Wallis test compared to healthy control. *p < 0.05, **p < 0.01, ***p < 0.001, and ****p < 0.0001

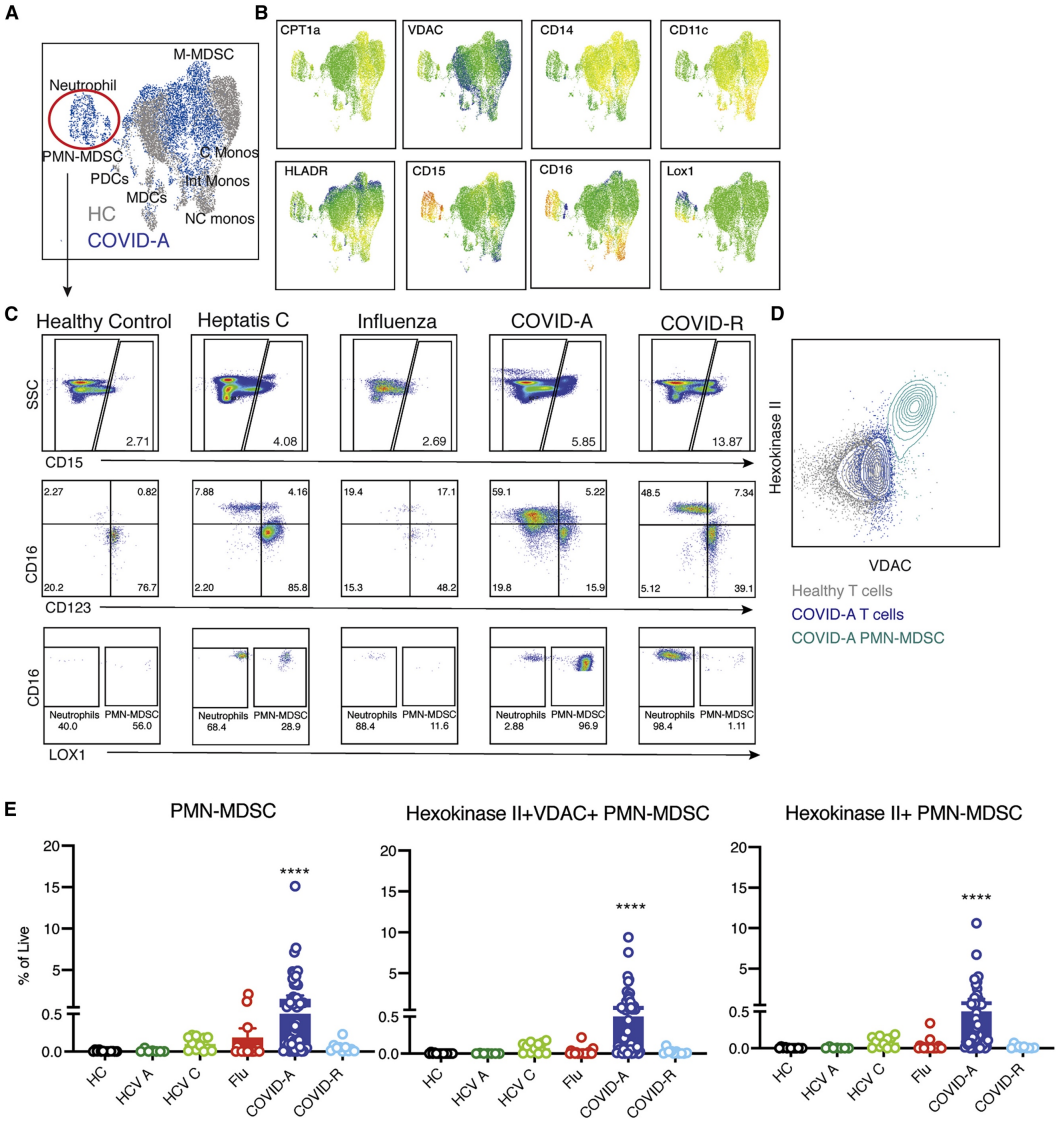

Figure 3.11. Identification of metabolically distinct monocytic myeloid derived suppressor cells in PBMC of COVID-19 patients track with disease severity.

A. Concatenated flow cytometry data depicted as UMAP projection of $CD3^{-}CD19^{-}CD56^{-}$ myeloid cells from healthy control (HC, grey) and acute COVID-19 patients (COVID-A, blue). B. Histogram overlays of MFI for metabolic markers CPT1a and VDAC1 from HC (grey) or COVID-A patients (blue). C. Representative gating of $CPT1a^{+}VDAC1^{+}$ myeloid cells (gated on $CD3^{-}CD19^{-}CD56^{-}$ and $CD33^{+}$) and subset of $CPT1a^{+}VDAC1^{+}$ cells based on HLA-DR expression. D. Histogram overlays of MFI for indicated proteins from CPT1a+VDAC1+HLA-DR+ (red) or CPT1a+VDAC1+HLA-DR- (orange) cells. E. UMAP projection of scRNA seq of myeloid cells from three COVID patients with detectable $CPT1a^{+}VDAC1^{+}$ myeloid cells by flow cytometry colored by identified clusters 0-3. Expression of indicated genes within cluster 0-3. Each dot represents a single cell. F. Genes identifying cluster 1 ($CPT1a^{+}VDAC1^{+}$ HLA-DR^{dim}) and cluster 3 ($CPT1a^{+}VDAC1^{+}$ HLA-DR^{high}) were evaluated for statistical over representation using GO biological processes as gene sets and categorized into higher level annotation using ReviGO. Heatmap color corresponds to the enrichment score in upregulated genes (red) and downregulated genes (blue), x indicates a non-significant enrichment. G. Expression of indicated gene within cluster 0-3. Each dot represents a single cell. H-I. Frequency of HLA-DR^{-} $CPT1a^{+}VDAC1^{+}$ myeloid cells and HLA-DR^{+} $CPT1a^{+}VDAC1^{+}$ myeloid cells as percent of total live cells. Each dot represents one individual, significance tested using unpaired Kruskal-Wallis test compared to healthy control. J. Frequency of $CPT1a^{+}VDAC1^{+}$ $DR^{+/-}$ cells in COVID-A patients were stratified by disease severity (Severe= deceased or required mechanical ventilation, Mild= hospitalized with low or high flow oxygen). Each dot represents one patient sample, significance tested using two-way ANOVA comparing either HLA-DR^{+} vs HLA-DR^{-} within each category or HLA-DR^{+} or HLA-DR^{-} across each category. *p < 0.05, **p < 0.01, ***p < 0.001, and ****p < 0.0001

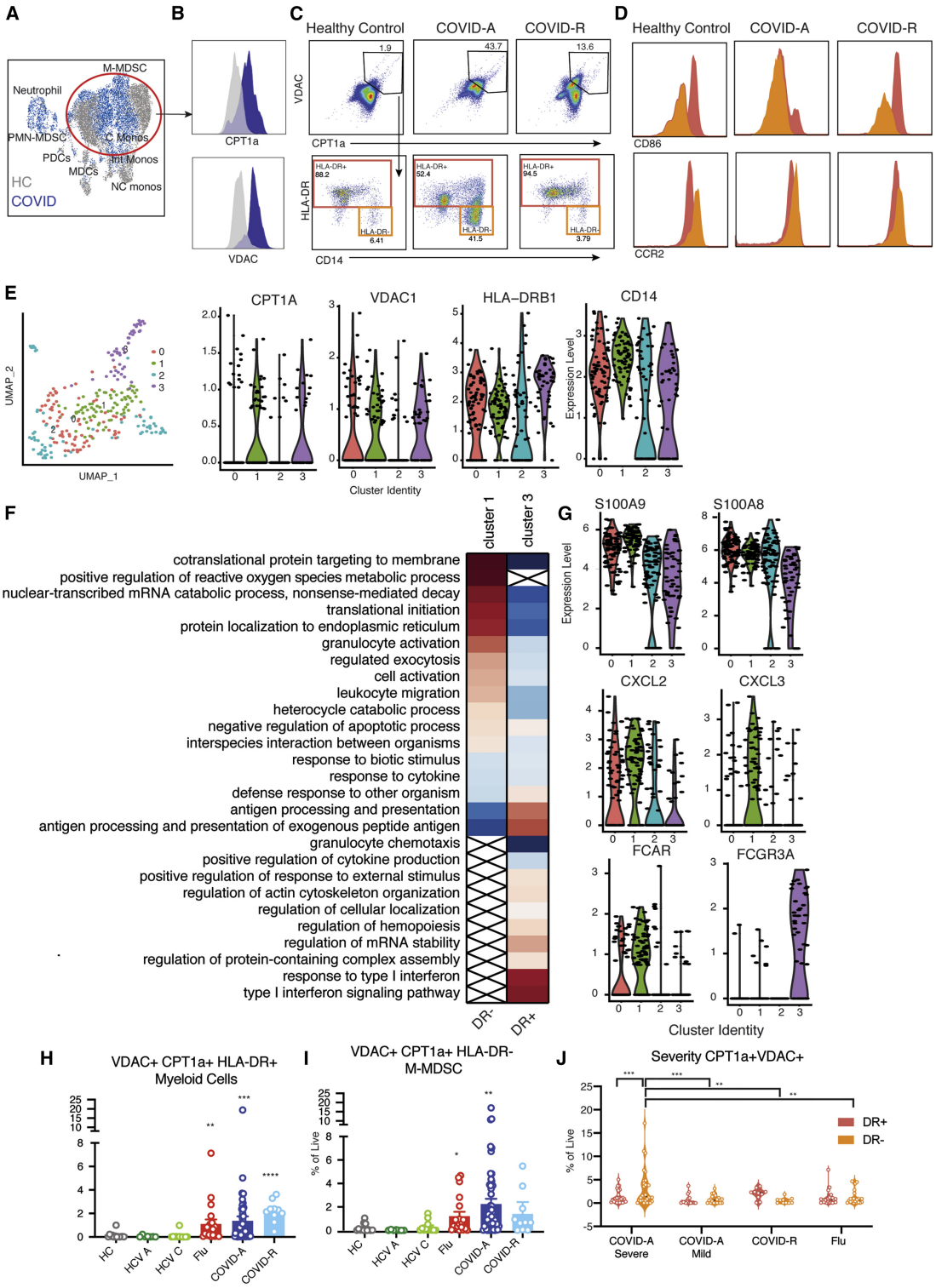
A
M-MDSC
Neutrophil
PMN-MDSC
C Monos
PDCs
Int Monos
MDCs
NC monos
HC
COVID
B
CPT1a
VDAC
C
Healthy Control
COVID-A
COVID-R
VDAC
CPT1a
HLA-DR
CD14
D
Healthy Control
COVID-A
COVID-R
CD86
CCR2
E
UMAP_2
UMAP_1
CPT1A
VDAC1
HLA–DRB1
CD14
Expression Level
Cluster Identity
F
cotranslational protein targeting to membrane
positive regulation of reactive oxygen species metabolic process
nuclear-transcribed mRNA catabolic process, nonsense-mediated decay
translational initiation
protein localization to endoplasmic reticulum
granulocyte activation
regulated exocytosis
cell activation
leukocyte migration
heterocycle catabolic process
negative regulation of apoptotic process
interspecies interaction between organisms
response to biotic stimulus
response to cytokine
defense response to other organism
antigen processing and presentation
antigen processing and presentation of exogenous peptide antigen
granulocyte chemotaxis
positive regulation of cytokine production
positive regulation of response to external stimulus
regulation of actin cytoskeleton organization
regulation of cellular localization
regulation of hemopoiesis
regulation of mRNA stability
regulation of protein-containing complex assembly
response to type I interferon
type I interferon signaling pathway
cluster 1
cluster 3
DR-
DR+
G
S100A9
S100A8
CXCL2
CXCL3
FCAR
FCGR3A
Expression Level
Cluster Identity
H
VDAC+ CPT1a+ HLA-DR+
Myeloid Cells
% of Live
HC
HCV A
HCV C
Flu
COVID-A
COVID-R
I
VDAC+ CPT1a+ HLA-DR-
M-MDSC
% of Live
J
Severity CPT1a+VDAC+
% of Live
DR+
DR-
COVID-A Severe
COVID-A Mild
COVID-R
Flu

Figure 3.12. Presence of immune cells with distinct metabolic profiles predicts disease severity.

A-D. Feature importance of distinguishing COVID-A patients and healthy controls, COVID-A patients and Flu patients, severe COVID-A patients and COVID-R patients, or severe COVID-A patients and mild COVID-A patients as indicated. Each feature is depicted as a frequency of total live cells, unless otherwise indicated in the case of proportion of cell subset with a specific metabolic phenotype. E. Feature importance analysis after adding basic clinical information (i.e., age, sex, and BMI) to the RF model for classifying severe vs. mild COVID-A. F. ROC curves for comparing the performance of prediction models trained using the top-five-ranked features (i.e., top5) and basic clinical information (i.e., baseline) for classifying severe vs. mild COVID-A. AUC is indicated. G. The data were confirmed using a validation cohort including 5 COVID-R, 10 severe COVID-A, 8 mild COVID-A and 5 healthy controls (HC).

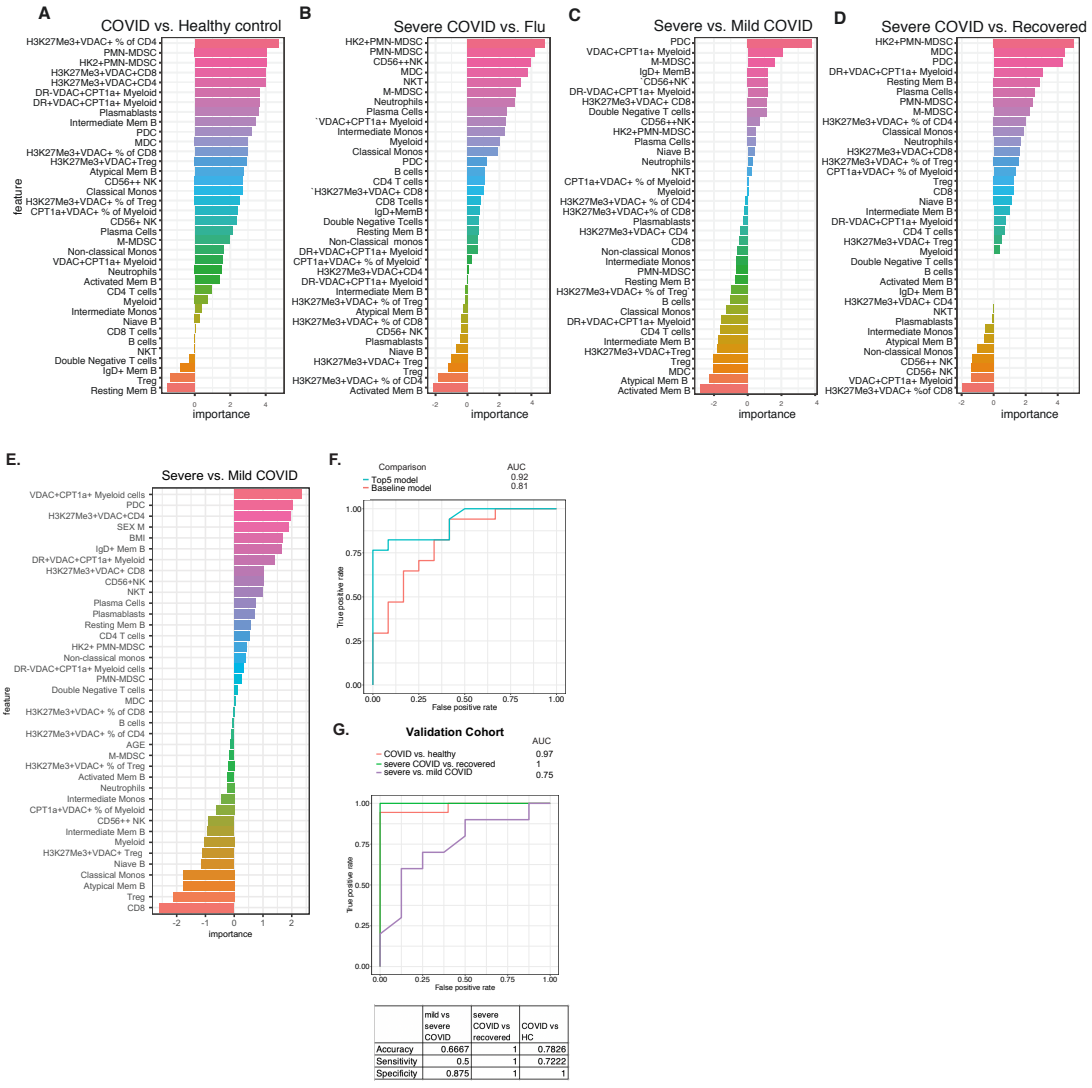

References

1. Chaplin, D. D. Overview of the immune response. *J. Allergy Clin. Immunol.* **125**, S3 (2010).
2. Takeuchi, O. & Akira, S. Innate immunity to virus infection. *Immunol. Rev.* **227**, 75–86 (2009).
3. Koyama, S., Ishii, K. J., Coban, C. & Akira, S. Innate immune response to viral infection. *Cytokine* **43**, 336–341 (2008).
4. Amulic, B., Cazalet, C., Hayes, G. L., Metzler, K. D. & Zychlinsky, A. Neutrophil function: From mechanisms to disease. *Annual Review of Immunology* **30**, 459–489 (2012).
5. Vivier, E., Tomasello, E., Baratin, M., Walzer, T. & Ugolini, S. Functions of natural killer cells. *Nature Immunology* **9**, 503–510 (2008).
6. Fitzgerald-Bocarsly, P., Dai, J. & Singh, S. Plasmacytoid dendritic cells and type I IFN: 50 years of convergent history. *Cytokine Growth Factor Rev.* **19**, 3–19 (2008).
7. Webster, B. *et al.* Plasmacytoid dendritic cells control dengue and chikungunya virus infections via IRF7-regulated interferon responses. *Elife* **7**, (2018).
8. Ley, K. M1 Means Kill; M2 Means Heal. *J. Immunol.* **199**, 2191–2193 (2017).
9. Pawelec, G., Verschoor, C. P. & Ostrand-Rosenberg, S. Myeloid-derived suppressor cells: Not only in tumor immunity. *Frontiers in Immunology* **10**, 1099 (2019).
10. Sprent, J. Antigen-Presenting Cells: Professionals and amateurs. *Curr. Biol.* **5**, 1095–1097 (1995).

11. Kranich, J. & Krautler, N. J. How follicular dendritic cells shape the B-cell antigenome. *Frontiers in Immunology* **7**, 225 (2016).

12. Christensen, J. E. & Thomsen, A. R. Co-ordinating innate and adaptive immunity to viral infection: mobility is the key. *APMIS* **117**, 338–355 (2009).

13. Zhang, N. & Bevan, M. J. CD8+ T Cells: Foot Soldiers of the Immune System. *Immunity* **35**, 161–168 (2011).

14. Swain, S. L., McKinstry, K. K. & Strutt, T. M. Expanding roles for CD4 + T cells in immunity to viruses. *Nature Reviews Immunology* **12**, 136–148 (2012).

15. Miossec, P. & Kolls, J. K. Targeting IL-17 and T H 17 cells in chronic inflammation. *Nature Reviews Drug Discovery* **11**, 763–776 (2012).

16. Crotty, S. T Follicular Helper Cell Differentiation, Function, and Roles in Disease. *Immunity* **41**, 529–542 (2014).

17. Kondělková, K. *et al.* Regulatory T cells (TREG) and their roles in immune system with respect to immunopathological disorders. *Acta medica (Hradec Králové) / Universitas Carolina, Facultas Medica Hradec Králové* **53**, 73–77 (2010).

18. Lu, L. L., Suscovich, T. J., Fortune, S. M. & Alter, G. Beyond binding: Antibody effector functions in infectious diseases. *Nature Reviews Immunology* **18**, 46–61 (2018).

19. Fink, K. Origin and function of circulating plasmablasts during acute viral infections. *Front. Immunol.* **3**, 1–5 (2012).

20. Akkaya, M., Kwak, K. & Pierce, S. K. B cell memory: building two walls of protection against pathogens. *Nature Reviews Immunology* **20**, 229–238 (2020).

21. O'Neill, L. A. J., Kishton, R. J. & Rathmell, J. A guide to immunometabolism for immunologists. *Nature Reviews Immunology* **16**, 553–565 (2016).

22. Li, X. B., Gu, J. D. & Zhou, Q. H. Review of aerobic glycolysis and its key enzymes - new targets for lung cancer therapy. *Thoracic Cancer* **6**, 17–24 (2015).

23. Warburg, O., Wind, F. & Negelein, E. The metabolism of tumors in the body. *J. Gen. Physiol.* **8**, 519–530 (1927).

24. Heiden, M. G. V., Cantley, L. C. & Thompson, C. B. Understanding the warburg effect: The metabolic requirements of cell proliferation. *Science* **324**, 1029–1033 (2009).

25. Rodríguez-Prados, J.-C. *et al.* Substrate Fate in Activated Macrophages: A Comparison between Innate, Classic, and Alternative Activation. *J. Immunol.* **185**, 605–614 (2010).

26. Krawczyk, C. M. *et al.* Toll-like receptor-induced changes in glycolytic metabolism regulate dendritic cell activation. *Blood* **115**, 4742–4749 (2010).

27. Donnelly, R. P. *et al.* mTORC1-Dependent Metabolic Reprogramming Is a Prerequisite for NK Cell Effector Function. *J. Immunol.* **193**, 4477–4484 (2014).

28. Michalek, R. D. *et al.* Cutting Edge: Distinct Glycolytic and Lipid Oxidative Metabolic Programs Are Essential for Effector and Regulatory CD4 + T Cell Subsets . *J. Immunol.* **186**, 3299–3303 (2011).

29. Doughty, C. A. *et al.* Antigen receptor-mediated changes in glucose metabolism in B lymphocytes: Role of phosphatidylinositol 3-kinase signaling in the glycolytic control of growth. *Blood* **107**, 4458–4465 (2006).

30. O'Sullivan, D. *et al.* Memory CD8+ T Cells Use Cell-Intrinsic Lipolysis to Support the Metabolic Programming Necessary for Development. *Immunity* **41**, 75–88 (2014).

31. Martínez-Reyes, I. & Chandel, N. S. Mitochondrial TCA cycle metabolites control physiology and disease. *Nature Communications* **11**, 1–11 (2020).

32. Jha, A. K. *et al.* Network integration of parallel metabolic and transcriptional data reveals metabolic modules that regulate macrophage polarization. *Immunity* **42**, 419–430 (2015).

33. Tannahill, G. M. *et al.* Succinate is an inflammatory signal that induces IL-1β through HIF-1α. *Nature* **496**, 238–242 (2013).

34. Houten, S. M., Violante, S., Ventura, F. V. & Wanders, R. J. A. The Biochemistry and Physiology of Mitochondrial Fatty Acid β-Oxidation and Its Genetic Disorders. *Annu. Rev. Physiol.* **78**, 23–44 (2016).

35. Van Der Windt, G. J. W. *et al.* CD8 memory T cells have a bioenergetic advantage that underlies their rapid recall ability. *Proc. Natl. Acad. Sci. U. S. A.* **110**, 14336–14341 (2013).

36. Posokhova, E. N., Khoshchenko, O. M., Chasovskikh, M. I., Pivovarova, E. N. & Dushkin, M. I. Lipid synthesis in macrophages during inflammation in vivo: Effect of agonists of peroxisome proliferator activated receptors α and γ and of retinoid X receptors. *Biochem.* **73**, 296–304 (2008).

37. World Health Organization. *Global Hepatitis Report, 2017*. *World Health Organisation* (2017). doi:10.1016/j.poly.2012.11.010

38. Nelson, N. P. *et al.* Epidemiology of Hepatitis B Virus Infection and Impact of Vaccination on Disease. *Clin Liver dis* **20**, 607–628 (2016).

39. Hyams, K. C. Risks of Chronicity Following Acute Hepatitis B Virus Infection: A Review. *Clin. Infect. Dis.* **20**, 992–1000 (1995).

40. Gerlich, W. H. Prophylactic vaccination against hepatitis B: achievements, challenges and perspectives. *Med. Microbiol. Immunol.* **204**, 39–55 (2015).

41. Thio, C. L., Guo, N., Xie, C., Nelson, K. E. & Ehrhardt, S. Global elimination of mother-to-child transmission of hepatitis B: Revisiting the current strategy. *The Lancet Infectious Diseases* **15**, 981–985 (2015).

42. Liang, T. J. *et al.* Present and future therapies of hepatitis B: From discovery to cure. *Hepatology* **62**, 1893–1908 (2015).

43. Timothy M. Block, Tianlun Zhou, Nikhil Anbarasan, and R. G. Evolving new strategies for the medical management of chronic hepatitis B virus infection. *Gastroenterol. Hepatol.* **12**, 679–689 (2016).

44. Lamontagne, R. J., Bagga, S. & Bouchard, M. J. Hepatitis B virus molecular biology and pathogenesis. *Hepatoma Res.* **2**, 163 (2016).

45. Seeger, C. & Mason, W. S. Molecular biology of hepatitis B virus infection. *Virology* **479**–**480**, 672–686 (2015).

46. Schulze, A., Gripon, P. & Urban, S. Hepatitis B virus infection initiates with a large surface protein-dependent binding to heparan sulfate proteoglycans. *Hepatology* **46**, 1759–1768 (2007).

47. Bertoletti, A. & Ferrari, C. Adaptive immunity in HBV infection. *J. Hepatol.* **64**,

S71–S83 (2016).

48. Yan, H. *et al.* Sodium taurocholate cotransporting polypeptide is a functional receptor for human hepatitis B and D virus. *Elife* **1**, 1–28 (2012).

49. Tsukuda, S. & Watashi, K. Hepatitis B virus biology and life cycle. *Antiviral Res.* **182**, 104925 (2020).

50. T Jake, L. Hepatitis B: The Virus and Disease. *Hepatology* **49**, S13–S21 (2009).

51. Karayiannis, P. Hepatitis B virus: virology, molecular biology, life cycle and intrahepatic spread. *Hepatology International* **11**, 500–508 (2017).

52. Liu, S., Zhou, B., Valdes, J. D., Sun, J. & Guo, H. Serum Hepatitis B Virus RNA: A New Potential Biomarker for Chronic Hepatitis B Virus Infection. *Hepatology* **69**, 1816–1827 (2019).

53. Bill, C. A. & Summers, J. Genomic DNA double-strand breaks are targets for hepadnaviral DNA integration. *Proc. Natl. Acad. Sci. U. S. A.* **101**, 11135–11140 (2004).

54. Watanabe, T. *et al.* Involvement of host cellular multivesicular body functions in hepatitis B virus budding. *Proc. Natl. Acad. Sci. U. S. A.* **104**, 10205–10210 (2007).

55. Nowak, M. A. *et al.* Viral dynamics in hepatitis B virus infection. *Proc. Natl. Acad. Sci. U. S. A.* **93**, 4398–4402 (1996).

56. Chai, N. *et al.* Properties of Subviral Particles of Hepatitis B Virus. *J. Virol.* **82**, 7812–7817 (2008).

57. Milich, D. R. & Mclachlan, A. The nucleocapsid of hepatitis B virus is both a T-cell-independent and a T-cell-dependent antigen. *Science (80-.).* **234**, 1398–1401

(1986).

58. Gerlich, W. H. Medical Virology of Hepatitis B: how it began and where we are now. *Virol. J.* **10**, 239 (2013).

59. Croagh, C. M. N. & Lubel, J. S. Natural history of chronic hepatitis B: Phases in a complex relationship. *World J. Gastroenterol.* **20**, 10395–10404 (2014).

60. Yuen, M. F. *et al.* Hepatitis B virus infection. *Nature Reviews Disease Primers* **4**, 1–20 (2018).

61. Thimme, R. *et al.* CD8+ T Cells Mediate Viral Clearance and Disease Pathogenesis during Acute Hepatitis B Virus Infection. *J. Virol.* **77**, 68–76 (2003).

62. Guidotti, L G; Ishikawa, T; Hobbs, M V; Matzke, B; Schreiber, R; Chisari, F. V. Intracellular inactivation of the hepatitis B virus by the immune response. *Immunity* **4**, 25–36 (1996).

63. Guidotti, L. G. *et al.* Viral clearance without destruction of infected cells during acute HBV infection. *Science (80-.).* **284**, 825–829 (1999).

64. Webster, G. J. M. *et al.* Incubation phase of acute hepatitis B in man: Dynamic of cellular immune mechanisms. *Hepatology* **32**, 1117–1124 (2000).

65. Asabe, S. *et al.* The Size of the Viral Inoculum Contributes to the Outcome of Hepatitis B Virus Infection. *J. Virol.* **83**, 9652–9662 (2009).

66. Penna, A. *et al.* Cytotoxic T lymphocytes recognize an HLA-A2-restricted epitope within the hepatitis B virus nucleocapsid antigen. *J. Exp. Med.* **174**, 1565–1570 (1991).

67. Nayersina, R. *et al.* HLA A2 restricted cytotoxic T lymphocyte responses to

multiple hepatitis B surface antigen epitopes during hepatitis B virus infection. *J. Immunol.* **150**, (1993).

68. Rehermann, B. *et al.* The cytotoxic T lymphocyte response to multiple hepatitis B virus polymerase epitopes during and after acute viral hepatitis. *J. Exp. Med.* **181**, 1047–1058 (1995).

69. Boni, C. *et al.* Restored function of HBV-specific T cells after long-term effective therapy with nucleos(t)ide analogues. *Gastroenterology* **143**, 963-973.e9 (2012).

70. Hoogeveen, R. C. *et al.* Phenotype and function of HBV-specific T cells is determined by the targeted epitope in addition to the stage of infection. *Gut* **0**, 1–12 (2018).

71. Maini, M. K. *et al. Direct Ex Vivo Analysis of Hepatitis B Virus-Specific CD8 T Cells Associated With the Control of Infection*.

72. Ferrari, C. *et al.* Cellular immune response to hepatitis B virus-encoded antigens in acute and chronic hepatitis B virus infection. *J. Immunol.* **145**, (1990).

73. Boni, C. *et al.* Characterization of Hepatitis B Virus (HBV)-Specific T-Cell Dysfunction in Chronic HBV Infection. *J. Virol.* **81**, 4215–4225 (2007).

74. Schuch, A. *et al.* Phenotypic and functional differences of HBV core-specific versus HBV polymerase-specific CD8+ T cells in chronically HBV-infected patients with low viral load. *Gut* gutjnl-2018-316641 (2019). doi:10.1136/gutjnl-2018-316641

75. Kim, J. H. *et al.* circulating serum HBsAg level is a biomarker for HBV-specific T and B cell responses in chronic hepatitis B patients. *Sci. RepoRtS* | **10**, 1835 (2020).

76. Le Bert, N. *et al.* Effects of Hepatitis B Surface Antigen on Virus-Specific and

Global T Cells in Patients With Chronic Hepatitis B Virus infection. *Gastroenterology* **159**, 652–664 (2020).

77. Boettler, T. *et al.* Expression of the Interleukin-7 Receptor Alpha Chain (CD127) on Virus-Specific CD8+ T Cells Identifies Functionally and Phenotypically Defined Memory T Cells during Acute Resolving Hepatitis B Virus Infection. *J. Virol.* **80**, 3532–3540 (2006).

78. Heim, K., Neumann-Haefelin, C., Thimme, R. & Hofmann, M. Heterogeneity of HBV-Specific CD8+ T-Cell Failure: Implications for Immunotherapy. *Frontiers in Immunology* **10**, 2240 (2019).

79. Cheng, Y. *et al.* Multifactorial heterogeneity of virus-specific T cells and association with the progression of human chronic hepatitis B infection. *Sci. Immunol.* **4**, 6905 (2019).

80. Speiser, D. E. *et al.* T cell differentiation in chronic infection and cancer: Functional adaptation or exhaustion? *Nature Reviews Immunology* **14**, 768–774 (2014).

81. Schurich, A. *et al.* Role of the coinhibitory receptor cytotoxic T lymphocyte antigen-4 on apoptosis-Prone CD8 T cells in persistent hepatitis B virus infection. *Hepatology* **53**, 1494–1503 (2011).

82. Wu, W. *et al.* Blockade of Tim-3 signaling restores the virus-specific CD8 + T-cell response in patients with chronic hepatitis B. *Eur. J. Immunol.* **42**, 1180–1191 (2012).

83. Bengsch, B., Martin, B. & Thimme, R. Restoration of HBV-specific CD8+ T cell

function by PD-1 blockade in inactive carrier patients is linked to T cell differentiation. *J. Hepatol.* **61**, 1212–1219 (2014).

84. Fisicaro, P. *et al.* Antiviral Intrahepatic T-Cell Responses Can Be Restored by Blocking Programmed Death-1 Pathway in Chronic Hepatitis B. *Gastroenterology* **138**, 682-693.e4 (2010).

85. El-Khoueiry, A. B. *et al.* Nivolumab in patients with advanced hepatocellular carcinoma (CheckMate 040): an open-label, non-comparative, phase 1/2 dose escalation and expansion trial. *Lancet* **389**, 2492–2502 (2017).

86. Gane, E. *et al.* Anti-PD-1 blockade with nivolumab with and without therapeutic vaccination for virally suppressed chronic hepatitis B: A pilot study. *J. Hepatol.* **71**, 900–907 (2019).

87. Corti, D., Benigni, F. & Shouval, D. Viral envelope-specific antibodies in chronic hepatitis B virus infection. *Curr. Opin. Virol.* **30**, 48–57 (2018).

88. Lee, C., Gong, Y., Brok, J., Boxall, E. H. & Gluud, C. Effect of hepatitis B immunisation in newborn infants of mothers positive for hepatitis B surface antigen: Systematic review and meta-analysis. *British Medical Journal* **332**, 328–332 (2006).

89. Cholongitas, E., Goulis, J., Akriviadis, E. & Papatheodoridis, G. V. Hepatitis B immunoglobulin and/or nucleos(t)ide analogues for prophylaxis against hepatitis b virus recurrence after liver transplantation: A systematic review. *Liver Transplant.* **17**, 1176–1190 (2011).

90. Loomba, R. & Liang, T. J. Hepatitis B Reactivation Associated With Immune

Suppressive and Biological Modifier Therapies: Current Concepts, Management Strategies, and Future Directions. *Gastroenterology* **152**, 1297–1309 (2017).

91. Lee, J. *et al.* Rituximab and hepatitis B reactivation in HBsAg-negative/anti-HBc-positive kidney transplant recipients. *Nephrol. Dial. Transplant.* **32**, 722–729 (2017).

92. Paul, S. *et al.* Role of surface antibody in hepatitis B reactivation in patients with resolved infection and hematologic malignancy: A meta-analysis. *Hepatology* **66**, 379–388 (2017).

93. Leandro, M. J. B-cell subpopulations in humans and their differential susceptibility to depletion with anti-CD20 monoclonal antibodies. *Arthritis Research and Therapy* **15**, S3 (2013).

94. Oliviero, B. *et al.* Enhanced B-cell differentiation and reduced proliferative capacity in chronic hepatitis C and chronic hepatitis B virus infections. *J. Hepatol.* **55**, 53–60 (2011).

95. Xu, X. *et al.* Reversal of B-cell hyperactivation and functional impairment is associated with HBsAg seroconversion in chronic hepatitis B patients. *Cell. Mol. Immunol.* **12**, 309–316 (2015).

96. Das, A. *et al.* IL-10-Producing Regulatory B Cells in the Pathogenesis of Chronic Hepatitis B Virus Infection. *J. Immunol.* **189**, 3925–3935 (2012).

97. Gong, Y. *et al.* Role of IL-10-Producing Regulatory B Cells in Chronic Hepatitis B Virus Infection. *Dig. Dis. Sci.* **60**, 1308–1314 (2015).

98. Salimzadeh, L. *et al.* PD-1 blockade partially recovers dysfunctional virus-specific B

cells in chronic hepatitis B infection. *J. Clin. Invest.* **128**, 4573–4587 (2018).

99. Burton, A. R. *et al.* Circulating and intrahepatic antiviral B cells are defective in hepatitis B. *J. Clin. Invest.* **128**, 4588–4603 (2018).

100. Gerlich, W. H. The enigma of concurrent hepatitis B surface antigen (HBsAg) and antibodies to HBsAg. *Clinical Infectious Diseases* **44**, 1170–1172 (2007).

101. Rydell, G. E., Prakash, K., Norder, H. & Lindh, M. Hepatitis B surface antigen on subviral particles reduces the neutralizing effect of anti-HBs antibodies on hepatitis B viral particles in vitro. *Virology* **509**, 67–70 (2017).

102. Barnaba, V., Franco, A., Alberti, A., Benvenuto, R. & Balsano, F. Selective killing of hepatitis B envelope antigen-specific B cells by class I-restricted, exogenous antigen-specific T lymphocytes. *Nature* **345**, 258–260 (1990).

103. Madaliński, K. & Bragiel, I. HBsAg immune complexes in the course of infection with hepatitis B virus. *Clin. Exp. Immunol.* **36**, 371–8 (1979).

104. Portugal, S., Obeng-Adjei, N., Moir, S., Crompton, P. D. & Pierce, S. K. Atypical memory B cells in human chronic infectious diseases: An interim report. *Cell. Immunol.* **321**, 18–25 (2017).

105. Le Bert, N. *et al.* Comparative characterization of B cells specific for HBV nucleocapsid and envelope proteins in patients with chronic hepatitis B. *J. Hepatol.* **72**, 34–44 (2020).

106. Vanwolleghem, T. *et al.* Hepatitis B core-specific memory B cell responses associate with clinical parameters in patients with chronic HBV. *J. Hepatol.* **73**, 52–61 (2020).

107. Ma, Z., Zhang, E., Gao, S., Xiong, Y. & Lu, M. Toward a functional cure for hepatitis B: The rationale and challenges for therapeutic targeting of the b cell immune response. *Frontiers in Immunology* **10**, 2308 (2019).

108. Thio, C. L. Hepatitis B and human immunodeficiency virus coinfection. *Hepatology* **49**, S138–S145 (2009).

109. Alter, M. J. Epidemiology of viral hepatitis and HIV co-infection. in *Journal of Hepatology* **44**, S6–S9 (Elsevier, 2006).

110. Bodsworth, N. J., Cooper, D. A. & Donovan, B. The influence of human immunodeficiency virus type 1 infection on the development of the hepatitis b virus carrier state. *J. Infect. Dis.* **163**, 1138–1140 (1991).

111. Hadler, S. C. *et al.* Outcome of hepatitis B virus infection in homosexual men and its relation to prior human immunodeficiency virus infection. *J. Infect. Dis.* **163**, 454–459 (1991).

112. Gilson, R. J. C. *et al.* Interactions between HIV and hepatitis B virus in homosexual men: Effects on the natural history of infection. *AIDS* **11**, 597–606 (1997).

113. Colin, J. F. *et al.* Influence of human immunodeficiency virus infection on chronic hepatitis B in homosexual men. *Hepatology* **29**, 1306–1310 (1999).

114. RJ, B., JJ, G. & J, H. Accelerated Loss of Antibody to Hepatitis B Surface Antigen among Immunodeficient Homosexual Men Infected with HIV. *N. Engl. J. Med.* **316**, 630–631 (1987).

115. Laukamm-Josten, U. *et al.* Decline of naturally acquired antibodies to hepatitis B surface antigen in HIV-1 infected homosexual men. *AIDS (London, England)* **2**,

400–401 (1988).

116. Thio, C. L. *et al.* HIV-1, hepatitis B virus, and risk of liver-related mortality in the Multicenter Cohort Study (MACS). *Lancet* **360**, 1921–1926 (2002).

117. Hoffmann, C. J. & Thio, C. L. Clinical implications of HIV and hepatitis B co-infection in Asia and Africa. *Lancet Infectious Diseases* **7**, 402–409 (2007).

118. Dong, E., Du, H. & Gardner, L. An interactive web-based dashboard to track COVID-19 in real time. *The Lancet Infectious Diseases* **20**, 533–534 (2020).

119. Wu, Z. & McGoogan, J. M. Characteristics of and Important Lessons from the Coronavirus Disease 2019 (COVID-19) Outbreak in China: Summary of a Report of 72314 Cases from the Chinese Center for Disease Control and Prevention. *JAMA - Journal of the American Medical Association* **323**, 1239–1242 (2020).

120. Ye, Z. W. *et al.* Zoonotic origins of human coronaviruses. *International Journal of Biological Sciences* **16**, 1686–1697 (2020).

121. Astuti, I. & Ysrafil. Severe Acute Respiratory Syndrome Coronavirus 2 (SARS-CoV-2): An overview of viral structure and host response. *Diabetes Metab. Syndr. Clin. Res. Rev.* **14**, 407–412 (2020).

122. Hoffmann, M. *et al.* SARS-CoV-2 Cell Entry Depends on ACE2 and TMPRSS2 and Is Blocked by a Clinically Proven Protease Inhibitor. *Cell* **181**, 271-280.e8 (2020).

123. V'kovski, P., Kratzel, A., Steiner, S., Stalder, H. & Thiel, V. Coronavirus biology and replication: implications for SARS-CoV-2. *Nature Reviews Microbiology* **19**, 155–170 (2020).

124. Huang, C. *et al.* Clinical features of patients infected with 2019 novel coronavirus

in Wuhan, China. *Lancet* **395**, 497–506 (2020).

125. Kuri-Cervantes, L. *et al.* Comprehensive mapping of immune perturbations associated with severe COVID-19. *Sci. Immunol.* **5**, (2020).

126. Laing, A. G. *et al.* A dynamic COVID-19 immune signature includes associations with poor prognosis. *Nat. Med.* **26**, 1623–1635 (2020).

127. Mathew, D. *et al.* Deep immune profiling of COVID-19 patients reveals distinct immunotypes with therapeutic implications. *Science (80-.).* eabc8511 (2020). doi:10.1126/science.abc8511

128. Wilk, A. J. *et al.* A single-cell atlas of the peripheral immune response in patients with severe COVID-19. *Nat. Med.* **26**, 1070–1076 (2020).

129. Nolan, J. P. & Condello, D. Spectral flow cytometry. *Curr. Protoc. Cytom.* **Chapter 1**, (2013).

130. Hartmann, F. J. & Bendall, S. C. Immune monitoring using mass cytometry and related high-dimensional imaging approaches. *Nature Reviews Rheumatology* **16**, 87–99 (2020).

131. Mahnke, Y. D. & Roederer, M. Optimizing a Multicolor Immunophenotyping Assay. *Clin. Lab. Med.* **27**, 469–485 (2007).

132. Maciorowski, Z., Chattopadhyay, P. K. & Jain, P. Basic multicolor flow cytometry. *Curr. Protoc. Immunol.* **2017**, 5.4.1-5.4.38 (2017).

133. Nguyen, R., Perfetto, S., Mahnke, Y. D., Chattopadhyay, P. & Roederer, M. Quantifying Spillover Spreading for Comparing Instrument Performance and Aiding in Multicolor Panel Design. *Cytom. Part A* **83**, 306–315 (2013).

134. Roederer, M. Compensation in flow cytometry. *Curr. Protoc. Cytom.* **Chapter 1**, (2002).

135. Kaslow, R. A. *et al.* The Multicenter AIDS Cohort Study: Rationale, Organization, and Selected Characteristics of the Participants. *Am. J. Epidemiol.* **126**, 310–318 (1987).

136. Falade-Nwulia, O. *et al.* Incident hepatitis B virus infection in HIV-infected and HIV-uninfected men who have sex with men from Pre-HAART to HAART periods: A cohort study. *Ann. Intern. Med.* **163**, 673–680 (2015).

137. Cascino, K., Roederer, M. & Liechti, T. OMIP-068: High-Dimensional Characterization of Global and Antigen-Specific B Cells in Chronic Infection. *Cytom. Part A* **97**, 1037–1043 (2020).

138. Hoffman, W., Lakkis, F. G. & Chalasani, G. B cells, antibodies, and more. *Clin. J. Am. Soc. Nephrol.* **11**, 137–154 (2016).

139. Mahnke, Y. D. & Roederer, M. OMIP-001: Quality and phenotype of Ag-responsive human T-cells. *Cytom. Part A* **77**, 819–820 (2010).

140. Hystad, M. E. *et al.* Characterization of Early Stages of Human B Cell Development by Gene Expression Profiling. *J. Immunol.* **179**, 3662–3671 (2007).

141. Bemark, M. Translating transitions - How to decipher peripheral human B cell development. *J. Biomed. Res.* **29**, 264–284 (2015).

142. Mesin, L., Ersching, J. & Victora, G. D. Germinal Center B Cell Dynamics. *Immunity* **45**, 471–482 (2016).

143. De Silva, N. S. & Klein, U. Dynamics of B cells in germinal centres. *Nat. Rev.*

Immunol. **15**, 137–148 (2015).

144. O'Connor, B. P. *et al.* Imprinting the Fate of Antigen-Reactive B Cells through the Affinity of the B Cell Receptor. *J. Immunol.* **177**, 7723–7732 (2006).

145. Taylor, J. J., Pape, K. A. & Jenkins, M. K. A germinal center-independent pathway generates unswitched memory B cells early in the primary response. *J. Exp. Med.* **209**, 597–606 (2012).

146. Kurosaki, T., Kometani, K. & Ise, W. Memory B cells. *Nat. Rev. Immunol.* **15**, 149–159 (2015).

147. Sims, G. P. *et al.* Identification and characterization of circulating human transitional B cells. *Blood* **105**, 4390–4398 (2005).

148. Klein, U., Rajewsky, K. & Küppers, R. Human immunoglobulin (Ig)M+IgD+ peripheral blood B cells expressing the CD27 cell surface antigen carry somatically mutated variable region genes: CD27 as a general marker for somatically mutated (memory) B cells. *J. Exp. Med.* **188**, 1679–1689 (1998).

149. Wu, Y. C. B., Kipling, D. & Dunn-Walters, D. K. The relationship between CD27 negative and positive B cell populations in human peripheral blood. *Front. Immunol.* **2**, 1–12 (2011).

150. Arpin, C. *et al.* The normal counterpart of IgD myeloma cells in germinal center displays extensively mutated IgVH gene, Cμ-Cδ switch, and λ light chain expression. *J. Exp. Med.* **187**, 1169–1178 (1998).

151. Koelsch, K. *et al.* Mature B cells class switched to IgD are autoreactive in healthy individuals. *J. Clin. Invest.* **117**, (2007).

152. Weller, S. *et al.* Human blood IgM 'memory' B cells are circulating splenic marginal zone B cells harboring a prediversified immunoglobulin repertoire. *Blood* **104**, 3647–3654 (2004).

153. Cerutti, A., Cols, M. & Puga, I. Marginal zone B cells: Virtues of innate-like antibody-producing lymphocytes. *Nature Reviews Immunology* **13**, 118–132 (2013).

154. Weill, J.-C., Weller, S. & Reynaud, C.-A. Human Marginal Zone B Cells. *Annu. Rev. Immunol.* **27**, 267–285 (2009).

155. Rothstein, T. L., Griffin, D. O., Holodick, N. E., Quach, T. D. & Kaku, H. Human B-1 cells take the stage. *Ann NY Acad Sci* **1285**, 97–114 (2013).

156. Griffin, D. O., Holodick, N. E. & Rothstein, T. L. Human B1 cells in umbilical cord and adult peripheral blood express the novel phenotype CD20+CD27+CD43+CD70-. *J. Exp. Med.* **208**, 67–80 (2011).

157. Covens, K. *et al.* Characterization of proposed human B-1 cells reveals pre-plasmablast phenotype. *Blood* **121**, 5176–5183 (2013).

158. Tangye, S. G. To B1 or not to B1: that really is still the question! *Blood* **121**, 5109–5110 (2013).

159. Lee, J., Kuchen, S., Fischer, R., Chang, S. & Lipsky, P. E. Identification and Characterization of a Human CD5 + Pre-Naive B Cell Population . *J. Immunol.* **182**, 4116–4126 (2009).

160. Sen, G., Bikah, G., Venkataraman, C. & Bondada, S. Negative regulation of antigen receptor-mediated signaling by constitutive association of CD5 with the SHP-1

protein tyrosine phosphatase in B-1 B cells. *Eur. J. Immunol.* **29**, 3319–3328 (1999).

161. Kardava, L. *et al.* Abnormal B cell memory subsets dominate HIV-specific responses in infected individuals. *J. Clin. Invest.* **124**, 3252–3262 (2014).

162. Tipton, C. M. *et al.* Diversity, cellular origin and autoreactivity of antibody-secreting cell population expansions in acute systemic lupus erythematosus. *Nat. Immunol.* **16**, 755–765 (2015).

163. Jenks, S. A. *et al.* Distinct Effector B Cells Induced by Unregulated Toll-like Receptor 7 Contribute to Pathogenic Responses in Systemic Lupus Erythematosus. *Immunity* **49**, 725-739.e6 (2018).

164. Liechti, T. *et al.* Widespread B cell perturbations in HIV-1 infection afflict naive and marginal zone B cells. *J. Exp. Med.* **216**, 2071–2090 (2019).

165. Zuniga, E. I., Macal, M., Lewis, G. M. & Harker, J. A. Innate and Adaptive Immune Regulation During Chronic Viral Infections. *Annu. Rev. Virol.* **2**, 573–597 (2015).

166. Griffith, J. W., Sokol, C. L. & Luster, A. D. Chemokines and Chemokine Receptors: Positioning Cells for Host Defense and Immunity. *Annu. Rev. Immunol.* **32**, 659–702 (2014).

167. Groom, J. R. & Luster, A. D. CXCR3 in T cell function. *Exp. Cell Res.* **317**, 620–631 (2011).

168. Perez-Andres, M. *et al.* Human peripheral blood B-Cell compartments: A crossroad in B-cell traffic. *Cytom. Part B - Clin. Cytom.* **78**, 47–60 (2010).

169. Larrubia, J. R. *et al.* The role of CCR5/CXCR3 expressing CD8+ cells in liver damage

and viral control during persistent hepatitis C virus infection. *J. Hepatol.* **47**, 632–641 (2007).

170. Zeremski, M. *et al.* Intrahepatic Levels of CXCR3-Associated Chemokines Correlate with Liver Inflammation and Fibrosis in Chronic Hepatitis C. *Hepatology* **48**, 1440–1450 (2008).

171. Collins, M., Ling, V. & Carreno, B. M. The B7 family of immune-regulatory ligands. *Genome Biol.* **6**, 1–7 (2005).

172. Vendel, A. C. *et al.* B and T Lymphocyte Attenuator Regulates B Cell Receptor Signaling by Targeting Syk and BLNK. *J. Immunol.* **182**, 1509–1517 (2009).

173. Figueiro, F. *et al.* Phenotypic and functional characteristics of CD39high human regulatory B cells (Breg). *Oncoimmunology* **5**, e1082703 (2016).

174. Tharinger, H. *et al.* Antibody-dependent and antibody-independent uptake of HBsAg across human leucocyte subsets is similar between individuals with chronic hepatitis B virus infection and healthy donors. *J. Viral Hepat.* **24**, 506–513 (2017).

175. Townsend, S. E., Goodnow, C. C. & Cornall, R. J. Single epitope multiple staining to detect ultralow frequency B cells. *J. Immunol. Methods* **249**, 137–146 (2001).

176. Amanna, I. J. & Slifka, M. K. Quantitation of rare memory B cell populations by two independent and complementary approaches. *J. Immunol. Methods* **317**, 175–185 (2006).

177. Keating, G. M. & Noble, S. Recombinant Hepatitis B Vaccine (Energix-B) A Review of its Immunogenicity and Protective Efficacy against Hepatitis B. *Drugs* **63**, 1021–1051 (2003).

178. Huang, J. *et al.* Isolation of human monoclonal antibodies from peripheral blood B cells. *Nat. Protoc.* **8**, 1907–1915 (2013).

179. Wong, P. & Pamer, E. G. CD8 T cell responses to infectious pathogens. *Annual Review of Immunology* **21**, 29–70 (2003).

180. Sant, A. J. & McMichael, A. Revealing the role of CD4+ T cells in viral immunity. *Journal of Experimental Medicine* **209**, 1391–1395 (2012).

181. Xia, A., Zhang, Y., Xu, J., Yin, T. & Lu, X. J. T Cell Dysfunction in Cancer Immunity and Immunotherapy. *Frontiers in immunology* **10**, 1719 (2019).

182. Rosenblum, M. D., Remedios, K. A. & Abbas, A. K. Mechanisms of human autoimmunity. *J. Clin. Invest.* **125**, 2228–2233 (2015).

183. Rehermann, B. Intrahepatic T cells in hepatitis B: Viral control versus liver cell injury. *Journal of Experimental Medicine* **191**, 1263–1268 (2000).

184. Seder, R. A. & Ahmed, R. Similarities and differences in CD4+ and CD8+ effector and memory T cell generation. *Nature Immunology* **4**, 835–842 (2003).

185. Miyara, M. & Sakaguchi, S. Natural regulatory T cells: mechanisms of suppression. *Trends in Molecular Medicine* **13**, 108–116 (2007).

186. Borsellino, G. *et al.* Expression of ectonucleotidase CD39 by Foxp3+ Treg cells: Hydrolysis of extracellular ATP and immune suppression. *Blood* **110**, 1225–1232 (2007).

187. Antonioli, L., Pacher, P., Vizi, E. S. & Haskó, G. CD39 and CD73 in immunity and inflammation. *Trends in Molecular Medicine* **19**, 355–367 (2013).

188. Germain, R. N. T-cell development and the CD4-CD8 lineage decision. *Nature*

Reviews Immunology **2**, 309–322 (2002).

189. Kaech, S. M., Wherry, E. J. & Ahmed, R. Effector and memory T-cell differentiation: Implications for vaccine development. *Nature Reviews Immunology* **2**, 251–262 (2002).

190. Mahnke, Y. D., Brodie, T. M., Sallusto, F., Roederer, M. & Lugli, E. The who's who of T-cell differentiation: Human memory T-cell subsets. *Eur. J. Immunol.* **43**, 2797–2809 (2013).

191. Testi, R., D'Ambrosio, D., De Maria, R. & Santoni, A. The CD69 receptor: a multipurpose cell-surface trigger for hematopoietic cells. *Immunol. Today* **15**, 479–483 (1994).

192. Chattopadhyay, P. K. & Roederer, M. Good cell, bad cell: Flow cytometry reveals T-cell subsets important in HIV disease. *Cytometry Part A* **77**, 614–622 (2010).

193. Croft, M., So, T., Duan, W. & Soroosh, P. The significance of OX40 and OX40L to T-cell biology and immune disease. *Immunological Reviews* **229**, 173–191 (2009).

194. Jacobi, F. J. *et al.* OX40 stimulation and PD-L1 blockade synergistically augment HBV-specific CD4 T cells in patients with HBeAg-negative infection. *J. Hepatol.* **70**, 1103–1113 (2019).

195. Bacher, P. & Scheffold, A. Flow-cytometric analysis of rare antigen-specific T cells. *Cytom. Part A* **83A**, 692–701 (2013).

196. Elgueta, R. *et al.* Molecular mechanism and function of CD40/CD40L engagement in the immune system. *Immunological Reviews* **229**, 152–172 (2009).

197. Betts, M. R. *et al.* Sensitive and viable identification of antigen-specific CD8+ T

cells by a flow cytometric assay for degranulation. *J. Immunol. Methods* **281**, 65–78 (2003).

198. Kalliolias, G. D. & Ivashkiv, L. B. TNF biology, pathogenic mechanisms and emerging therapeutic strategies. *Nat. Rev. Rheumatol.* **12**, 49–62 (2016).

199. Kang, S., Brown, H. M. & Hwang, S. Direct antiviral mechanisms of interferon-gamma. *Immune Network* **18**, (2018).

200. Ross, S. H. & Cantrell, D. A. Signaling and Function of Interleukin-2 in T Lymphocytes. *Annu. Rev. Immunol.* **36**, 411–433 (2018).

201. Spolski, R. & Leonard, W. J. IL-21 and T follicular helper cells. *International Immunology* **22**, 7–12 (2009).

202. Ai, W., Li, H., Song, N., Li, L. & Chen, H. Optimal method to stimulate cytokine production and its use in immunotoxicity assessment. *Int. J. Environ. Res. Public Health* **10**, 3834–3842 (2013).

203. Pardoll, D. M. The blockade of immune checkpoints in cancer immunotherapy. (2012). doi:10.1038/nrc3239

204. Saeidi, A. *et al.* T-cell exhaustion in chronic infections: Reversing the state of exhaustion and reinvigorating optimal protective immune responses. *Front. Immunol.* **9**, 2569 (2018).

205. Qin, S. *et al.* Novel immune checkpoint targets: Moving beyond PD-1 and CTLA-4. *Molecular Cancer* **18**, 1–14 (2019).

206. Wieland, D. *et al.* TCF1+ hepatitis C virus-specific CD8+ T cells are maintained after cessation of chronic antigen stimulation. *Nat. Commun.* **8**, 1–13 (2017).

207. Escobar, G., Mangani, D. & Anderson, A. C. *T cell factor 1: A master regulator of the T cell response in disease*. *Sci. Immunol* **5**, (2020).

208. Wang, Y. *et al.* The Transcription Factor TCF1 Preserves the Effector Function of Exhausted CD8 T Cells During Chronic Viral Infection. *Front. Immunol.* **10**, 169 (2019).

209. Chen, Z. *et al.* TCF-1-Centered Transcriptional Network Drives an Effector versus Exhausted CD8 T Cell-Fate Decision. *Immunity* **51**, 840-855.e5 (2019).

210. Takahashi, T., Dejbakhsh-Jones, S. & Strober, S. Expression of CD161 (NKR-P1A) Defines Subsets of Human CD4 and CD8 T Cells with Different Functional Activities. *J. Immunol.* **176**, 211–216 (2006).

211. Northfield, J. W. *et al.* CD161 expression on hepatitis C virus-specific CD8+ T cells suggests a distinct pathway of T cell differentiation. *Hepatology* **47**, 396–406 (2008).

212. Henson, S. M. & Akbar, A. N. KLRG1-more than a marker for T cell senescence. *Age* **31**, 285–291 (2009).

213. Ye, B. *et al.* T-cell exhaustion in chronic hepatitis B infection: current knowledge and clinical significance. *Cell death & disease* **6**, e1694 (2015).

214. Tassignon, J. *et al.* Monitoring of cellular responses after vaccination against tetanus toxoid: Comparison of the measurement of IFN-γ production by ELISA, ELISPOT, flow cytometry and real-time PCR. *J. Immunol. Methods* **305**, 188–198 (2005).

215. Thompson, E. A. *et al.* Metabolic programs define dysfunctional immune

responses in severe COVID-19 patients. *Cell Rep.* (2021). doi:10.1016/j.celrep.2021.108863

216. Pearce, E. L. & Shen, H. Making sense of inflammation, epigenetics, and memory CD8+ T-cell differentiation in the context of infection. *Immunological Reviews* **211**, 197–202 (2006).

217. Mazzoni, A. *et al.* Impaired immune cell cytotoxicity in severe COVID-19 is IL-6 dependent. *J. Clin. Invest.* **130**, 4694–4703 (2020).

218. Ben-Hail, D. *et al.* Novel compounds targeting the mitochondrial protein VDAC1 inhibit apoptosis and protect against mitochondrial dysfunction. *J. Biol. Chem.* **291**, 24986–25003 (2016).

219. Kim, J. *et al.* VDAC oligomers form mitochondrial pores to release mtDNA fragments and promote lupus-like disease. *Science (80-.).* **366**, 1531–1536 (2019).

220. Cox, A. L. *et al.* Prospective evaluation of community-acquired acute-phase hepatitis C virus infection. *Clin. Infect. Dis.* **40**, 951–958 (2005).

221. Dugas, A. F. *et al.* Derivation and Validation of a Clinical Decision Guideline for Influenza Testing in 4 US Emergency Departments. *Clin. Infect. Dis.* **70**, 49–58 (2020).

222. Klein, S. L. *et al.* Sex, age, and hospitalization drive antibody responses in a COVID-19 convalescent plasma donor population. *J. Clin. Invest.* **130**, 6141–6150 (2020).

223. Zhang, J. Y. *et al.* Single-cell landscape of immunological responses in patients with COVID-19. *Nat. Immunol.* **21**, 1107–1118 (2020).

224. Camara, A. K. S., Zhou, Y. F., Wen, P. C., Tajkhorshid, E. & Kwok, W. M. Mitochondrial VDAC1: A key gatekeeper as potential therapeutic target. *Frontiers in Physiology* **8**, (2017).

225. Garrido, C. *et al.* Mechanisms of cytochrome c release from mitochondria. *Cell Death and Differentiation* **13**, 1423–1433 (2006).

226. Kuri-Cervantes, L. *et al.* Immunologic perturbations in severe COVID-19/SARS-CoV-2 infection. *bioRxiv* 2020.05.18.101717 (2020). doi:10.1101/2020.05.18.101717

227. Abu-Hamad, S. *et al.* The VDAC1 N-terminus is essential both for apoptosis and the protective effect of anti-apoptotic proteins. *J. Cell Sci.* **122**, 1906–1916 (2009).

228. Shimizu, S., Ide, T., Yanagida, T. & Tsujimoto, Y. Electrophysiological study of a novel large pore formed by Bax and the voltage-dependent anion channel that is permeable to cytochrome c. *J. Biol. Chem.* **275**, 12321–12325 (2000).

229. Laing, A. G. *et al.* A consensus Covid-19 immune signature combines immuno-protection with discrete sepsis-like traits associated with poor prognosis. *medRxiv* 2020.06.08.20125112 (2020). doi:10.1101/2020.06.08.20125112

230. Silvestre-Roig, C., Fridlender, Z. G., Glogauer, M. & Scapini, P. Neutrophil Diversity in Health and Disease. *Trends in Immunology* **40**, 565–583 (2019).

231. Zhou, J., Nefedova, Y., Lei, A. & Gabrilovich, D. Neutrophils and PMN-MDSC: Their biological role and interaction with stromal cells. *Seminars in Immunology* **35**, 19–28 (2018).

232. Shoshan-Barmatz, V., Zakar, M., Rosenthal, K. & Abu-Hamad, S. Key regions of

VDAC1 functioning in apoptosis induction and regulation by hexokinase. *Biochim. Biophys. Acta - Bioenerg.* **1787**, 421–430 (2009).

233. Hall, C. J. *et al.* Immunoresponsive gene 1 augments bactericidal activity of macrophage-lineage cells by regulating β-oxidation-dependent mitochondrial ros production. *Cell Metab.* **18**, 265–278 (2013).

234. Moon, J. S. *et al.* NOX4-dependent fatty acid oxidation promotes NLRP3 inflammasome activation in macrophages. *Nat. Med.* **22**, 1002–1012 (2016).

235. Lucas, C. *et al.* Longitudinal analyses reveal immunological misfiring in severe COVID-19. *Nature* **584**, 463–469 (2020).

236. Bronte, V. *et al.* Recommendations for myeloid-derived suppressor cell nomenclature and characterization standards. *Nature Communications* **7**, 1–10 (2016).

237. Arunachalam, P. S. *et al.* Systems biological assessment of immunity to mild versus severe COVID-19 infection in humans. *Science (80-.).* **369**, 1210–1220 (2020).

238. Schulte-Schrepping, J. *et al.* Severe COVID-19 Is Marked by a Dysregulated Myeloid Cell Compartment. *Cell* **182**, 1419-1440.e23 (2020).

239. Chen, G. *et al.* Clinical and immunological features of severe and moderate coronavirus disease 2019. *J. Clin. Invest.* **130**, 2620–2629 (2020).

240. La Gruta, N. L. & Turner, S. J. T cell mediated immunity to influenza: Mechanisms of viral control. *Trends in Immunology* **35**, 396–402 (2014).

241. Shoshan-Barmatz, V. *et al.* VDAC, a multi-functional mitochondrial protein

regulating cell life and death. *Molecular Aspects of Medicine* **31**, 227–285 (2010).

242. Cheng, E. H. Y., Sheiko, T. V., Fisher, J. K., Craigen, W. J. & Korsmeyer, S. J. VDAC2 inhibits BAK activation and mitochondrial apoptosis. *Science (80-.).* **301**, 513–517 (2003).

243. Shimizu, S., Matsuoka, Y., Shinohara, Y., Yoneda, Y. & Tsujimoto, Y. Essential role of voltage-dependent anion channel in various forms of apoptosis in mammalian cells. *J. Cell Biol.* **152**, 237–250 (2001).

244. Shimizu, S., Narita, M. & Tsujimoto, Y. Bcl-2 family proteins regulate the release of apoptogenic cytochrome c by the mitochondrial channel VDAC. *Nature* **399**, 483–487 (1999).

245. Bratic, A. & Larsson, N. G. The role of mitochondria in aging. *Journal of Clinical Investigation* **123**, 951–957 (2013).

246. Quinn, K. M., Palchaudhuri, R., Palmer, C. S. & La Gruta, N. L. The clock is ticking: the impact of ageing on T cell metabolism. *Clin. Transl. Immunol.* **8**, e01091 (2019).

247. Vabret, N. *et al.* Immunology of COVID-19: Current State of the Science. *Immunity* **52**, 910–941 (2020).

248. Grifoni, A. *et al.* Targets of T Cell Responses to SARS-CoV-2 Coronavirus in Humans with COVID-19 Disease and Unexposed Individuals. *Cell* **181**, 1489-1501.e15 (2020).

249. Sekine, T. *et al.* Robust T Cell Immunity in Convalescent Individuals with Asymptomatic or Mild COVID-19. *Cell* **183**, 158-168.e14 (2020).

250. Lauvau, G., Boutet, M., Williams, T. M., Chin, S. S. & Chorro, L. Memory CD8+ T Cells: Innate-Like Sensors and Orchestrators of Protection. *Trends in Immunology* **37**, 375–385 (2016).

251. Pearce, E. L., Poffenberger, M. C., Chang, C. H. & Jones, R. G. Fueling immunity: Insights into metabolism and lymphocyte function. *Science* **342**, (2013).

252. Vangeti, S., Yu, M. & Smed-Sörensen, A. Respiratory Mononuclear Phagocytes in Human Influenza A Virus Infection: Their Role in Immune Protection and As Targets of the Virus. *Frontiers in Immunology* **9**, 1521 (2018).